

# Nanotechnology for hydrometallurgy

Extraction and separation of rare earth elements by  
hybrid nanoadsorbents

Elizabeth Polido Legaria

*Faculty of Natural Resources and Agricultural Sciences*

*Department of Molecular Sciences*

*Uppsala*

Doctoral thesis

Swedish University of Agricultural Sciences

Uppsala 2018

Acta Universitatis agriculturae Sueciae

2018:7

ISSN 1652-6880

ISBN (print version) 978-91-7760-154-8

ISBN (electronic version) 978-91-7760-155-5

© 2018 Elizabeth Polido Legaria, Uppsala

Print: SLU Service/Repro, Uppsala 2018

# Nanotechnology for hydrometallurgy. Extraction and separation of rare earth elements by hybrid nanoadsorbents.

## Abstract

Rare Earth Elements (REE) are a group of 17 chemically similar metals that have gained an increasing importance over the past decades, due to their unique properties that make them crucial for many applications, especially in high-tech products. The term “rare” is rather historical than descriptive, since they are quite abundant in the Earth’s crust. However, their extraction and separation can be challenging. This thesis aims to develop a competitive technology, based on functional nanoadsorbents, for extraction and separation of REE in solution that can be industrially applied.

Silica (SiO<sub>2</sub>) nanoparticles (NPs) with an iron oxide core were selected as the base for the nanoadsorbents. Nanoscale SiO<sub>2</sub> exhibits a large surface area that is very advantageous for adsorption purposes. Furthermore, they can be surface functionalized with different organic molecules (ligands). The iron oxide core allows the solid nanoadsorbents to be easily removed magnetically from solution.

First, the synthesis of the nanoadsorbents was optimized and three different organosilanes were synthesized, grafted onto SiO<sub>2</sub> NPs and tested for REE uptake. One of the three organosilanes showed to be reasonably efficient and was further tested with magnetic NP for selective uptake of REE. Structural studies of molecular model compounds gave molecular insights into the observed selectivity.

Next, adsorption conditions were carefully modified to, presumably, double the obtained REE uptake. Unexpectedly, the uptake increased up to 30 times, which suggested that a different uptake mechanism was involved. The mechanism was investigated and revealed the induced seeding of a crystalline phase of REE(OH)<sub>3</sub> on the surface. Preliminary tests on REE carbonate from REE ores gave very encouraging results.

Finally, a deeper understanding into the selective REE uptake was achieved via structural studies of different ligands and their interaction with different REE, creating the basis for molecular recognition approach. Four ligands specific to different REE were identified and their interaction with REE explained from a molecular point of view. One of these ligands was chosen for upscaling of the technology, by evaluating its potential as packing material for chromatographic separation of REE. The studies provided very attractive results, with good separation of 6 different REE from a solution.

*Keywords:* Rare earth elements, silica nanoparticles, magnetic silica nanoparticles, nanoadsorbents, hydrometallurgy, selective adsorption

*Author’s address:* Elizabeth Polido Legaria, SLU, Department of Molecular Sciences  
P.O. Box 7015, 750 07 Uppsala, Sweden

## Dedication

A mis padres, mi hermana y Jon, las personas más importantes de mi vida.

*When you see yourself doing something badly and nobody is bothering to tell you anymore, that's a very bad place to be. You may not want to hear it, but your critics are often the ones telling you they still love you and care about you.*

Randy Pausch, The Last Lecture

*If you trust in yourself...and believe in your dreams...and follow your star...you'll still get beaten by people who spent their time working hard and learning things and weren't so lazy.*

Terry Pratchett, The Wee Free Men.

# Contents

<b>List of publications</b>	<b>9</b>
<b>List of tables</b>	<b>13</b>
<b>List of figures</b>	<b>15</b>
<b>Abbreviations</b>	<b>19</b>
<b>1 Introduction</b>	<b>21</b>
<b>2 Background</b>	<b>25</b>
2.1 Rare Earth Elements. Definitions and occurrence in nature.	25
2.2 Importance of REE. Main applications.	29
2.3 Technologies for REE Extraction and Separation	31
2.4 Silica (SiO <sub>2</sub> ) nanoparticles.	32
2.5 Magnetic Iron Oxide nanoparticles.	33
2.5.1 Iron oxides and magnetic nanoparticles.	34
2.5.2 Iron oxide MNPs as nanoadsorbents for REE extraction and separation.	35
<b>3 Silica (SiO<sub>2</sub>) and magnetic SiO<sub>2</sub> nanoparticles</b>	<b>37</b>
3.1 Synthesis of SiO <sub>2</sub> nanoparticles.	37
3.2 Synthesis of magnetic SiO <sub>2</sub> nanoparticles ( $\gamma$ -Fe <sub>2</sub> O <sub>3</sub> -SiO <sub>2</sub> core-shell magnetic nanoparticles –MNPs-).	39
<b>4 Organosilane derivatives: Synthesis and applications as selective ligands on hybrid nanoadsorbents (Papers I&amp;II)</b>	<b>41</b>
4.1 Background	41
4.2 Synthesis of organosilane derivatives (Paper I)	42
4.3 Synthesis of organic ligand grafted magnetic and non-magnetic SiO <sub>2</sub> NPs	43
4.4 Nuclear magnetic resonance (NMR) spectroscopy	43
4.4.1 Solution <sup>1</sup> H-NMR and <sup>13</sup> C-NMR spectroscopy (Paper I)	43
4.4.2 Solid state <sup>29</sup> Si and <sup>13</sup> C-NMR spectroscopy (Paper I)	44

4.5	Fourier-transform infrared spectroscopy (FTIR)	45
4.5.1	Functionalized SiO <sub>2</sub> NPs (Paper I)	46
4.5.2	Functionalized magnetic $\gamma$ -Fe <sub>2</sub> O <sub>3</sub> -SiO <sub>2</sub> MNPs (Paper II)	48
4.6	Thermo-gravimetric analysis (TGA).	49
4.7	REE uptake and release studies on magnetic and non-magnetic nanoadsorbents	50
4.7.1	Adsorption studies. Kinetic curves.	50
4.7.2	Desorption and selectivity studies.	51
4.8	Luminescence studies (Paper I)	53
4.9	Molecular insights into the observed selectivity. X-ray crystallography (Paper II).	54
4.10	Conclusions	55
<b>5</b>	<b>Exploring new possibilities for enhanced REE uptake (Paper III &amp; IV).</b>	<b>57</b>
5.1	Background	57
5.2	REE uptake at controlled pH conditions	58
5.3	REE release under mild conditions	59
5.4	Reusability of the nanoadsorbents. Consecutive adsorption-desorption cycles.	60
5.5	Solid state <sup>13</sup> C and <sup>29</sup> Si CP-MAS NMR spectroscopy for the study of the interaction of the functional layer with REE cations.	60
5.6	Enhanced adsorption mechanism: What is really happening?	62
5.7	Study of the simultaneity of coordination and seeding mechanisms by EXAFS (Paper IV).	66
5.8	Magnetic characterization and quantification of REE by magnetometry (Paper IV)	70
5.9	Possible practical applications.	73
5.10	Conclusions	75
<b>6</b>	<b>Comparative study of amino-polycarboxylic acids as complexonate ligands for molecular recognition of REEs (Paper V).</b>	<b>77</b>
6.1	Background	77
6.2	Synthesis of aminopolycarboxylic acid-functionalized nanoadsorbents.	78
6.3	Characterization of the functionalized nano-adsorbents.	78
6.3.1	FTIR spectroscopy.	78
6.3.2	Microscopy characterization (AFM, SEM and TEM).	80
6.3.3	Thermogravimetric analysis (TGA).	81
6.4	REE uptake and selectivity studies.	81

6.4.1	Adsorption isotherms with La <sup>3+</sup> , Nd <sup>3+</sup> and Dy <sup>3+</sup> . Influence of different ligands.	81
6.4.2	Selectivity studies with ternary and quinary mixtures of REE.	83
6.5	Structural studies.	85
6.5.1	Crystal structure of the TTHA-Dy molecular model compound.	85
6.5.2	Molecular insights into selective action of different complexonate functions.	86
6.6	Conclusions	90
<b>7</b>	<b>Proof of concept: Evaluation of chromatographic applications for DTPA-functionalized SiO<sub>2</sub>-based adsorbents (Paper VI).</b>	<b>91</b>
7.1	Background	91
7.2	Upscaling of the production of functional adsorbents.	92
7.2.1	DTPA-functionalization of SiO <sub>2</sub> NPs from Sigma-Aldrich.	92
7.2.2	DTPA-functionalized Kromasil® silica particles.	92
7.3	Characterization of the adsorbents.	93
7.3.1	Thermogravimetric analysis.	93
7.3.2	SEM, TEM and AFM imaging.	93
7.4	HPCIC evaluation of DTPA-functionalized Kromasil® column.	95
7.4.1	Isocratic and gradient elution.	95
7.4.2	Influence of column temperature.	96
7.4.3	Column efficiency and long-term stability.	96
7.4.4	Column overloading.	99
7.5	Conclusions	100
<b>8</b>	<b>Conclusions and future prospects.</b>	<b>101</b>
	<b>References</b>	<b>103</b>
	<b>Popular science summary</b>	<b>113</b>
	<b>Populärvetenskaplig sammanfattning</b>	<b>114</b>
	<b>Acknowledgements</b>	<b>115</b>



## List of publications

This thesis is based on the work contained in the following papers, referred to by Roman numerals in the text:

- I S.D Topel, E.P. Legaria, C. Tiseanu, J. Rocha, J-M. Nedelec, V. G. Kessler, G. A. Seisenbaeva\* (2014). Hybrid silica nanoparticles for sequestration and luminescence detection of trivalent rare-earth ions ( $\text{Dy}^{3+}$  and  $\text{Nd}^{3+}$ ) in solution. *Journal of Nanoparticle Research* 16:2783.
- II E. P. Legaria, S. D. Topel, V. G. Kessler, G. A. Seisenbaeva\* (2015). Molecular insights into the selective action of a magnetically removable complexone-grafted adsorbent. *Dalton Transactions* 44, 1273-1282.
- III E. P. Legaria\*, J. Rocha, C. W. Tai, V. G. Kessler, G. A. Seisenbaeva (2017). Unusual seeding mechanism for enhanced performance in solid-phase magnetic extraction of Rare Earth Elements. *Scientific Reports* 7: 43740.
- IV E. P. Legaria, I. Saldan, P. Svedlindh, E. Wetterskog, K. Gunnarsson. V. G. Kessler, G. A. Seisenbaeva\* (2018). Coordination of REE cations on the surface of  $\text{SiO}_2$ -derived nanoadsorbents. *Dalton Transactions*, Advance Article. DOI: 10.1039/C7DT04388K
- V E. P. Legaria\*, M. Samouchos, V. G. Kessler, G. A. Seisenbaeva\* (2017). Towards molecular recognition of REE: Comparative analysis of hybrid nanoadsorbents with different complexonate ligands- EDTA, DTPA and TTHA. *Inorganic Chemistry* 56 (22), 13938-13948.

VI R. A. Mahmoud, M. Samouchos, E. P. Legaria, M. Svärd, J. Hogblom, K. Forsberg, M. Palmlof, V. G. Kessler, G. A. Seisenbaeva, Å. Rasmusson (2017). DTPA-functionalised nanoadsorbents for REE separation: evaluation of chromatographic applications. (manuscript).

Papers I-V are reproduced with the permission of the publishers.

The contribution of E. P. Legaria to the papers included in this thesis was as follows:

- I Performed the synthesis of SiO<sub>2</sub> nanoparticles, rare earth adsorption determination by complexometric titration, characterization by SEM-EDS and TGA. Took part in the discussion and writing of the manuscript together with other co-authors.
- II Performed the synthesis of magnetic SiO<sub>2</sub> nanoparticles, their functionalization and characterization by TGA, FTIR and SEM-EDS, rare earth adsorption determination and analysis of the rare earth loaded material with SEM-EDS. Took part in the discussion and writing of the manuscript together with co-authors.
- III Planned the work together with the co-authors. Coordinated the experimental work and conducted almost all experiments, including synthesis of the magnetic nanoadsorbents, characterization (except for TEM), design of the adsorption-desorption experiments and determination of the rare earth uptake capacity. Compiled all the results and took the leading role in their interpretation and writing of the manuscript. Corresponding author of this paper.
- IV Planned the work together with the co-authors. Designed the experimental work and conducted all the experiments except single crystal X-ray and magnetic measurements. Compiled all the results and took the leading role in their interpretation and writing of the manuscript.
- V Planned the work together with the co-authors. Designed and coordinated the experimental work. Conducted almost all experiments, including synthesis and functionalization of the nanoadsorbents, adsorption-

desorption studies, full characterization of the materials (TGA, FTIR, SEM-EDS) except AFM and X-ray data collection and analysis. Compiled all the data and took very active role in their interpretation and writing of the manuscript. Shared corresponding author of this paper.

- VI Synthesized the DTPA-functionalized nanoadsorbents and conducted their characterization, including TGA, FTIR and REE uptake test. Took part in the discussion and writing of the manuscript together with the other co-authors.

## List of tables

Table 1. Classifications of REE in LREE and HREE. Source: GEUS, 2017.	26
Table 2. Reaction parameters of two different synthetic routes for SiO <sub>2</sub> nanoparticles.	38
Table 3. Summary of the FTIR spectra of SiO <sub>2</sub> and functionalized SiO <sub>2</sub> NPs	46
Table 4. Summary of the FTIR spectra of Fe <sub>3</sub> O <sub>4</sub> , $\gamma$ -Fe <sub>2</sub> O <sub>3</sub> -SiO <sub>2</sub> and functionalized $\gamma$ -Fe <sub>2</sub> O <sub>3</sub> -SiO <sub>2</sub> NPs.	48
Table 5. Quantification of organic ligand grafting on different nanoadsorbents	50
Table 6. Desorption efficiency for different nanoadsorbents loaded with REE.	52
Table 7. Selectivity in adsorption and desorption of REE by magnetic nanoadsorbents	52
Table 8. Nd <sup>3+</sup> uptake in different types of nanoadsorbents, varying adsorption conditions and molar ratios.	58
Table 9. Multi-step desorption with NH <sub>4</sub> (SO <sub>4</sub> ) <sub>2</sub> and comparison with acidic desorption.	59
Table 10. EDS analysis on $\gamma$ -Fe <sub>2</sub> O <sub>3</sub> -SiO <sub>2</sub> NPs for three consecutive adsorption-desorption cycles of Dy <sup>3+</sup> . Values are given in relative weight %.	60
Table 11. EXAFS fitting data for functionalized and non-functionalized SiO <sub>2</sub> NPs loaded with the indicated REE at high pH conditions.	68
Table 12. Comparison of REE uptake capacity obtained from magnetometry (magn.) and from titration (titr.).	72
Table 13. Chemical composition as determined by EDS analysis of the REE carbonate from Tanbreez ore and its leachate solution after treatment with HNO <sub>3</sub> .	74
Table 14. Chemical composition as determined by EDS of the SiO <sub>2</sub> NPs after adsorption at high pH of the leachate coming from Tanbreez ore.	74
Table 15. Summary of FTIR spectra of SiO <sub>2</sub> and functionalized SiO <sub>2</sub> NPs	79
Table 16. Amount of EDTA, DTPA and TTHA grafted onto the NPs, as obtained from TGA.	81

Table 17. Average maximum adsorption capacity ( $q_e$ ) for each nanoadsorbent, followed by the standard deviation from three measurements.	82
Table 18. EDS analysis of functionalized SiO <sub>2</sub> NPs with Ternary and Quinary Mixtures of REE	83
Table 19. Selectivity trends in desorption for functionalized SiO <sub>2</sub> NPs under different conditions. Expressed in molar ratios.	84
Table 20. Experimental parameters and column efficiency for some reported HPCIC REE separation studies and the present work.	98

## List of figures

- Figure 1.* Integrated knowledge management system for European REE exploitation industry. Source: [www.eurare.org](http://www.eurare.org) 22
- Figure 2.* Abundance of chemical elements in the Earth's upper continental crust. (Haxel et al., 2002). Note: The abundance is measured as a function of atomic number. REE are by orders of magnitude more abundant than precious metals such as Pt, Au and Ag. 27
- Figure 3.* Uses of the Rare Earth Elements. Source: [www.eurare.org](http://www.eurare.org) 29
- Figure 4.* Estimated worldwide REO consumption in 2015. Source: Roskill, 2016 29
- Figure 5.* HR-TEM images of SiO<sub>2</sub> nanoparticles (scale bar is 200, 50 and 20 nm for **a**, **c** and **e**, **f**, respectively). **b** and **d** are size distribution histograms of **a** and **c** images, respectively. 38
- Figure 6.* HR-TEM images of  $\gamma$ -Fe<sub>2</sub>O<sub>3</sub>-SiO<sub>2</sub> nanoparticles (the scale bar is 100, 20 and 5 nm in A, B and C respectively. D is the EF-TEM mapping image. 39
- Figure 7.* Core-shell  $\gamma$ -Fe<sub>2</sub>O<sub>3</sub>-SiO<sub>2</sub> NPs: 1) dispersed in ethanol ; 2) retracted by a magnet. 39
- Figure 8.* Synthetic pathway for the three organosilane derivatives. 42
- Figure 9.* <sup>13</sup>C CP-MAS NMR and <sup>29</sup>Si CP-MAS NMR spectra of SiO<sub>2</sub> NPs functionalized with organosilanes. 45
- Figure 10.* Q<sub>n</sub> type (Q<sub>4</sub>, Q<sub>3</sub>, Q<sub>2</sub>) and T<sub>n</sub> type (T<sub>3</sub>, T<sub>2</sub>, T<sub>1</sub>) Si local environments. 45
- Figure 11.* FTIR spectra of SiO<sub>2</sub> and functionalized SiO<sub>2</sub> NPs (A series) and functionalized SiO<sub>2</sub> NPs with and without adsorbed RE<sup>3+</sup> cations (B series). 47
- Figure 12.* FTIR spectra of Fe<sub>3</sub>O<sub>4</sub>,  $\gamma$ -Fe<sub>2</sub>O<sub>3</sub>-SiO<sub>2</sub> and functionalized  $\gamma$ -Fe<sub>2</sub>O<sub>3</sub>-SiO<sub>2</sub> (left) and comparison between functionalized  $\gamma$ -Fe<sub>2</sub>O<sub>3</sub>-SiO<sub>2</sub> with and without adsorbed RE<sup>3+</sup> cations (right.) 49

- Figure 13.* Kinetic curves of adsorption of Dy<sup>3+</sup> and Nd<sup>3+</sup> on functionalized SiO<sub>2</sub> NPs. 51
- Figure 14.* Kinetic curves of adsorption of Dy<sup>3+</sup>, Nd<sup>3+</sup> and La<sup>3+</sup> by magnetic  $\gamma$ -Fe<sub>2</sub>O<sub>3</sub>-SiO<sub>2</sub> NPs functionalized with L3 (mmol RE<sup>3+</sup>/g in black and mg RE<sup>3+</sup>/g in blue). 51
- Figure 15.* Photoluminescence spectra of a) SiO<sub>2</sub>-L2-Dy<sup>3+</sup> b) SiO<sub>2</sub>-L1-Dy<sup>3+</sup> and c) SiO<sub>2</sub>-L3-Dy<sup>3+</sup>. Excitation and emission wavelengths and the delays after the laser pulse used in the experiments are indicated. 53
- Figure 16.* Structures of 2D coordination polymers of REE : IDA complexes as models for binding the REE on the surface of nanoadsorbents with covalently grafted IDA molecules. 54
- Figure 17.* <sup>13</sup>C CP-MAS NMR and <sup>29</sup>Si CP-MAS NMR spectra of SiO<sub>2</sub> NPs functionalized with IDA-derivative ligand. 61
- Figure 18.* <sup>13</sup>C CP-MAS NMR spectra of functionalized SiO<sub>2</sub> NPs (red) and La<sup>3+</sup>-loaded functionalized SiO<sub>2</sub> NPs (black). 62
- Figure 19.* <sup>29</sup>Si MAS and <sup>29</sup>Si CP-MAS NMR spectra of SiO<sub>2</sub> NPs (black), functionalized SiO<sub>2</sub> NPs (red), and the corresponding La<sup>3+</sup>-loaded NPs (pink and blue, respectively). Every spectrum is normalized to the highest peak. 62
- Figure 20.* BF-TEM (upper two rows) and HAADF-STEM (lower row) images of SiO<sub>2</sub> nanoadsorbents loaded with a) Dy<sup>3+</sup>; b) Nd<sup>3+</sup>; c) La<sup>3+</sup> at high pH. 63
- Figure 21.* BF-TEM (upper two rows) and HAADF-STEM (lower row) images of  $\gamma$ -Fe<sub>2</sub>O<sub>3</sub>-SiO<sub>2</sub> NPs loaded with a)Dy<sup>3+</sup>; b)Nd<sup>3+</sup>; c)La<sup>3+</sup> at high pH. 64
- Figure 22.* BF-TEM images and EFTEM elemental mapping of SiO<sub>2</sub> nanoparticles loaded with REE. 64
- Figure 23.* XRPD patterns of functionalized SiO<sub>2</sub> NPs loaded with REE. The blue lines represent the pattern of the corresponding REE hydroxides. 65
- Figure 24.* AFM 3D images of SiO<sub>2</sub> NPs loaded with Nd<sup>3+</sup> (top) and 2D image of pure SiO<sub>2</sub> NPs. 66
- Figure 25.* EXAFS spectra for SiO<sub>2</sub>-Nd<sup>3+</sup> (left), SiO<sub>2</sub>-IDA-Dy<sup>3+</sup> (middle) and SiO<sub>2</sub>-IDA-La<sup>3+</sup> (right). Experimental data in black and fitted data in red. 69
- Figure 26.* (a)  $1/M$  versus  $T$  and (b)  $M \times T$  versus  $T$  for the REE : IDA compounds. The magnetic moment was normalized by weight of the REE : IDA sample. 70
- Figure 27.* (a)  $1/M$  versus  $T$  and (b)  $M \times T$  versus  $T$  for the SiO<sub>2</sub> NPs loaded with REE at high pH (SiO<sub>2</sub>-Dy(OH)<sub>3</sub> and SiO<sub>2</sub>-Nd(OH)<sub>3</sub>). The magnetic moment was normalized by weight of the sample. 71

- Figure 28.* Magnetization versus field for SiO<sub>2</sub>-IDA-Dy<sup>3+</sup> (solid lines) and SiO<sub>2</sub>-Dy(OH)<sub>3</sub> (open circles). 72
- Figure 29.* Synthesis scheme for the functionalization of NPs with aminopolycarboxylic acids. 78
- Figure 30.* FTIR spectra of functionalized SiO<sub>2</sub> NPs and the corresponding aminopolycarboxylic acid. 79
- Figure 31.* AFM, SEM and TEM images of pure SiO<sub>2</sub> NPs (first row); EDTA-functionalized SiO<sub>2</sub> NPs loaded with REE (second row); DTPA-functionalized  $\gamma$ -Fe<sub>2</sub>O<sub>3</sub>-SiO<sub>2</sub> NPs loaded with REE (third row) and TTHA-functionalized  $\gamma$ -Fe<sub>2</sub>O<sub>3</sub>-SiO<sub>2</sub> NPs loaded with REE (fourth row). 80
- Figure 32.* REE adsorption isotherms for the six different functional nanoadsorbents tested. A series shows the data sorted by type of ligand grafted (EDTA, DTPA or TTHA), and B series shows the data sorted by REE adsorbed (La<sup>3+</sup>, Nd<sup>3+</sup> or Dy<sup>3+</sup>). 82
- Figure 33.* Molecular structure of the complex anion in (NH<sub>4</sub>)<sub>3</sub>[HDyTTHA](NO<sub>3</sub>)·4H<sub>2</sub>O. 85
- Figure 34.* Crystal structures of Na[Dy(EDTA)(H<sub>2</sub>O)<sub>3</sub>]·5H<sub>2</sub>O (left) and (H<sub>3</sub>O)[Dy(EDTA)]·H<sub>2</sub>O (right). (You and Ng, 2007). 87
- Figure 35.* Crystal structures of K<sub>2</sub>[Yb(DTPA)(H<sub>2</sub>O)]·7H<sub>2</sub>O (left) (Hardcastle et al., 2000) and (NH<sub>4</sub>)<sub>4</sub>[Dy<sub>2</sub>(DTPA)<sub>2</sub>]·8H<sub>2</sub>O (right) (Inomata et al., 2003). 88
- Figure 36.* Crystal structures of K<sub>3</sub>[Dy(TTHA)]·5H<sub>2</sub>O (right) and K<sub>4</sub>[Tb<sub>2</sub>(HTTHA)<sub>2</sub>]·14H<sub>2</sub>O (left) (Wang et al., 2006b). 89
- Figure 37.* SEM (A-B) and AFM (C-F) images of Kromasil® microparticles (A, C and D correspond to pure Kromasil® and B, E, F to DTPA-functionalized Kromasil®) 94
- Figure 38.* TEM images of A) DTPA-functionalized SiO<sub>2</sub> NPs; B) DTPA functionalized SiO<sub>2</sub> NPs bearing La<sup>3+</sup>, Nd<sup>3+</sup> and Dy<sup>3+</sup>; C) Acid treated DTPA-functionalized SiO<sub>2</sub> NPs (pH= 1.9) and D) Acid treated DTPA-functionalized SiO<sub>2</sub> NPs (pH=1.3). 94
- Figure 39.* Chromatograms from A) isocratic and B) linear gradient elution studies at different concentrations of HNO<sub>3</sub> in the eluent. Eluent flow rate = 1 mL min<sup>-1</sup>, column temperature = 55°C, injected volume = 50  $\mu$ L and total REE concentration = 1000 mg L<sup>-1</sup>. 95
- Figure 40.* Chromatograms obtained at different column temperatures for linear gradient elution experiments (from 0M - 0.15M HNO<sub>3</sub> over 55 min). Eluent flow rate= 1 mL min<sup>-1</sup>, injected volume = 50  $\mu$ L, total REE concentration= 1000mg L<sup>-1</sup>. 96

- Figure 41.* Effect of the eluent flow rate on the column efficiency (HETP) for  $\text{La}^{3+}$ ,  $\text{Ce}^{3+}$ ,  $\text{Pr}^{3+}$ ,  $\text{Nd}^{3+}$ ,  $\text{Y}^{3+}$  and  $\text{Dy}^{3+}$ , for linear gradient elution experiments (from 0M-0.15M  $\text{HNO}_3$  over 55 min). Column temperature =  $55^\circ\text{C}$ , injected volume =  $50\mu\text{L}$ , and total REE concentration =  $1000\text{ mg L}^{-1}$ . 97
- Figure 42.* Comparison of retention times obtained for the six REE with a freshly packed column after 54 experimental runs. 98
- Figure 43.* A) Chromatograms of experiments with increasing sample load, with linear gradient elution (0M-0.15M  $\text{HNO}_3$  over 55 min), eluent flow rate =  $1\text{ mL min}^{-1}$ , column temperature =  $55^\circ\text{C}$ . B) ICP element-resolved fraction analysis of experiments with the highest total sample loads. 99

## Abbreviations

AFM	Atomic force microscopy
BF-TEM	Bright-field transmission electron microscopy
CP	Cross-polarization
CP-MAS	Cross-polarization magic-angle spinning
DTPA	Diethylenetriaminepentaacetic acid
EDS	Energy-dispersive X-ray spectroscopy
EDTA	Ethylenediaminetetraacetic acid
EFTEM	Energy-filtered transmission electron microscopy
EXAFS	X-ray absorption fine structure spectroscopy
FCC	Fluid catalytic cracking
FTIR	Fourier-transform infrared
FWMH	Full width at half maximum
HAADF-STEM	High-angle annular dark-field scanning transmission electron microscopy
HETP	Height of a theoretical plate
HPCIC	High-performance chelation ion chromatography
HREE	Heavy rare earth elements
HR-TEM	High resolution transmission electron microscopy
ICP	Inductively coupled plasma
ICPTES	3-isocyanatopropyltriethoxysilane
IDA	Iminodiacetic acid
IR	Infrared
IUPAC	International union of pure and applied chemistry
LED	Light-emitting diode
LREE	Light rare earth elements
MAS	Magic angle spinning

MNPs	Magnetic nanoparticles
MREE	Medium rare earth elements
MRI	Magnetic resonance imaging
MRT	Molecular recognition technology
NMR	Nuclear magnetic resonance
NPs	Nanoparticles
NTA	Nitrilotriacetic acid
REE	Rare earth elements
REO	Rare earth oxides
SEM	Scanning electron microscopy
TEM	Transmission electron microscopy
TEOS	Tetraethyl orthosilicate
TGA	Thermo-gravimetric analysis
TLC	Thin layer chromatography
TMS	Tetramethylsilane
TTHA	Triethylenetetraaminehexaacetic acid
UV	Ultra-violet
XANES	X-ray absorption near edge structure
XRF	X-ray fluorescence

# 1 Introduction

“What do cars, precision-guided missiles and the television you are watching right now have in common? They all depend on something called rare earth elements, unusual metals that are sprinkled inside almost every piece of high-tech you can think of. Most people have never heard of them. But we have become so reliant on rare earths that a few years ago, an intense global power struggle broke out over their free flow. The reason is that one country has a virtual monopoly – roughly 90 percent- of the mining, refining and processing of rare earths- China. And in 2010, it used that power to disrupt the world’s supply.”

Lesley Stahl, correspondent journalist, 2015, in an episode called “Rare Earth Elements” of the series *60 minutes* produced by CBS News.

Rare Earth Elements (REE) are a group of metals that are fundamental for innumerable products in a very broad spectrum of applications, but especially in many high-tech products (US Geological Survey, 2013). Both the European Commission and the U.S. Department of Energy have declared REE as critical and/or strategic raw materials (European Commission, 2010, U.S. Department of Energy, 2010, European Commission, 2014). The term “criticality” generally refers to the relevance of a specific material for a vital sector of the economy, whereas the term “strategic” is related to a material that is, from a national point of view, essential for defence issues, industrial development, medicine etc. Additionally, it usually alludes to materials that are difficult to replace and primarily imported from foreign countries (U.S. Department of Energy, 2010).

Taking this into account, it can be understood that the group of materials or minerals regarded as critical varies over time. REE have only been considered critical within the past decade, as demand increased and there was a growing awareness that China had quasi-monopolized the REE market, accounting for around 88% of the global production (Roskill Ltd, 2016).

To the surprise of many, the reasons for this Chinese quasi-monopoly are not exclusively geological. While it is true that China possesses an important share of the global reserves - roughly 40% (U.S. Geological Survey, 2017), there are plenty of resources outside China that were neither being exploited nor assessed until China started to limit REE exports. At this point, the REE supply to the non-Chinese consumers was put at risk.

In view of this, the European Commission funded the EURARE project, through the Seventh Framework Programme (FP7) scheme. The main goal of EURARE project was to ensure a sustainable supply of REE minerals and develop from scratch the basis of a European REE extraction and processing industry, that was non-existent at the time (Efythymios Balomenos, 2017, EURARE, 2013). The project aimed to embrace all aspects of the REE industry, from surveying and assessing available resources to developing REE end-products (Figure 1).



Figure 1. Integrated knowledge management system for European REE exploitation industry.

Source: [www.eurare.org](http://www.eurare.org)

This thesis describes work carried out within the EURARE project, focusing on the development of efficient procedures for the extraction of separation of REE. These processes are intended to support an economically viable REE industry that has a minimal impact on the environment.

REE are chemically very similar, they tend to occur jointly in nature, and almost ironically, they are needed in very high degrees of purity for their applications. Their separation is therefore imperative, and this very challenging task is being addressed using a variety of methods. Developing a technology for REE extraction and separation that is competitively efficient, environmentally friendly and economically viable is of course no easy task. The EURARE project has therefore gathered experts from diverse areas to develop and evaluate technologies and optimized processes. The three separation technologies investigated are solvent extraction, ionic liquids and separation by novel specific nanoadsorbents. The latter method constitutes the focus of this work.

Solvent extraction is currently one of the most used technologies in industry due to its good efficiency (Xie et al., 2014, Wilden et al., 2015, Johnson and Nash, 2015), but it generally produces large quantities of organic solvent wastes. Ionic liquids come to the stage as a greener alternative to solvent extraction. These are typically organic salts with a melting point below 100°C (Earle and Seddon, 2002). Their main advantages are their reduced flammability and lower risk of air pollution compared to conventional organic solvents (Dietz, 2006), although some of them, e.g. fluorinated IL can be harmful (Ghandi, 2014). However, they are generally expensive and require high temperatures, which can also increase costs from an industrial point of view. It is here where nanoadsorbents for solid phase extraction and separation of REE appear as an interesting and innovative technology. To the best of our knowledge, nanomaterials have not been so far used in industry for this purpose, so the field is quite new and the questions to tackle are many, starting from the lab scale. Nanomaterials offer huge potential for adsorption purposes since they provide a larger specific area than bulk material, and more specifically, SiO<sub>2</sub> based nanomaterials have numerous advantages for the production of efficient adsorbent materials. Besides their high surface-to-volume ratio, they offer the possibility of surface functionalization, which opens doors for selective adsorption (Yurchenko et al., 2012, Dudarko et al., 2008, Melnyk et al., 2012, A.Kavosi; F. Faridbod; Ganjali, 2015, Liou, 2004, Florek et al., 2015). Having set the goal on a technology that can be applied in industry, being able to easily separate the nanomaterials from solution becomes an attractive asset. Magnetic SiO<sub>2</sub> nanoparticles (NPs), consisting of a magnetic iron oxide core and a covering layer of SiO<sub>2</sub>, emerge then as very interesting materials. These offer the combined advantages for adsorption characteristic of SiO<sub>2</sub>-based nanomaterials and the easy removal of the NPs from solution thanks to the magnetic properties of the iron oxide core.

This work aims to explore the potential of this type of nanomaterials for the extraction and separation of REE, starting from the lab scale and the chemical mechanisms behind adsorption, to the application in a scaled up process.

## 2 Background

### 2.1 Rare Earth Elements. Definitions and occurrence in nature.

Rare Earth Elements is a collective name for 17 chemically similar metallic elements. According to the International Union of Pure and Applied Chemistry (IUPAC) definition, it includes the 15 lanthanide elements, from lanthanum (atomic no. 57) to lutetium (atomic no. 71) along with scandium (atomic no. 21) and yttrium (atomic no. 39). The latter two are included as they share many physical and chemical properties with the lanthanides (IUPAC, 2005).

REE are usually divided in Light Rare Earth Elements (LREE) and Heavy Rare Earth Elements (HREE), but several different classifications are used by different organizations. Within the EURARE project and in agreement with the European Commission, we have applied a common classification, in which the five elements from La to Sm (atomic no. 57-62) belong to LREE and the elements from Eu to Lu along with Y (atomic no. 63-71, 39) belong to the HREE. Y is usually considered a HREE despite its low atomic mass because it has a similar occurrence, ionic radius and properties to the other HREE (Gupta and Krishnamurthy, 2004). Although Sc is, as mentioned before, considered a REE, it is usually sourced as a by-product of nickel and aluminium production and therefore was not one of the target elements of the project (GEUS, 2017). It is important to mention that in some of the work in this thesis, Nd has been treated as a medium REE (MREE) but just as a comparison to the lighter REE La, since the actual term MREE, used by some organizations, denotes the elements from Sm to Dy. Some of the classifications used are presented in Table 1.

Table 1. Classifications of REE in LREE and HREE. Source: GEUS, 2017.

Element	Symbol	EURARE	IUPAC	China MLR		China State Council White Paper
				I	II	
Lanthanum	La	LREE	Unpaired electrons in 4f shells (LREE)	LREE	LREE	LREE
Cerium	Ce					
Praseodymium	Pr					
Neodymium	Nd					
Samarium	Sm	HREE	Paired electrons in 4f shells (HREE)	MREE	MREE	HREE
Europium	Eu					
Gadolinium	Gd					
Terbium	Tb					
Dysprosium	Dy					
Holmium	Ho					
Erbium	Er					
Thulium	Tm					
Ytterbium	Yb					
Lutetium	Lu					
Yttrium	Y					
Scandium	Sc					

The term “rare” is quite a misnomer, since REE are actually quite abundant in the earth crust, with variations within different REE. This slightly misleading term comes historically from the chemist Carl Axel Arrhenius (1757-1824), after he discovered REE in 1784 in the dumps of Ytterby (Sweden) quarries. They were then called “rare” because they were totally unknown and when discovered, Arrhenius thought that they were present in very small amounts, whilst the term “earths” comes from the fact that, when forming oxides, REEs have an earthy appearance (Massari and Ruberti, 2013).

The abundance of an element or group of elements is however not necessarily related to the ease of their exploitation. The Earth’s upper crust is assumed to contain 63 ppm of Ce and 33 ppm of La (the two most abundant REE) and 0.3 ppm of Tm and Lu, which are the rarest (Weng et al., 2015). The rarer HREE are more abundant in the Earth’s crust than other metals such as Au, Ag and Pt (Figure 2).



carbonatites of Fen in Norway and Sokli in Finland and the eudialyte in Norra Kärr in Sweden. As of September 2015, at least 66 advanced stage REE-projects were being developed outside China (Technology Metals Research, 2015), including the three deposits under license to EURARE partners (Norra Kärr, Klingerne and Kvanefjeld) .

It can be now understood that the issue with REE lies not in their scarcity as the misleading term “rare” might hint, but in the difficulty to find economically exploitable deposits and technologies to efficiently separate them, due to their joint occurrence in nature.

## 2.2 Importance of REE. Main applications.

The REE are essential raw materials for countless technological applications in various fields. The major applications include high field strength magnets, metallurgy, catalysts in the automotive and petro-chemical industry, colouring of glass/ceramics, phosphors (LEDs, flat panel displays...), lasers, NiMH batteries, fibre optics and so on. (Zhang et al., 2014, Jin et al., 1997, Shibasaki and Yoshikawa, 2002, Bünzli and Piguet, 2002, Sprecher et al., 2014, Alonso et al., 2012, Dasari et al., 2016, Carron et al., 2016). Figure 3 shows some of the most important uses of REE and Figure 4 shows the estimated worldwide consumption of Rare Earth Oxides (REO) in 2015 in different sectors (Roskill Ltd, 2016).

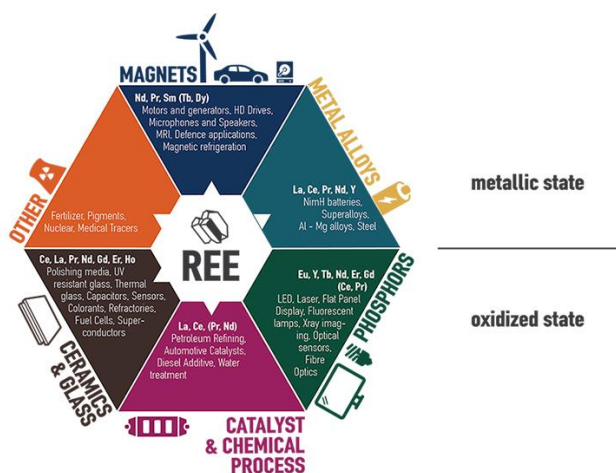


Figure 3. Uses of the Rare Earth Elements. Source: [www.eurare.org](http://www.eurare.org)

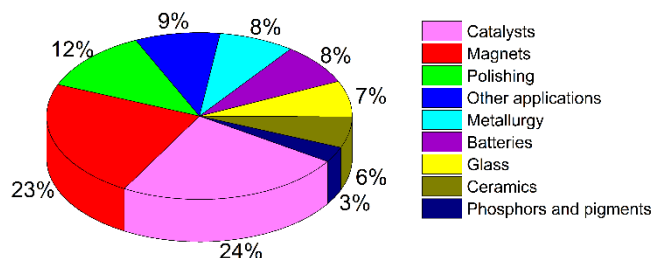


Figure 4. Estimated worldwide REO consumption in 2015. Source: Roskill, 2016

**Catalysts:** REE are used in both Fluid Catalytic Cracking (FCC) catalysts and automotive catalysts. The FCC process is used in the petroleum industry to obtain light fractions from high-molecular weight hydrocarbon fractions. The use of REE, particularly La, Ce and Nd, in this type of catalyst, increased in the 1960s when zeolite-based cracking catalysts started to be used (Sousa-Aguiar et al., 2013, Henriques, 2012). The main REE used in automotive catalysts are La, Ce and Nd.

**High field strength magnets:** NdFeB magnets constitute an important part of the global production of permanent magnets (Binnemans, 2015). Permanent magnets have a broad spectrum of uses, such as acoustic transducers, motors and generators, magneto mechanical devices and imaging systems. They are also used in amplifiers, loudspeakers, smartphones and other communication technologies, as well as in magnetic refrigeration.

**Polishing:** REE are used in polishing powders to finish the surface of glass products and electrical components (display panels, flat glass, optical glass etc), and can be also used in jewellery to polish precious metals. CeO<sub>2</sub> is the most used compound for this purpose (GEUS, 2017).

**Metallurgy:** REEs are employed in the construction and automotive sectors (in hybrid electric vehicles and electric vehicles), in portable electronics, fuel cell components, aircraft manufacture and magnesium alloys among others.

**Batteries:** REE are used in the anode formulation of rechargeable batteries, typically NiMH batteries. Lanthanum is the most employed REE in NiMH batteries, followed by Ce, Pr and Nd.

**Glass:** REE can be used as colouring agents, protective agents against different types of radiation or to remove impurities from glass (decolouring agents). For example, Ce is used as a glass stabilizer or as a decolouring agent to remove natural impurities present in glass.

**Ceramics:** REE are essential raw materials in the manufacturing of refractories, electronic ceramics and engineering ceramics. In this sector, the most important REE are La, Ce, Nd and Pr.

**Phosphors:** REE are used as doping elements or activators, whereas REE-pigments are used to stain ceramic tiles and to convey colours or improve the finish of ceramic glazes (Ronda et al., 1998, Nazarov and Noh, 2010, Rapaport et al., 2006, Ye et al., 2010).

Other applications of REE include those like laser or microwave crystals, nuclear applications, textile additives, medical applications, fertilizers and other<sup>1</sup>.

---

1. Source: GEUS and D'Appolonia, 2017, *Road map for REE material supply autonomy in Europe*.

## 2.3 Technologies for REE Extraction and Separation

Before the advent of industrial scale solvent extraction in the 1960s, ion exchange was the only practical way to separate REE in large quantities (Xie et al., 2014, Kumar, 1994, Reddy et al., 1992). Ion exchange methods were first developed to remove U and Th from the REE, and then to separate the REE. The method allowed the separation of REE into high purity metal fractions in a single operation. The disadvantages of the method were its long duration and the need for discontinuity. Nowadays this technology is only used for separation of small quantities of REE to a high degree of purity (Taniguchi and Doty, 1989).

Currently, solvent extraction is the most extensively used technology for REE separation. In hydrometallurgy, solvent extraction is the process of extraction of a metal from an aqueous phase into an immiscible organic phase, where the selectivity of the process for a particular metal arises from the interaction between the metal and the solvent (Thakur, 2000). Solvent extraction offers good separation factors and the possibility to treat large quantities. However, it is associated with a number of environmental issues due to the large volumes of organic solvents used (Sheldon, 2012, Dunn, 2012, Ghernaout et al., 2011, Capello et al., 2007). A typical solvent extraction plant has a multitude of mixer-settlers (also known as batteries), which require a high initial capital investment, and a conventional process requires several sequential steps to obtain an individual REE product.

Ionic liquids have been presented as a greener alternative to conventional organic solvents. According to some solvent selection guides available in the literature, ionic liquids are amongst the most desired solvents to use (Capello et al., 2007, Slater and Savelski, 2007). Ionic liquids are salts that are liquid below 100°C and due to their low flammability and volatility along with their recyclability, are considered green solvents. Nevertheless, the substitution of conventional organic solvents for ionic liquids can translate into higher costs, and the toxicity and environmental impact of some of the conventional ionic liquids, e.g. fluorinated ionic liquids, is not yet fully understood and can be potentially harmful (Ghandi, 2014, Dietz, 2006). Within the EURARE project, an ionic liquid extraction and separation technology was investigated, making use of a non-fluorinated ionic liquid (Larsson and Binnemans, 2015, Larsson and Binnemans, 2017).

In February 2016, Ucore Rare Metals (Ucore) and IBC Advanced stage technologies Inc., released a white paper on a highly selective green chemistry procedure based on molecular recognition technology (MRT) that has been applied for the separation of individual REE at >99% purity levels from pregnant leach solutions (Izatt et al., 2016). However, the process makes use of crown

ethers, which are rather expensive and hazardous (Carey and Sundberg, 2007, Mohapatra et al., 2009).

Our approach aims to avoid all or most of the issues presented above, making use of solid inorganic adsorbents in the nanoscale with specific ligands. The technology resembles the MRT technology, which can achieve much greater selectivity than solvent extraction or ionic exchange with considerably fewer steps in the process (Izatt et al., 2000, Ariga et al., 2012). However, our aim is to use more easily accessible complexonates that entail minimal hazards to humans and the environment, such as amino carboxylic acids, which are frequently used in medicine for magnetic resonance imaging (MRI). The nanoadsorbents developed are silica ( $\text{SiO}_2$ ) based magnetic and non-magnetic nanoparticles (NPs). The magnetic  $\text{SiO}_2$  NPs consist of a core of magnetic iron oxide NPs covered by a layer of  $\text{SiO}_2$  that not only protects the iron oxide core from leaching, but also allows functionalization of the surface. This type of nanoadsorbents will be described in more detail in the following sections, together with an explanation of why they are optimal for REE extraction and separation.

## 2.4 Silica ( $\text{SiO}_2$ ) nanoparticles.

Silica is a basic raw material that is widely used in many fields, for example as a food additive, excipient in drugs and vitamins, filler for paints and rubber ceramics and lubricant, as well as in electronics and medical devices such as silicon implants. Silica is indeed widespread and abundant, and while there are dangers with the inhalation of crystalline silica, there are many other forms of silica in nature that entail no toxicity (Martin, 2007).

At the nanoscale,  $\text{SiO}_2$  NPs exhibit a much higher surface area than the bulk material, and therefore has significant potential as a high performance sorbent material.  $\text{SiO}_2$  NPs have been widely studied as adsorbents of different compounds such as heavy metals, dyes and lanthanides (Arce et al., 2015, He et al., 2015, Dutta et al., 2015, Shiri-Yekta et al., 2013, Yurchenko et al., 2012, Melnyk et al., 2012, Dudarko et al., 2008, Renu et al., 2017).  $\text{SiO}_2$  NPs have also been investigated and applied in biomedical applications, drug delivery systems and so on (Popat et al., 2011, Davis, 2002, Bitar et al., 2012)

There are quite a number of methods to synthesize  $\text{SiO}_2$  NPs, namely micro emulsion processing, chemical vapour deposition, combustion synthesis, hydrothermal techniques, plasma synthesis, sol-gel processes etc. (Nagao et al., 2004, Vemury et al., 2011, Tani et al., 2003, Singh et al., 2014). Among all the methods used, the eminent and broadly studied Stöber method (Stöber et al.,

1968) is known to lead to silica nanoparticles with a narrow size distribution. The reaction parameters can also be adapted to obtain particles of the desired size. Stöber synthesis of SiO<sub>2</sub> NPs is based on the ammonia-catalyzed hydrolysis of a silica precursor, typically tetraethyl orthosilicate (TEOS), in ethanol media. When using this method for synthesis of SiO<sub>2</sub> NPs, the resulting NPs retain silanol (Si-OH) groups on their surface, which is very beneficial for their further functionalization. This is a very important asset for our purpose, since the goal is to identify specific ligands for REE and attach them on the surface of the nanoadsorbents, creating thus hybrid nanoadsorbents.

Nevertheless, if SiO<sub>2</sub> NPs were to be applied industrially for separation of REE, the most feasible way to separate them from solution would be via centrifugation, and this can involve high costs or high initial investments in equipment. Therefore, the idea of a material that can combine the advantageous adsorption properties of SiO<sub>2</sub> NPs with the easy removal from solution characteristic of magnetic NPs becomes of great interest. This is possible using core-shell magnetic SiO<sub>2</sub> NPs, consisting of a magnetic iron oxide core and a covering silica layer.

## 2.5 Magnetic Iron Oxide nanoparticles.

Magnetic nanoparticles (MNPs) possess many interesting properties for diverse applications in fields such as catalysis (Cornell and Schwertmann, 2003, Azhar Uddin et al., 2008, Li et al., 2008, Shi et al., 2007, Zhang et al., 2007, Wang and Willey, 1998, Al-Sayari et al., 2007, Wang and Davis, 1999, Bautista et al., 2007), biomedical applications including immunoassays, magnetic resonance imaging contrast agents, targeted drug delivery vehicles and magnetic hyperthermia among others (Tartaj et al., 2003, Jurgons et al., 2006, Qiang et al., 2006, Xu et al., 2006, Lübbe et al., 1999, Zheng et al., 2006, Ai et al., 2005, Gonzales and Krishnan, 2005, Lee et al., 2005, Sadeghiani et al., 2005), data storage (Reiss and Hutten, 2005) or environmental protection applications such as wastewater treatment (Jiang et al., 2011, Nassar, 2010).

### 2.5.1 Iron oxides and magnetic nanoparticles.

Iron oxides are common compounds in nature. There are fourteen known iron oxides or sixteen including iron hydroxides (often included in the iron oxides family). Magnetite ( $\text{Fe}_3\text{O}_4$ ), maghemite ( $\gamma\text{-Fe}_2\text{O}_3$ ) and hematite ( $\alpha\text{-Fe}_2\text{O}_3$ ) are the most common phases of iron oxide (Cornell and Schwertmann, 2003).

Hematite does not exhibit magnetic properties, whereas magnetite possesses the strongest magnetism of any transition metal oxide (Majewski and Thierry, 2007, Cornell and Schwertmann, 2003). Maghemite has a crystal structure similar to that of magnetite but without Fe (II), and it forms continuous solid solutions with magnetite (Majewski, 2008). Magnetite and maghemite can be transformed one into another via redox reactions.

Magnetic iron oxides (magnetite and maghemite) contain Fe (III) in a spinel structure occupying octahedral spaces between densely packed oxide anions.

In a bulk ferromagnetic material, the magnetization vector  $M$  is the sum of all the magnetic moments of the atoms in the material per unit volume of the material. The bulk is constituted by domains, having each domain its own magnetization vector. The magnetization moments of all the domains might not be aligned and this can result in a decrease in the overall magnetic properties of the material. But when we go down to the nanoscale, the number of domains decreases until the size of the material is below a critical size  $d_c$ , in which case there is one single domain (Teja and Koh, 2009). A single magnetic domain has no hysteresis loop and is said to be superparamagnetic. Hence, iron oxide nanoparticles below 20 nm often have superparamagnetic behaviour at room temperature (Cornell and Schwertmann, 2003).

Magnetite nanoparticles exhibit the most interesting magnetic properties, but they are not the most stable in the nanoscale and can be easily transformed into maghemite by oxidation. This oxidation to maghemite carries along a loss of some magnetic properties, but nanoscale maghemite retain enough magnetization for the desired purpose.

## 2.5.2 Iron oxide MNPs as nanoadsorbents for REE extraction and separation.

As it has already been mentioned, the main advantages of magnetic iron oxide NPs for REE adsorption arise from their magnetism, which makes possible a facile separation of the solid nanoadsorbents from the solution, just via application of an external magnetic field (Shen et al., 2009).

Iron oxide MNPs require simple equipment, offer facile operation and high efficiency and they have high potential for restoration and reusability (Shahriari et al., 2014). Moreover, they are feasible for industrial upscaling in economic terms and have good stability and very low toxicity compared to other counterpart ions (Soenen et al., 2012, Wilkinson et al., 2012).

One factor to consider is the fact that iron oxide MNP are usually unstable under harsh conditions (such as acid media). In the REE extraction and separation process, release of REE is usually aided by washing with acid solutions, therefore it is necessary to stabilize MNPs against iron leaching via deposition of a protecting layer. Synthesis of core-shell MNPs is a good solution for this issue, and among diverse types of coating materials (including noble metals, metal oxides and polymer materials), silica coating presents many advantages. As a protecting agent, silica is highly stable in aqueous solutions, prevents direct contact of the iron oxide core with external agents and enhances the biocompatibility, hydrophilicity and dielectric properties of the NPs (Stjerndahl et al., 2008, Im et al., 2005, Lu et al., 2007a). But what is even more interesting and has already been mentioned in section 2.4, a silica coating allows further functionalization of the NPs thanks to the  $-\text{SiOH}$  groups on the surface. The silanol groups can be functionalized with amino, thiol and carboxyl group among others, leading to functionalized nanoadsorbents useful in bio-labeling, drug delivery and adsorption applications (Gupta and Gupta, 2005, Lu et al., 2007b). There are a few methods known to produce core-shell silica coated MNPs, microemulsion and alkaline hydrolysis of TEOS are the major ones (Santra et al., 2001, Stöber et al., 1968, Abbas et al., 2014). The latter is known to lead to uniform spherical colloidal nanoparticles of tuneable sizes, and therefore was the method chosen in this work.

A previous study has shown by X-ray absorption near edge structure (XANES) spectroscopy that encapsulation of magnetite MNP leads to oxidation from magnetite to maghemite with the consequent partial loss of magnetic properties. Nevertheless, the magnetic measurements showed that the material keeps a magnetic susceptibility of about 6 emu/g, which is competitive for the industrial requirements of magnetic separation (Pogorilyi et al., 2014). This depends of course of the thickness of the silica layer, given that the thicker the

layer of silica, the longer the encapsulation process is and therefore higher degree of oxidation to maghemite and stronger dilution by a non-magnetic phase. The process must be optimized to obtain a silica layer that can protect the MNP without hindering their unique magnetic properties.

Adsorption of pollutants (especially heavy metals) by iron oxide MNPs has been extensively studied, including, among others, oil refinery wastewater treatment (Rasheed et al., 2011), paper mill wastewater treatment (Zhang et al., 2011), colour removal from water (Absalan et al., 2011, Iram et al., 2010), methylene blue removal from aquatic environments (Rakhshae and Panahandeh, 2011), reduction of polybrominated diphenyl ethers (Fang et al., 2011a), adsorption of cadmium from aquatic environments (Chen et al., 2011, Tu et al., 2012), copper and chromium (VI) removal from electroplating wastewater (Fang et al., 2011b), removal of nickel, cadmium and lead ions from water (Badruddoza et al., 2013), decontamination of medical samples (Melnyk and Zub, 2012) and removal of chromium (III) (Shahriari et al., 2014).

In recent years, a number of investigations have been carried out regarding adsorption of REE by functionalized magnetic silica based nanoadsorbents (Dudarko et al., 2008, Almeida and Toma, 2016, Condomitti et al., 2012, Zhang et al., 2016). However, to the best of our knowledge, no work has aimed at addressing the mechanism behind the interactions of REE and the specific ligands, which are necessary to understand in order to control the process and develop a competitive technology for the extraction and separation of REE. This technology must be grounded and understood at the lab scale, but easily applicable and efficient at industrial scale.

## 3 Silica (SiO<sub>2</sub>) and magnetic SiO<sub>2</sub> nanoparticles

### 3.1 Synthesis of SiO<sub>2</sub> nanoparticles.

Several methods are reported in literature for the synthesis of SiO<sub>2</sub> NPs, namely chemical vapour condensation, arc discharge, micro-emulsion, hydrothermal methods, sol-gel, etc. Among these, the Stöber method (Stöber et al., 1968) is a sol-gel method that is considered one of the simplest and most effective ones, leading to spherical silica nanoparticles with a narrow size-dispersion. This synthetic method has been widely used and studied since it allows to easily perform modifications of the reaction parameters controlling the desired size. Therefore, it was the method of choice in this work for the synthesis of the raw materials, that is, magnetic and non-magnetic nanoadsorbents. Stöber process is based on the hydrolysis of a silica precursor (typically tetraethylorthosilicate –TEOS-) in an alcoholic solution and in presence of ammonia as catalyst. The effect of the reaction parameters on the size of SiO<sub>2</sub> NPs obtained by this method was studied, given that the particle size is a determinant factor in adsorption processes. The smaller the nanoparticles the larger is surface area available to attach specific organic ligands, but when the particles become too small they can be difficult to handle and use as adsorbents. For our purpose we set the target particle size between 60-100 nm, therefore, several different concentration and temperature conditions were tested. Table 2 shows two of the synthesis conducted, the first one leading to relatively large NPs and the second one leading to the optimal average size of 80 nm.

Table 2. Reaction parameters of two different synthetic routes for SiO<sub>2</sub> nanoparticles.

Synthesis	H <sub>2</sub> O	EtOH	[NH <sub>4</sub> OH]	[TEOS]	Temp.	Reaction time (h.)	Particle size
I	-	40 mL	6.75 M	0.29 M	25°C	2	600 nm
II	9.5 M	200 mL	0.5 M	0.25 M	65°C	1	80 nm

Figure 5 shows transmission electron microscopy (TEM) images of the SiO<sub>2</sub> nanoparticles obtained with the synthesis designated as II. The figure shows that the particles are indeed spherical and quite narrowly dispersed in size as can be seen in the size distribution histograms.

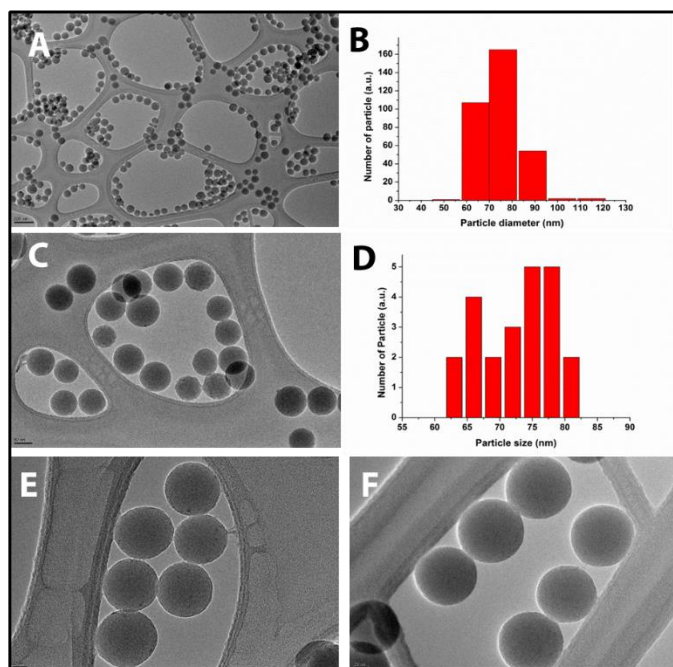


Figure 5. HR-TEM images of SiO<sub>2</sub> nanoparticles (scale bar is 200, 50 and 20 nm for **a**, **c** and **e**, **f**, respectively). **b** and **d** are size distribution histograms of **a** and **c** images, respectively.

### 3.2 Synthesis of magnetic SiO<sub>2</sub> nanoparticles ( $\gamma$ -Fe<sub>2</sub>O<sub>3</sub>-SiO<sub>2</sub> core-shell magnetic nanoparticles –MNPs-).

A modified Stöber method (Abbas et al., 2014) was followed for the encapsulation of magnetic iron oxide MNP into a protective layer of SiO<sub>2</sub>. Fe<sub>3</sub>O<sub>4</sub> nanoparticles have been previously synthesized via the well-known coprecipitation of iron (II) and iron (III) (Martínez-Mera et al., 2007, Qiu et al., 2005). The effect of the thickness of the silica shell on the protection of the iron oxide core against leaching and loss of magnetic properties had been investigated in our group previously by R. Pogorilyi et al (Pogorilyi et al., 2014). A silica layer of approximately 25 nm in thickness proved to be optimal in order to protect the iron core yet keeping their magnetic properties (Figure 7). Particles with an average diameter of 100 nm were produced in this work (see Figure 6). Their stability under acidic conditions was tested with a solution of 0.1M HNO<sub>3</sub> containing 0.5% KSCN, and they were found to be stable for years, without any observable iron leaching.

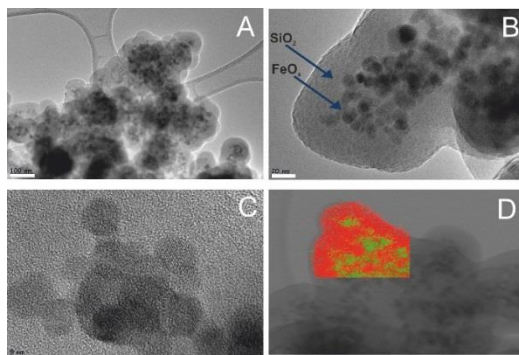


Figure 6. HR-TEM images of  $\gamma$ -Fe<sub>2</sub>O<sub>3</sub>-SiO<sub>2</sub> nanoparticles (the scale bar is 100, 20 and 5 nm in A, B and C respectively. D is the EF-TEM mapping image).

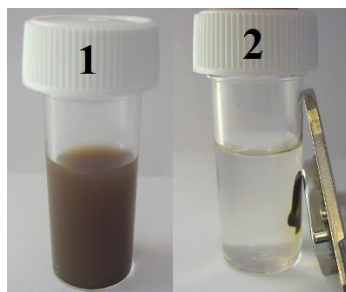


Figure 7. Core-shell  $\gamma$ -Fe<sub>2</sub>O<sub>3</sub>-SiO<sub>2</sub> NPs: 1) dispersed in ethanol ; 2) retracted by a magnet.



## 4 Organosilane derivatives: Synthesis and applications as selective ligands on hybrid nanoadsorbents (Papers I&II)

### 4.1 Background

Silica based nanoadsorbents offer great opportunities for surface functionalization, the silanol groups present on the surface allow easy grafting of organosilanes. An organosilane is a monomeric silicon chemical (silane) that contains at least one carbon-silicon bond (Si-C) in its structure (Materne, 2004). Organosilanes contain both organic and inorganic reactivity in the same molecule, and therefore can be applied in the development of hybrid materials. These organic molecules can be tailored for different purposes with specific functional groups. The first work focused on the synthesis of organosilane derivatives with carboxylic and amine functional groups, initially meant for the chelation of REE, and their attachment onto the surface of SiO<sub>2</sub> nanoparticles. The resulting hybrid nanoadsorbents possess interesting REE adsorption and luminescence detection properties. The following work focused on the organosilane derivative that showed to be the most efficient and tested it on magnetic  $\gamma$ -Fe<sub>2</sub>O<sub>3</sub>-SiO<sub>2</sub> NPs. The selectivity of this specific ligand toward different groups of REE was studied and structural studies of molecular model compounds were carried out to understand the observed selectivity.

## 4.2 Synthesis of organosilane derivatives (Paper I)

Three different organosilane derivatives denoted as **L1**, **L2** and **L3**, were synthesized according to the synthetic routes schematized in Figure 8. The choice of ligands with carboxylic acid and amine groups was based on the idea that these functional groups would take part in the chelation with REE. Ligand 1 and Ligand 3 bear an iminodiacetic acid (IDA) fragment, which offers attractive coordination potential with REE through the carboxylic groups. L1 showed afterwards poor stability properties, which is the reason why we did not proceed further on adsorption studies with this material, while L3 showed much better stability due to the fact that the imino function of IDA is attached to the silica surface via an alkyl group, which is chemically more stable than the urea-based group in L1. On the other hand, the pyridine ring present in L2, offers potentially good stability towards radioactivity, which is very beneficial when working with REE, since they often appear together with radioactive elements in nature. L1 was synthesized from the reaction between 3-isocyanatopropyltriethoxysilane (ICPTES) and dimethyl iminodiacetate in chloroform at 80°C. L2 and L3 were synthesized following previously reported synthetic routes (Claramunt et al., 2005, Franville et al., 1998).

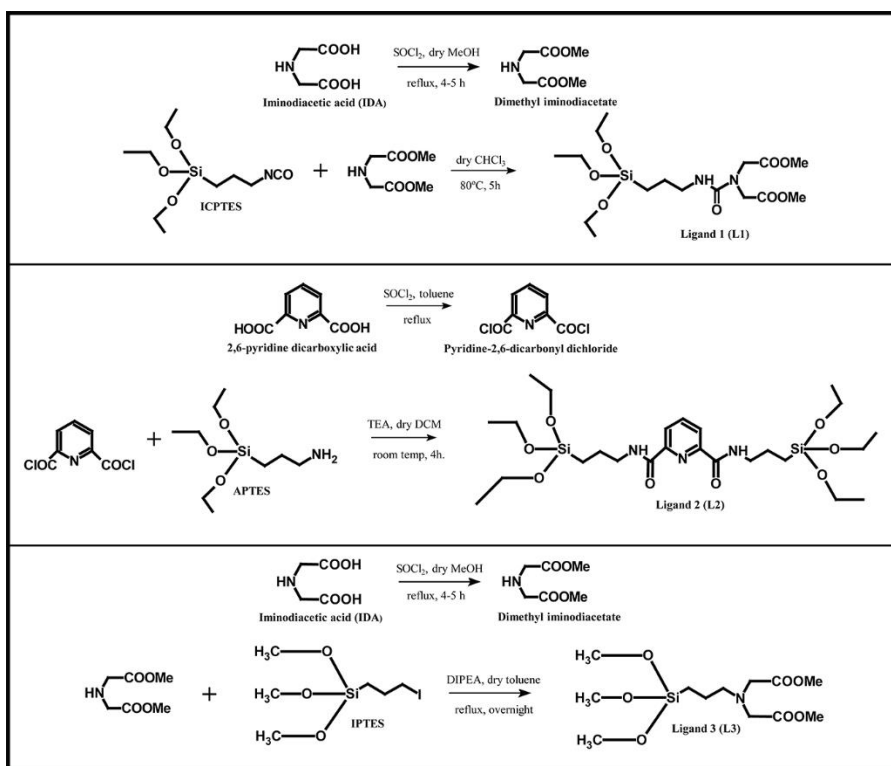


Figure 8. Synthetic pathway for the three organosilane derivatives.

### 4.3 Synthesis of organic ligand grafted magnetic and non-magnetic SiO<sub>2</sub> NPs

The synthesized SiO<sub>2</sub> and magnetic SiO<sub>2</sub> NPs were functionalized by the synthesized organosilane derivatives. For this, the amount of ligand that can fit on the NPs surface was estimated, knowing the active surface area of the silica substrate and the space required for the attachment of a single siloxane group. In practice, an excess of this calculated amount was used in order to guarantee full reaction. All of the reactions were carried out using dry toluene as solvent. The magnetic SiO<sub>2</sub> NPs were functionalized with only the third organosilane (L3), since it proved in the previous study with SiO<sub>2</sub> NPs to be the most stable and efficient, as it will be described in section 4.7.

### 4.4 Nuclear magnetic resonance (NMR) spectroscopy

#### 4.4.1 Solution <sup>1</sup>H-NMR and <sup>13</sup>C-NMR spectroscopy (Paper I)

Solution NMR spectroscopy is a powerful technique in organic chemistry for confirming the efficiency and purity of a synthesis, and therefore was used in this work to verify the successful synthesis of the organosilanes. NMR spectroscopy is based on the fact that some atomic nuclei possess a magnetic moment ( $\mu$ ) and an angular momentum ( $P$ ), i.e. a non-zero spin. All nuclei with an odd mass or atomic number have non-zero spin and are therefore NMR active. When the nuclei are subjected to a magnetic field, they absorb electromagnetic radiation and the excess energy is dissipated, producing then an observable signal. This energy is at a specific resonance frequency, which depends on the applied static magnetic field, the type of nuclei and the chemical environment of the nuclei. The variations of nuclear magnetic resonance frequencies of the same type of nucleus, due to variations in the electron distribution, are called chemical shifts, and are often diagnostic of the structure of a molecule (Silverstein et al., 2014, Balci, 2005). The chemical shift is given with respect to a reference frequency, usually a molecule with a barely distorted electron distribution. For <sup>1</sup>H, <sup>13</sup>C and <sup>29</sup>Si nuclei, the internal reference often used is tetramethylsilane (TMS).

The spectra of the final products and the intermediates were recorded on a Bruker Avance spectrometer, at 25°C, operating at 600 MHz for  $^1\text{H}$ -NMR and 150 MHz for  $^{13}\text{C}$ -NMR. The solvent used was  $\text{CDCl}_3$  and TMS as internal standard<sup>2</sup>.

#### 4.4.2 Solid state $^{29}\text{Si}$ and $^{13}\text{C}$ -NMR spectroscopy (Paper I)

Solid state NMR is a type of NMR where the experimental sample is contained in a media with little or no mobility (such as crystalline or powder state, membrane-bound system or aligned solutions). In solution NMR, the spectra consist of a series of very sharp transitions, due to the averaging of anisotropic NMR interactions by rapid random tumbling. However, solid-state NMR spectra are very broad, as the full effects of anisotropic, or orientation-dependent interactions, are observed in the spectrum. High-resolution solid state NMR spectra can provide the same type of information than the corresponding solution NMR spectra, but some special techniques and equipment are needed, such as magic-angle spinning (MAS), cross polarization (CP), enhanced probe electronics etc. The technique was used in order to confirm the grafting of organosilanes onto the surface of the NPs. For technical reasons, the analysis was carried out on non-magnetic  $\text{SiO}_2$  NPs and the results were used as a model for magnetic nanoadsorbents in the further study. Solid state  $^{13}\text{C}$  and  $^{29}\text{Si}$  CP-MAS NMR spectra of the functionalized NPs were recorded at the Aveiro Institute of Materials, CICECO, University of Aveiro (Portugal) in a Bruker Avance III 400 (9.4 T) spectrometer. Figure 9 shows the spectra for  $\text{SiO}_2$  NPs functionalized with the three synthesized organosilanes. On the left of the image, the  $^{13}\text{C}$  CP-MAS NMR spectra is shown, followed by the structure of the corresponding organosilane used, with tags a-g appointing all carbon atoms (identified in the spectrum with the letter). The right part shows the  $^{29}\text{Si}$  CP-MAS spectra of the NPs. All the characteristic carbon atoms could be identified in the  $^{13}\text{C}$  CP-MAS spectra, which gives strong proof of the effective chemical bonding between the synthesized organosilanes and the  $\text{SiO}_2$  NPs.

Furthermore, the  $^{29}\text{Si}$  CP-MAS spectra showed several peaks that can be assigned to Qn and Tn local environments of silica,  $\text{Si}(\text{OH})_{(4-n)}$ ,  $(\text{OSi})_n$  and  $\text{RSi}(\text{OH})_{(3-n)}(\text{OSi})_n$  (Peng et al., 2005, Sharma and Sharma, 2014). Figure 10 shows the different Qn and Tn type of Si local environments.

---

2. The NMR spectra are provided in Supplementary of Paper I.

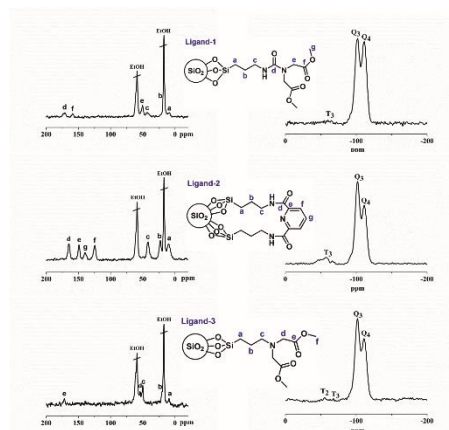


Figure 9.  $^{13}\text{C}$  CP-MAS NMR and  $^{29}\text{Si}$  CP-MAS NMR spectra of  $\text{SiO}_2$  NPs functionalized with organosilanes.

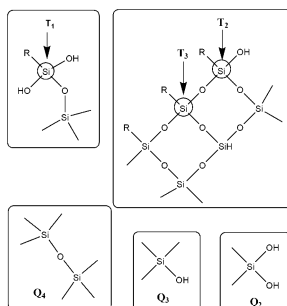


Figure 10.  $Q_n$  type ( $Q_4$ ,  $Q_3$ ,  $Q_2$ ) and  $T_n$  type ( $T_3$ ,  $T_2$ ,  $T_1$ ) Si local environments.

## 4.5 Fourier-transform infrared spectroscopy (FTIR)

Infrared spectroscopy (IR spectroscopy) involves the interaction of infrared radiation with matter. Infrared radiation refers broadly to that part of the electromagnetic spectrum between the visible and microwave regions (Silverstein et al., 2014). IR spectroscopy exploits the fact that molecules absorb radiation at frequencies that are characteristic of their structure. Different functional groups give rise to characteristic bands, both in terms of intensity and position (frequency). FTIR is a type of absorption spectroscopy technique in which the spectrometer collects high-spectral-resolution data over a wide spectral range, unlike dispersive spectrometers, where intensity is measured over a narrow range of wavelengths at a time. The term *Fourier transform* comes from the fact that the mathematical operation Fourier transform is needed to

convert the spectrum from intensity vs. time into an intensity vs. frequency spectrum.

FTIR provides an easy way to identify the presence of certain functional groups in a molecule, and there comes its importance in this work to confirm the efficient attachment of the organic molecules (organosilanes) onto the surface of the nanoadsorbents.

#### 4.5.1 Functionalized SiO<sub>2</sub> NPs (Paper I)

Figure 11 shows the obtained FTIR spectra. The A series shows the spectra of SiO<sub>2</sub> NPs and SiO<sub>2</sub> NPs functionalized with each of the three organosilanes, while the B series shows spectra comparing functionalized SiO<sub>2</sub> NPs and the same particles bearing REE (Dy<sup>3+</sup> or Nd<sup>3+</sup>) cations. Several characteristic peaks could be identified in each spectrum, supporting the conclusion that the organosilanes were successfully attached onto the surface of the SiO<sub>2</sub> NPs. All this information is summarized in Table 3.

Table 3. Summary of the FTIR spectra of SiO<sub>2</sub> and functionalized SiO<sub>2</sub> NPs

Sample	Absorption peak location (cm <sup>-1</sup> )	Peak identification
SiO <sub>2</sub> NPs	1100 (saturated)	ν <sub>as</sub> (Si-O-Si)
	956	ν <sub>as</sub> (Si-OH)
	800	ν(Si-O-Si)
	464	δ(Si-O-Si)
SiO <sub>2</sub> -L1	1702	ν(C=O)
	1635	ν(C=O)
	1448	δ(N-H)
SiO <sub>2</sub> -L2	1664	ν(C=O)
	1546	ν(C=C)
	1448	δ(C-N-H)
SiO <sub>2</sub> -L3	1748	ν(C=O)

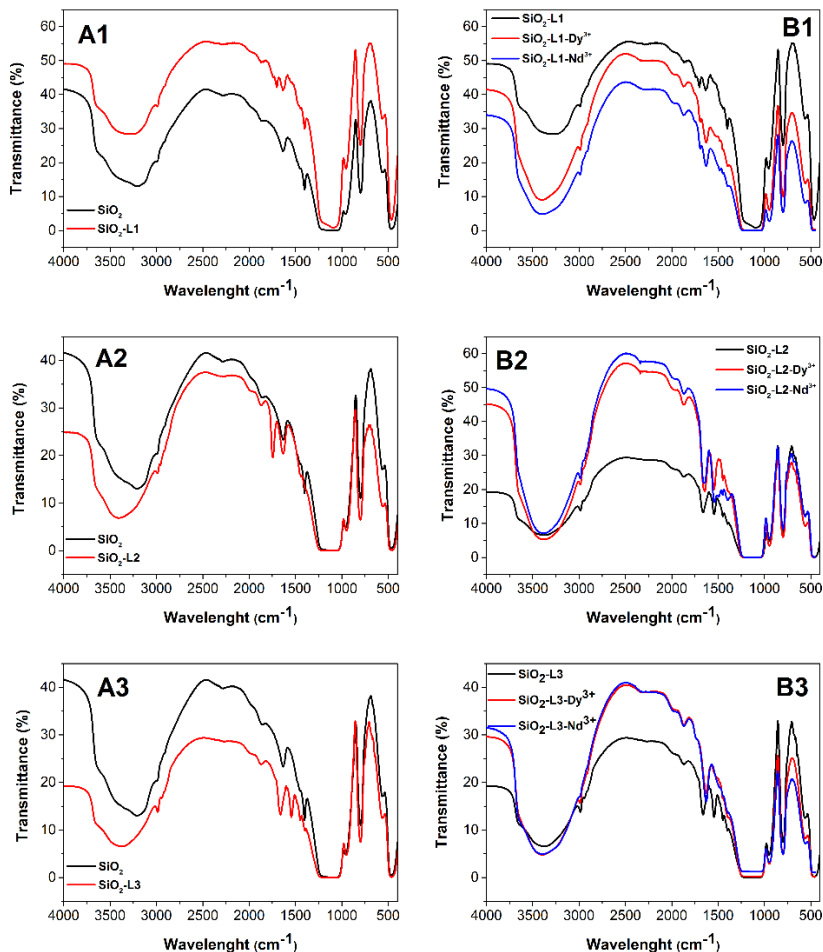


Figure 11. FTIR spectra of SiO<sub>2</sub> and functionalized SiO<sub>2</sub> NPs (A series) and functionalized SiO<sub>2</sub> NPs with and without adsorbed RE<sup>3+</sup> cations (B series).

It is noteworthy that REE adsorption by the nanoadsorbents leads to a shift in the  $\nu(\text{C}=\text{O})$  bands to lower frequencies, as a result of the coordination between the carboxylic group and REE cations.

#### 4.5.2 Functionalized magnetic $\gamma$ -Fe<sub>2</sub>O<sub>3</sub>-SiO<sub>2</sub> MNPs (Paper II)

Figure 12 shows the spectra of the initial Fe<sub>3</sub>O<sub>4</sub> magnetite NPs, the synthesized SiO<sub>2</sub> MNP and these MNPs functionalized with the organosilane designated as L3. The right spectra shows the comparison between the functionalized MNP with and without adsorbed REE cations. The characteristic identified bands, which again give proof of the successful functionalization of the MNPs, are summarized in Table 4.

Table 4. Summary of the FTIR spectra of Fe<sub>3</sub>O<sub>4</sub>,  $\gamma$ -Fe<sub>2</sub>O<sub>3</sub>-SiO<sub>2</sub> and functionalized  $\gamma$ -Fe<sub>2</sub>O<sub>3</sub>-SiO<sub>2</sub> NPs.

Sample	Absorption peak location (cm <sup>-1</sup> )	Peak identification
Fe <sub>3</sub> O <sub>4</sub>	3400	$\nu$ (O-H)
	570	$\nu$ (Fe-O)
	470	$\nu_{as}$ (Fe-O)
$\gamma$ -Fe <sub>2</sub> O <sub>3</sub> -SiO <sub>2</sub>	3400	$\nu$ (O-H)
	1090	$\nu_{as}$ (Si-O-Si)
	950	$\nu$ (Si-OH)
	800	$\nu$ (Si-O-Si)
	460	$\delta$ (Si-O-Si) -overlaps with $\nu_{as}$ (Fe-O)
	570	$\nu$ (Fe-O)
	470	$\nu_{as}$ (Fe-O)
$\gamma$ -Fe <sub>2</sub> O <sub>3</sub> -SiO <sub>2</sub> -L3	3400	$\nu$ (O-H)
	1740	$\nu$ (C=O)
	1630	$\delta$ (O-H)
	1090 (saturated)	$\nu_{as}$ (Si-O-Si)
	950	$\nu$ (Si-OH)
	800	$\nu$ (Si-O-Si)
	460	$\delta$ (Si-O-Si) -overlaps with $\nu_{as}$ (Fe-O)
	570	$\nu$ (Fe-O)
	470	$\nu_{as}$ (Fe-O)

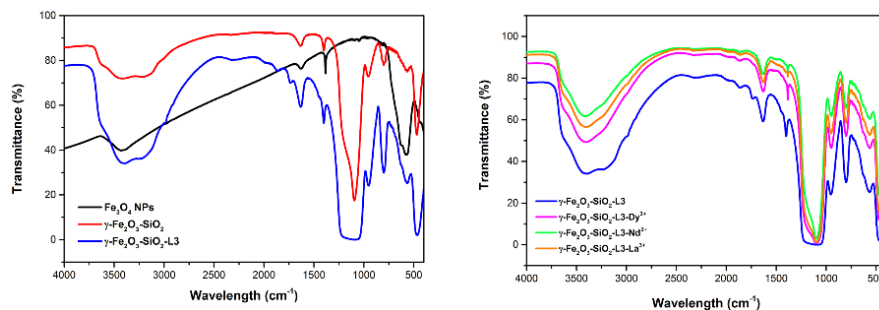


Figure 12. FTIR spectra of  $\text{Fe}_3\text{O}_4$ ,  $\gamma\text{-Fe}_2\text{O}_3\text{-SiO}_2$  and functionalized  $\gamma\text{-Fe}_2\text{O}_3\text{-SiO}_2$  (left) and comparison between functionalized  $\gamma\text{-Fe}_2\text{O}_3\text{-SiO}_2$  with and without adsorbed  $\text{RE}^{3+}$  cations (right).

As described in the previous section, it can be seen that the adsorption of REE cations by the nanoadsorbents leads to a shift in the  $\nu(\text{C}=\text{O})$  absorption band to lower frequencies, giving proof of the coordination between this functional group and the cations.

#### 4.6 Thermo-gravimetric analysis (TGA).

TGA is a method of thermal analysis in which the mass of a sample is measured over time as the temperature changes. This technique can be used to evaluate the thermal stability of a material, and it also can provide information about physical and chemical properties. In this work, TGA was used to quantify the amount of organic ligand grafted onto a specific nanoadsorbent. Monitoring the mass change in a functionalized nanoadsorbent as the temperature gradually increases allows quantification the amount of organic matter that has decomposed and thus the amount of organic ligand originally contained in the sample. The TG analyses were performed on functionalized magnetic and non-magnetic nanoadsorbents, in the range from 25 to 600°C at a heating rate of 5°C/min.

The first step of loss corresponds to water molecules and other remaining solvents from reaction (ethanol, toluene) and occurs until approximately 200°C. Decomposition and carbonization of organic matter usually occurs between 200-600 °C and above 600°C, the residual carbon burns out. Table 5 summarizes the amount of organic ligands grafted on different nanoadsorbents.

Table 5. Quantification of organic ligand grafting on different nanoadsorbents.

Sample	Amount of ligand grafted (weight %)
SiO <sub>2</sub> -L1	6.4
SiO <sub>2</sub> -L2	9.2
SiO <sub>2</sub> -L3	6.8
$\gamma$ -Fe <sub>2</sub> O <sub>3</sub> -SiO <sub>2</sub> -L3	5.6

## 4.7 REE uptake and release studies on magnetic and non-magnetic nanoadsorbents

### 4.7.1 Adsorption studies. Kinetic curves.

The REE adsorption efficiency of both magnetic and non-magnetic functionalized nanoadsorbents was tested. For this, a defined amount of the nanoadsorbents was put in contact with a calculated amount of REE(NO<sub>3</sub>)<sub>3</sub> corresponding to twice the amount of organic ligand grafted onto their surface (this information can be inferred from TGA analyses). Chelation between REE and the ligands would occur in a 1 : 1 molar ratio, therefore this amount was doubled to ensure full reaction. After addition of NaNO<sub>3</sub> in order to keep the ionic strength constant, the mixtures were shaken on an orbital shaker for different times (from 2 to 48 hours).

The amount of REE taken up by the adsorbent was determined by complexometric titration of REE in the mother liquor solutions. This method, although less automatized than others often used, such as inductively coupled plasma (ICP) or X-ray fluorescence (XRF), is very sensitive and accurate. The titrant chosen was EDTA tetrasodium salt, as it forms complexes with RE trivalent cations in a 1:1 ratio. Thus, knowing the REE content in the initial solution and the REE amount remaining in the solution after adsorption, the amount adsorbed by the nanoadsorbents can be determined by subtraction.

Figure 13 shows the kinetic curves, fitted according to the Langmuir isotherm model, obtained for non-magnetic nanoadsorbents (functionalized SiO<sub>2</sub> NPs). A quick achievement of the equilibria can be observed, reaching over 75% of the total uptake in the first two hours. It is also observable that the nanoadsorbents functionalized with L3 are more efficient, showing 4 times higher uptake than the nanoadsorbents functionalized with L2. This is the main reason why L2 was not used in further studies with magnetic nanoadsorbents, since its capacity was

not high enough to compete with other commonly used techniques for adsorption of REE, such as ion-exchange resins (El-Sofany, 2008, Texier et al., 1999).

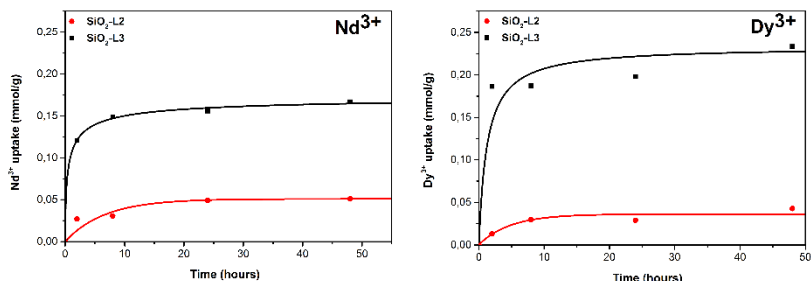


Figure 13. Kinetic curves of adsorption of  $\text{Dy}^{3+}$  and  $\text{Nd}^{3+}$  on functionalized  $\text{SiO}_2$  NPs.

The kinetic curves for magnetic  $\text{SiO}_2$  NPs functionalized with L3 (Figure 14) show as well a quick achievement of the adsorption equilibria, reaching over 65% of the total uptake in the first 2 hours. These magnetic nanoadsorbents proved to be very efficient for REE adsorption, specially for  $\text{Dy}^{3+}$ , with a maximum uptake of  $0.25 \text{ mmol Dy}^{3+}/\text{g}$ . The observed selectivity toward  $\text{Dy}^{3+}$  will be further studied and explained.

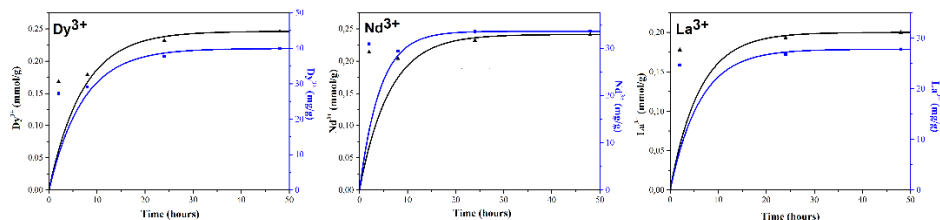


Figure 14. Kinetic curves of adsorption of  $\text{Dy}^{3+}$ ,  $\text{Nd}^{3+}$  and  $\text{La}^{3+}$  by magnetic  $\gamma\text{-Fe}_2\text{O}_3\text{-SiO}_2$  NPs functionalized with L3 ( $\text{mmol RE}^{3+}/\text{g}$  in black and  $\text{mg RE}^{3+}/\text{g}$  in blue).

#### 4.7.2 Desorption and selectivity studies.

Once the REE are adsorbed by the nanoadsorbents, it is crucial to be able to release them back into solution. The REE loaded nanoadsorbents were therefore treated with  $\text{HNO}_3$  1M for 24 hours. The amount of REE released to solution was then determined by complexometric titration (as previously described) after a prior step of neutralization by evaporation of the acid. Table 6 shows the percentage of REE released into solution for magnetic and non-magnetic

nanoadsorbents for different REE, displaying a highly efficient process, with more than 80% desorbed in all cases and well over 90% for most of them.

Table 6. *Desorption efficiency for different nanoadsorbents loaded with REE.*

<b>Sample</b>	<b>Percentage desorbed (%)</b>
SiO <sub>2</sub> -L3-Dy <sup>3+</sup>	83
SiO <sub>2</sub> -L3-Nd <sup>3+</sup>	93.1
γ-Fe <sub>2</sub> O <sub>3</sub> -SiO <sub>2</sub> -L3-Dy <sup>3+</sup>	91.3
γ-Fe <sub>2</sub> O <sub>3</sub> -SiO <sub>2</sub> -L3-Nd <sup>3+</sup>	98.4
γ-Fe <sub>2</sub> O <sub>3</sub> -SiO <sub>2</sub> -L3 La <sup>3+</sup>	93.9

In the case of magnetic nanoadsorbents, the kinetic curves showed quite distinct adsorption trends, with a higher capacity toward HREE. This suggested the possibility of selective adsorption in solutions with more than one REE present. Therefore, adsorption experiments on binary mixtures of REE were performed, followed by a desorption process that was tested at two different pH values. The obtained results are summarized in Table 7.

Table 7. *Selectivity in adsorption and desorption of REE by magnetic nanoadsorbents.*

	<b>Dy:Nd ratio</b>	<b>Dy:La ratio</b>
<b>Nanoadsorbent obtained after adsorption</b>	3.9 : 1	4.2 : 1
<b>Nanoadsorbent obtained after desorption at pH=3</b>	5.9 : 1	81 : 1
<b>Nanoadsorbent obtained after desorption at pH=1</b>	1.3 : 1	1.8 : 1
<b>Total uptake capacity (mmol RE<sup>3+</sup>/g)</b>	0.242	0.275

Desorption carried out under strong acidic conditions leads to total non-selective release of REE. However, less acidic conditions (pH=3) led to selective desorption, showing that the nanoadsorbents functionalized with L3 have clear preference toward Dy<sup>3+</sup>, especially in binary mixtures of La-Dy. The separation factors obtained are quite close to those reported in a parallel study by Binnemans and co-workers (Dupont et al., 2014).

## 4.8 Luminescence studies (Paper I)

The luminescence properties of the lanthanides are very well known and have been broadly studied (Anikina and Karyakin, 1964, Babai et al., 2014, Andres and Chauvin, 2011, Alammari et al., 2016, Bunzli et al., 2007). The luminescence of functionalized SiO<sub>2</sub> NPs bearing REE was first observed in a simple experiment, using UV-excitation. A common broad spectrum mercury lamp (Chromato-Vue Transilluminator TM-36) was used to excite SiO<sub>2</sub> NPs that had been spotted onto a TLC plate. These comprised SiO<sub>2</sub> NPs grafted with the three synthesized ligands and the same materials bearing Dy<sup>3+</sup> or Nd<sup>3+</sup>. In this test, the brightest spots were observed for SiO<sub>2</sub> NPs functionalized with L2, due to the pyridine ring present in its structure, and those with adsorbed Nd<sup>3+</sup>. The luminescence of Dy<sup>3+</sup> is in the green part of the spectrum, which may be difficult to observe over the background auto-luminescence from alumina in the TLC plates.

Photoluminescence studies were carried out at the National Institute for Laser, Plasma and Radiation Physics in Bucharest, Romania, using a Fluoromax 4 spectrofluorimeter (Horiba) operating in both fluorescence and phosphorescence modes. The spectral characterization (Figure 15) revealed that the better signal from SiO<sub>2</sub>-L2-Nd<sup>3+</sup> is caused exclusively by the luminescence of the ligand itself, which is apparently enhanced by complexation.

For Dy<sup>3+</sup> complexes on SiO<sub>2</sub> NPs, the data suggests a weak antenna sensitization for L1 and L2, but not for L3. The strongest emission was achieved for SiO<sub>2</sub>-L2-Dy<sup>3+</sup>.

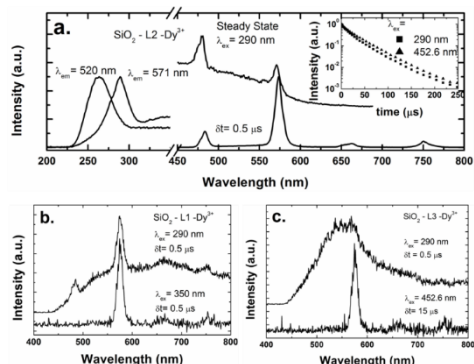


Figure 15. Photoluminescence spectra of a) SiO<sub>2</sub>-L2-Dy<sup>3+</sup> b) SiO<sub>2</sub>-L1-Dy<sup>3+</sup> and c) SiO<sub>2</sub>-L3-Dy<sup>3+</sup>. Excitation and emission wavelengths and the delays after the laser pulse used in the experiments are indicated.

## 4.9 Molecular insights into the observed selectivity. X-ray crystallography (Paper II)<sup>3</sup>.

The selectivity shown in section 4.7.2 is a very interesting phenomenon and warranted a deeper investigation of the molecular mechanisms. For this, we synthesized three molecular model compounds between each of the three REE ( $\text{La}^{3+}$ ,  $\text{Nd}^{3+}$  and  $\text{Dy}^{3+}$ ) used and IDA (since L3 is an IDA-derivative) at neutral pH. The structural information from these compounds allows a deeper understanding of the coordination mechanism. The composition of the surface complexes is  $\text{M} : \text{L} = 1 : 1$ , in a flat layer structure but with a remarkably different coordination number for each of the REE studied (Figure 16)<sup>4</sup>.

In all three structures, the nitrogen atoms remain protonated and are not involved in the coordination with metal cations, which occurs instead via concerted action of the carboxylic groups. The distances between the N-atoms in the model structures, corresponding to optimal distances between siloxane centers on the surface of the nanoparticles, are specific for each REE, being 4.9 Å for La, 5.7 Å for Nd and 6.4 Å for Dy. The earlier study of molecular models for  $\text{SiO}_2$  surface showed that the average distance between the silicon atoms on the surface of functional particles is in the range of 6.48-7.41 Å (Seisenbaeva et al., 2015, Polido, 2016). This explains the enhanced affinity toward  $\text{Dy}^{3+}$ , since the real N-N distance on the surface of functionalized silica suits best the required distance for the optimal structure of the surface layer formed by the  $\text{Dy}^{3+}$  complex.

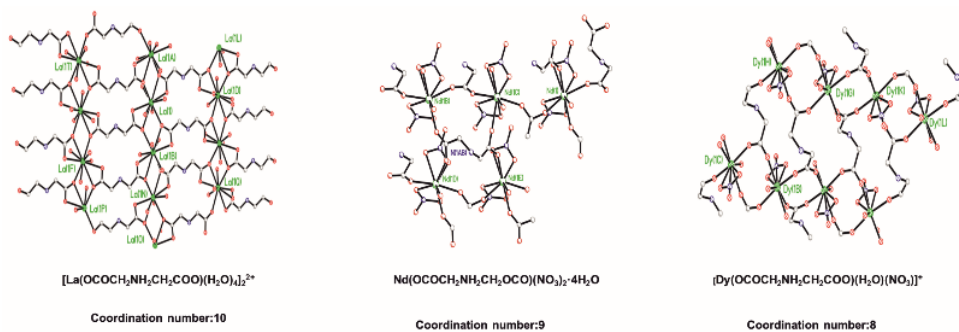


Figure 16. Structures of 2D coordination polymers of REE : IDA complexes as models for binding the REE on the surface of nanoadsorbents with covalently grafted IDA molecules.

3. The  $\text{Nd}^{3+}$  complex was actually presented in Paper IV.

4. For better resolution please see Figure 6 in Paper II and Figure 3 in Paper IV.

## 4.10 Conclusions

Three organosilane derivatives designated as L1, L2 and L3 were successfully synthesized and attached onto the surface of SiO<sub>2</sub> nanoparticles of 80 nm in average size. The first work focused on the synthesis of these three ligands and the study of their potential for REE adsorption. L1 showed poor stability over time and was therefore not tested for REE adsorption. The SiO<sub>2</sub> NPs functionalized with the L3, an IDA derivative, showed the best affinity for REE and was consequently chosen for further studies with magnetic  $\gamma$ -Fe<sub>2</sub>O<sub>3</sub>-SiO<sub>2</sub> NPs in the second work. Hence, we evaluated the REE uptake capacity of functionalized magnetic nanoadsorbents, obtaining values comparable to current techniques like ion-exchange resins. Even more interestingly, the selectivity study of this type of ligand showed that it has a much stronger affinity toward HREE (Dy<sup>3+</sup>) than to LREE (La<sup>3+</sup>). Molecular model compounds with three different REE (La<sup>3+</sup>, Nd<sup>3+</sup> and Dy<sup>3+</sup>) were synthesized and structurally studied to understand this selectivity, revealing very distinct coordination complexes with different coordination numbers. The higher affinity toward Dy<sup>3+</sup> could be explained based on these investigations, since the Dy<sup>3+</sup> coordination complex provides the most suitable distance for this type of silica based materials.



## 5 Exploring new possibilities for enhanced REE uptake (Paper III & IV).

### 5.1 Background

The previous study of the coordination mechanisms in bonding between different REE and IDA in molecular model compounds opened some gates for improvement of the REE uptake by the nanoadsorbents. Initially, the hypothesis was that REE cations would chelate with the organic ligand, involving the N atoms in the chelation. The crystallographic study of model compounds showed that the mechanism was governed only by concerted action of the carboxylic groups. This is due to the fact that the adsorption conditions were acidic for this organic ligand and therefore the N atoms were protonated and unable to be involved in the coordination mechanism.

With this information, a logical step to improve the efficiency of the nanoadsorbents was to modify the adsorption conditions, so that the N atoms could play a role in the coordination and thus increase the REE uptake. By controlling the pH to create basic conditions for adsorption, we expected to increase the uptake in approximately twice than previously observed. However, an uptake of more than 20 times higher was displayed. This was completely unanticipated and implied that a different mechanism was taking place. Therefore, unravelling this mechanism became the focus point of the study, using several techniques to analyze what is behind the observed unexpected increase in uptake.

## 5.2 REE uptake at controlled pH conditions

A similar procedure to the one presented in section 4.1.7 for adsorption studies was carried out. A known amount of the nanoadsorbents was put in contact with solutions of  $\text{REE}(\text{NO}_3)_3$  for two hours. The pH was then carefully tuned by dropwise addition of a 5%  $\text{NH}_4\text{OH}$  solution until  $\text{pH}=9$ . Different molar ratios of REE : Ligand were tested after observing the first promising results. In the beginning, functionalized nanoadsorbents were used (since the initial idea was to involve the N atoms in the chelation with REE), but in the view of the hugely enhanced uptake and under the suspicion that the mechanism was other than chelation, bare nanoparticles (both magnetic and non-magnetic  $\text{SiO}_2$  NPs) were also tested, indicating that indeed the presence of the ligands is not crucial in this case. Table 8 summarizes the REE uptake values obtained from complexometric titration. In this case, the complexometric titration is more time consuming than usual since it requires a prior step of neutralization of the solutions, which is performed via evaporation. Therefore only a number of representative materials were selected for this procedure.

Table 8.  $\text{Nd}^{3+}$  uptake in different types of nanoadsorbents, varying adsorption conditions and molar ratios.

Sample	Molar ratio Nd : Ligand	pH	Uptake capacity (mg $\text{Nd}^{3+}$ /g)
$\gamma\text{-Fe}_2\text{O}_3\text{-SiO}_2\text{-L3}$	1:1	Neutral	33.6
$\gamma\text{-Fe}_2\text{O}_3\text{-SiO}_2\text{-L3}$	1:1	9	90
$\gamma\text{-Fe}_2\text{O}_3\text{-SiO}_2\text{-L3}$	5:1	9	446.3
$\gamma\text{-Fe}_2\text{O}_3\text{-SiO}_2\text{-L3}$	10:1	9	907.7
$\gamma\text{-Fe}_2\text{O}_3\text{-SiO}_2$	5:1	9	861.6
$\text{SiO}_2$	5:1	9	442.8

It can be seen in the table that from the first attempt, the increase in  $\text{Nd}^{3+}$  uptake is higher than expected, which encouraged us to increase the amount of  $\text{Nd}^{3+}$  since this first observed uptake enhancement did not correlate with a chelation mechanism. The amount of  $\text{Nd}^{3+}$  adsorbed by the functionalized nanoadsorbents drastically increased and this gave the idea that perhaps the organic ligands were actually not necessary in this new mechanism. It was worthwhile to perform trials with bare  $\text{SiO}_2$  and  $\gamma\text{-Fe}_2\text{O}_3\text{-SiO}_2$  and it was proved that indeed huge uptake of REE ( $\text{Nd}^{3+}$  in this case) occurred even in the absence of specific ligands.

### 5.3 REE release under mild conditions

Desorption of REE using solutions of HNO<sub>3</sub>, although very effective as shown in previous sections, might not be the best choice when thinking about applying the technology to an industrial scale, since it would require large volumes of acid. Although this acid could be easily reused in several adsorption-desorption cycles, it could be beneficial to investigate less harmful alternatives from an environmental perspective. For this purpose, we studied (NH<sub>4</sub>)<sub>2</sub>SO<sub>4</sub> as desorbing agent, as well as a slightly acidified (NH<sub>4</sub>)<sub>2</sub>SO<sub>4</sub> solution (pH = 3.75). The method was implemented in three steps to increase efficiency: The loaded nanoadsorbents were first put in contact with the (NH<sub>4</sub>)<sub>2</sub>SO<sub>4</sub> solution for 3 hours (twice) and finally for a longer desorption step of 20 hours. Table 9 shows the summary of the desorption achieved for Dy<sup>3+</sup> loaded  $\gamma$ -Fe<sub>2</sub>O<sub>3</sub>-SiO<sub>2</sub> NPs, where the results are obtained by complexometric titration and given in percentage related to the initial amount adsorbed.

Table 9. *Multi-step desorption with NH<sub>4</sub>(SO<sub>4</sub>)<sub>2</sub> and comparison with acidic desorption.*

Desorption method	Dy <sup>3+</sup> adsorbed (mmol Dy <sup>3+</sup> /g)	Desorbed at first 3h. (%)	Desorbed at second 3h. (%)	Desorbed at last 20 h. (%)	Total desorbed (%)	Desorbed in one-step 24h. (%)
(NH <sub>4</sub> ) <sub>2</sub> SO <sub>4</sub> 0.5M	3.4	20.1	39.9	2	62	
Acidified	3.4	23	30.2	1.8	55	
(NH <sub>4</sub> ) <sub>2</sub> SO <sub>4</sub> 0.5M (pH=3.75)						
HCl 1M	3.4	-	-	-	-	51.1
HNO <sub>3</sub> 1M	3.4	-	-	-	-	40.9

The table shows that quite competent desorption can be achieved with (NH<sub>4</sub>)<sub>2</sub>SO<sub>4</sub> instead of acid, showing even higher desorption rates than with acids. Most of the Dy<sup>3+</sup> is released during the first two steps, whereas the last and longest step (20h.) does not really provide a significant improvement of the total desorption.

## 5.4 Reusability of the nanoadsorbents. Consecutive adsorption-desorption cycles.

Being able to develop a stable material and technology that can be used for several cycles in a continuous process is one of the ultimate goals of this work. The stability and efficiency of the nanoadsorbents needs to be tested hence in consecutive adsorption-desorption cycles. For this test, one-step 24 hours acidic desorption was chosen, so that the stability of the materials could be proven even under harsh conditions. The test was performed on  $\gamma$ -Fe<sub>2</sub>O<sub>3</sub>-SiO<sub>2</sub> NPs for Dy<sup>3+</sup> in three consecutive adsorption-desorption cycles. The results are summarized in Table 10, where it can be seen that the nanoadsorbents proved their total reusability, with high uptake values in all three cycles (up to 87%) and equal or less than 0.5% remaining on the nanoadsorbents after desorption.

Table 10. EDS analysis on  $\gamma$ -Fe<sub>2</sub>O<sub>3</sub>-SiO<sub>2</sub> NPs for three consecutive adsorption-desorption cycles of Dy<sup>3+</sup>. Values are given in relative weight %.

Process	%Fe	%Si	%Dy
1 <sup>st</sup> cycle adsorption	24.5	14.2	61.3
1 <sup>st</sup> cycle desorption	64.5	32.6	0.5
2 <sup>nd</sup> cycle adsorption	16.9	5.7	77.5
2 <sup>nd</sup> cycle desorption	71.7	28.3	0
3 <sup>rd</sup> cycle adsorption	10.9	2.5	86.9
3 <sup>rd</sup> cycle desorption	70.3	29.4	0.3

## 5.5 Solid state <sup>13</sup>C and <sup>29</sup>Si CP-MAS NMR spectroscopy for the study of the interaction of the functional layer with REE cations.

Aiming to unravel this new mechanism, one of the first things we wanted to evaluate was the interaction between the organic functional layer and the REE cations (if any) and any possible change in the silica network occurs after adsorption. For this, solid state NMR comes again as a very helpful technique. For technical reasons, we used functionalized non-magnetic SiO<sub>2</sub> NPs loaded with La<sup>3+</sup> (non-paramagnetic) and analysed them before and after adsorption at controlled pH. Figure 17 shows labelling of the C atoms of the IDA-derived ligand and the corresponding <sup>13</sup>C CP-MAS NMR resonances. The characteristic C=O peak appears at 171.7 ppm. It is important to note that the signal

corresponding to the C atom labelled as f does not appear in the spectrum. This indicates the hydrolysis of the ester, which leaves the ligand free for complexation with terminal carboxylic groups. The  $^{29}\text{Si}$  spectrum reveals several resonances assigned to  $\text{Q}_n$  and  $\text{T}_n$  Si local environments (Peng et al., 2005, Sharma and Sharma, 2014).

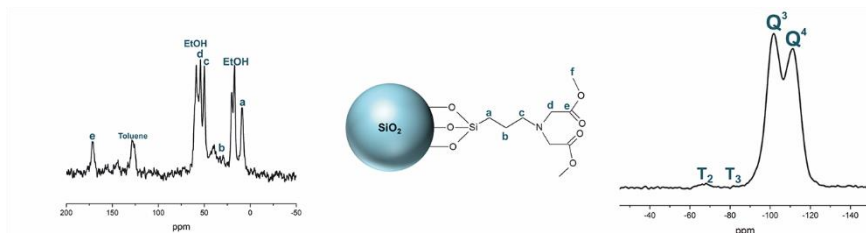


Figure 17.  $^{13}\text{C}$  CP-MAS NMR and  $^{29}\text{Si}$  CP-MAS NMR spectra of  $\text{SiO}_2$  NPs functionalized with IDA-derivative ligand.

The effect of REE adsorption on the nanoadsorbents under these new conditions was studied and the obtained spectra are shown in Figures 18 and 19. Figure 18 shows the  $^{13}\text{C}$  CP-MAS NMR spectra of the functionalized  $\text{SiO}_2$  NPs (red) and the same particles after adsorption of  $\text{La}^{3+}$  at high pH. In the latter one it can be observed that the carboxylate ( $\text{C}=\text{O}$ ) resonance shifts from 171.7 ppm to 174.5 ppm, which provides evidence of coordination of  $\text{La}^{3+}$  by the terminal carboxylic groups of the ligand. Figure 19 shows  $^{29}\text{Si}$  MAS and CP-MAS NMR spectra of both functionalized and non-functionalized  $\text{SiO}_2$  NPs with and without adsorbed REE. A decrease in the number of  $\text{Q}_3$  groups in functionalized  $\text{SiO}_2$  NPs, which is expected due to the grafting of the organic ligand, can be observed, but other than that, no significant change in the silica network is displayed, leading to the conclusion that this new adsorption mechanism does not affect in any way the silica structure.

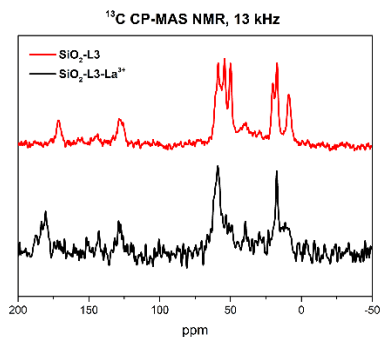


Figure 18.  $^{13}\text{C}$  CP-MAS NMR spectra of functionalized  $\text{SiO}_2$  NPs (red) and  $\text{La}^{3+}$ -loaded functionalized  $\text{SiO}_2$  NPs (black).

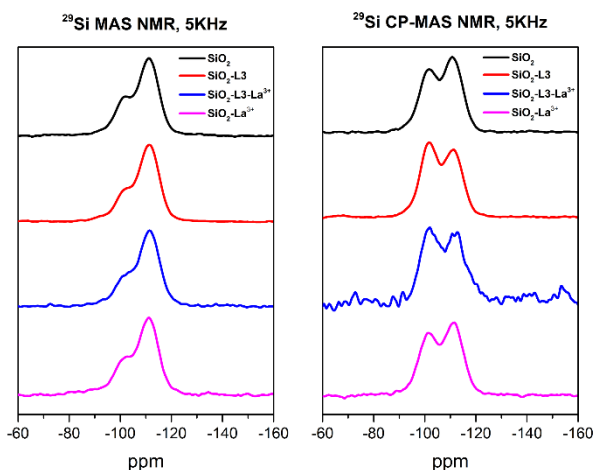


Figure 19.  $^{29}\text{Si}$  MAS and  $^{29}\text{Si}$  CP-MAS NMR spectra of  $\text{SiO}_2$  NPs (black), functionalized  $\text{SiO}_2$  NPs (red), and the corresponding  $\text{La}^{3+}$ -loaded NPs (pink and blue, respectively). Every spectrum is normalized to the highest peak.

## 5.6 Enhanced adsorption mechanism: What is really happening?

It has been confirmed that the adsorption efficiency increases to a very large extent with this method, that its efficiency remains intact after several adsorption-desorption cycles, that desorption can be achieved under mild conditions and that the silica network is not affected in the process, but what is really going on behind this wonders? In this section, we will try to understand

the mechanism that governs this increase in adsorption efficiency and prove it using several techniques.

The morphology of the loaded nanoadsorbents was studied by transmission electron microscopy (TEM) and atomic force microscopy (AFM). Bright-field TEM (BF-TEM) and high-angle annular dark-field scanning transmission electron microscopy (HAADF-STEM) images of magnetic and non-magnetic NPs loaded with REE are shown in Figure 20 and 21, where the formation of a new phase around the surface of NPs is easily visible and is confirmed by energy-filtered transmission electron microscopy (EFTEM) elemental mapping on REE loaded  $\text{SiO}_2$  NPs (Figure 22).

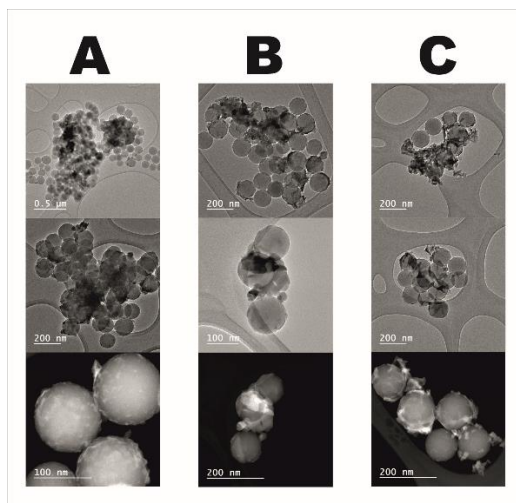


*Figure 20.* BF-TEM (upper two rows) and HAADF-STEM (lower row) images of  $\text{SiO}_2$  nanoadsorbents loaded with a)  $\text{Dy}^{3+}$ ; b)  $\text{Nd}^{3+}$ ; c)  $\text{La}^{3+}$  at high pH.

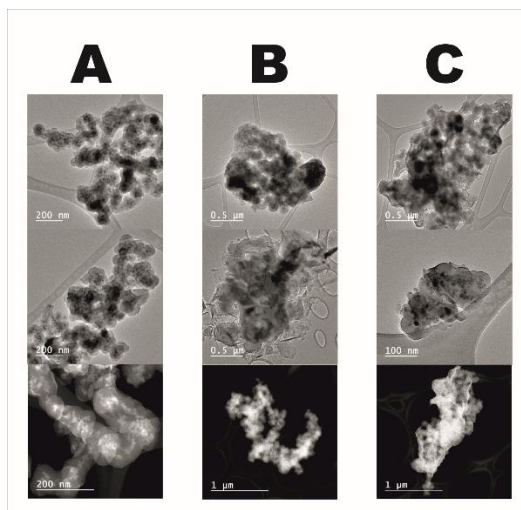


Figure 21. BF-TEM (upper two rows) and HAADF-STEM (lower row) images of  $\gamma\text{-Fe}_2\text{O}_3\text{-SiO}_2$  NPs loaded with a)  $\text{Dy}^{3+}$ ; b)  $\text{Nd}^{3+}$ ; c)  $\text{La}^{3+}$  at high pH.

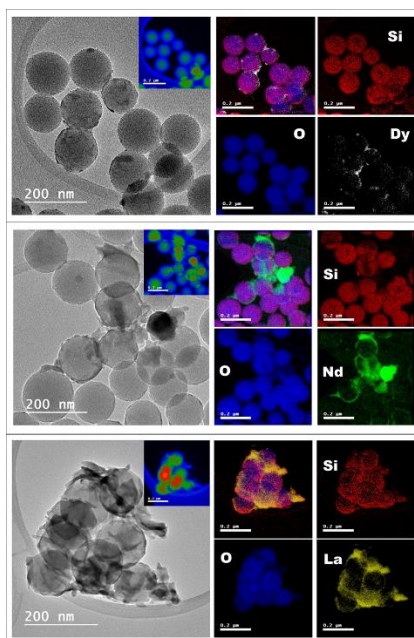


Figure 22. BF-TEM images and EFTEM elemental mapping of  $\text{SiO}_2$  nanoparticles loaded with REE.

TEM images showed that the adsorption process did not affect in any significant way the morphology of the NPs, and the EFTEM elemental mapping provided valuable information about the composition of this new phase,

confirming the formation of a REE compound on the surface of the nanoparticles. In some of the TEM images some needle-shaped motifs can be distinguished. To support this statement, the crystallinity of this new phase has been assessed by X-ray powder studies (Figure 23), revealing a structure that matches REE(OH)<sub>3</sub>. The X-ray diffractogram allows the calculation of the size of the crystallites using the Scherrer equation (equation 1), a formula that relates the size of crystallites to the broadening of a peak in a diffraction pattern.

$$\tau = \frac{K \cdot \lambda}{\beta \cdot \cos \theta} \quad (1)$$

where  $\tau$  is the size of the crystalline domains,  $K$  is a dimensionless shape factor with a typical value of about 0.9,  $\lambda$  is the X-ray wavelength (0.71073 Å for the instrument used),  $\beta$  is the line broadening at half maximum intensity (FWMH) and  $\theta$  is the Bragg angle of diffraction.

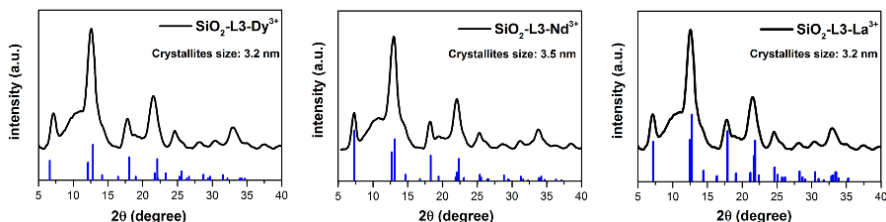


Figure 23. XRPD patterns of functionalized SiO<sub>2</sub> NPs loaded with REE. The blue lines represent the pattern of the corresponding REE hydroxides.

The compilation of these results gives quite compelling proof that the mechanism for REE adsorption under basic conditions involves a controlled growth of a crystalline phase of REE(OH)<sub>3</sub> that is initiated by the SiO<sub>2</sub> NPs, both magnetic and non-magnetic. The driving force for this seems to be the formation of outer sphere complexes between the negatively charged surface of silica at high pH and the positively charged REE cations.

Figure 24 shows the 3D AFM images of SiO<sub>2</sub> NPs loaded with Nd<sup>3+</sup> at high pH, obtained with a Bruker FastScan Bio atomic force microscope operating in tapping mode, in which a considerable increase in roughness after deposition of the Nd(OH)<sub>3</sub> crystalline layer can be noticed.

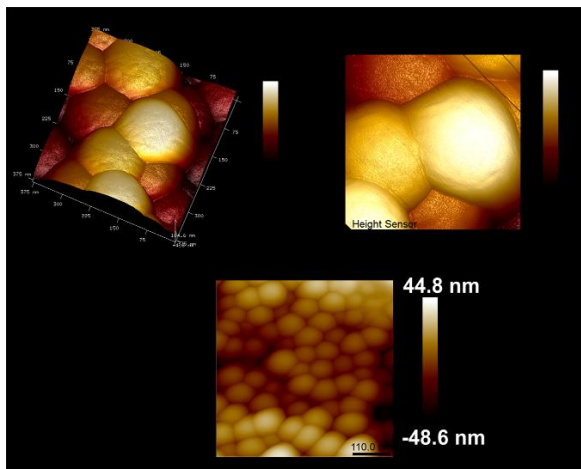


Figure 24. AFM 3D images of SiO<sub>2</sub> NPs loaded with Nd<sup>3+</sup> (top) and 2D image of pure SiO<sub>2</sub> NPs.

This supports the hypothesis that the mechanism differs from coordination, since coordination does not usually lead to such a high amount of REE on the surface that could cause observable morphology changes using AFM.

## 5.7 Study of the simultaneity of coordination and seeding mechanisms by EXAFS (Paper IV).

In the previous section, it was demonstrated that the adsorption of REE at high pH conditions is governed by the crystallization of a REE(OH)<sub>3</sub> layer induced by magnetic or non-magnetic SiO<sub>2</sub> NPs. The mechanism is very different from coordination, and specific organic ligands are, in principle, not necessary for this process. But what happens when the method is implemented on functionalized NPs? We have seen that the REE uptake efficiency is huge in both cases, which implies that seeding of REE(OH)<sub>3</sub> also takes place here, but, does coordination occur at all? Do both mechanisms co-exist? Is the coordination monolayer preserved after the growth of the hydroxide layer? This is investigated in this section.

For this, we followed the process by extended X-ray absorption fine structure (EXAFS), since it is a technique that is sensitive to changes in the atomic environment and will allow us to distinguish if both coordination with the ligand and REE(OH)<sub>3</sub> seeding are present. Three systems where the adsorption of REE was performed at high pH were selected for this analysis: bare SiO<sub>2</sub> NPs loaded with Nd<sup>3+</sup> (SiO<sub>2</sub>-Nd), IDA-derivative functionalized SiO<sub>2</sub> NPs loaded with Dy<sup>3+</sup> and La<sup>3+</sup> (SiO<sub>2</sub>-IDA-Dy and SiO<sub>2</sub>-IDA-La). The first system will allow us to

confirm the formation of the REE(OH)<sub>3</sub> layer and with the other two systems we will study the influence of the organic ligand in the process.

Fluorescence EXAFS data were collected at the wiggler beam I811 at Max IV Laboratory in Lund, Sweden. The station is equipped with a Si (111) double crystal monochromator and the absorption edge energy was calibrated using the first inflection point of the spectrum of a Mn foil (6.54 keV). Four scans were collected for each sample and the data was averaged. The obtained EXAFS spectra were processed using the program IFEFFIT included in the DEMETER software package. Using the crystal structures for REE : IDA models (previously solved, see section 4.7.3) and REE(OH)<sub>3</sub> (taken from crystallographic database) for the fitting of the obtained EXAFS spectra, we would be able to evaluate the contribution of both mechanisms. Table 11 compiles the obtained fitting data for the three evaluated samples. Each scattering path in the table is followed by an indication in square brackets to clarify what structure the path comes from.

Table 11. EXAFS fitting data for functionalized and non-functionalized SiO<sub>2</sub> NPs loaded with the indicated REE at high pH conditions.

Sample	Scattering path	N	R(Å)	E <sub>0</sub> (eV)	R factor
<b>SiO<sub>2</sub>-Nd</b>	Nd-O	9	2.49 ± 0.03	3.33 ± 1.46	<b>0.033</b>
	Nd-Nd	2	3.75 ± 0.01		
	Nd-O	3	3.77 ± 0.2		
	Nd-O	6	4.23 ± 0.02		
	Nd-O-O	12	4.04 ± 0.27		
	Nd-O-O	24	4.01 ± 0.12		
	Nd-O-Nd	24	4.38 ± 0.2		
<b>SiO<sub>2</sub>-IDA-Dy</b>	Nd-O-O	12	4.58 ± 0.32	4.44 ± 1.38	<b>0.034</b>
	Dy-O	9	2.35 ± 0.09		
	[Dy(OH) <sub>3</sub> ]				
	Dy-Dy	2	3.61 ± 0.03		
	[Dy(OH) <sub>3</sub> ]				
	Dy-O	2	2.34 ± 0.07		
	[Dy-IDA]				
	Dy-O	2	2.39 ± 0.11		
	[Dy-IDA]				
	Dy-N	1	3.21 ± 0.3		
	[Dy-IDA]				
	Dy-C	2	3.25 ± 0.16		
	[Dy-IDA]				
	Dy-O-C	4	3.73 ± 0.26		
	[Dy-IDA]				
Dy-O-C	2	3.73 ± 0.27			
[Dy-IDA]					
Dy-O	1	3.94 ± 0.04			
[Dy-IDA]					
<b>SiO<sub>2</sub>-IDA-La</b>	La-O	3	1.99 ± 0.49	-6.6 ± 0.53	<b>0.019</b>
	[La(OH) <sub>3</sub> ]				
	La-O	6	2.94 ± 0.16		
	[La(OH) <sub>3</sub> ]				
	La-La	2	3.8 ± 0.05		
	[La(OH) <sub>3</sub> ]				
	La-O	6	2.26 ± 0.3		
	[La-IDA]				
	La-O	2	2.79 ± 0.17		
	[La-IDA]				
	La-O	2	2.74 ± 0.03		
	[La-IDA]				
	La-C	2	3.11 ± 0.06		
	[La-IDA]				
	La-C	2	3.59 ± 0.11		
[La-IDA]					
La-O-C	4	3.95 ± 0.18			
[La-IDA]					

This summary of the EXAFS parameters obtained after fitting indicates the coexistence of both coordination of REE with the molecules of organic ligand, and seeding of REE(OH)<sub>3</sub> on the surface of the NPs. The best fit for the spectra of bare SiO<sub>2</sub> NPs loaded with Nd<sup>3+</sup> (SiO<sub>2</sub>-Nd), indicated by the low R factor, is achieved with the Nd(OH)<sub>3</sub> structure, as expected. However, for the other two samples, with functionalized NPs, it is a combination of scattering paths both

from the REE : IDA and the REE(OH)<sub>3</sub> structure that gives the best fit, indicating the coexistence of both mechanisms.

In EXAFS, the parameter R-factor represents the relative error of a fit. There are no standard guidelines for the interpretation of this factor, but generally an R-factor < 0.05 is accepted as a good fit, and the smaller the better fit (Calvin, 2013). In our study, considering the complexity of the samples and the fact that some unidentified scattering paths could possibly come from interactions with the silica network (which we were unable to consider in the fit), the obtained R factor were quite acceptable. in all three cases.

Figure 25 shows the EXAFS spectra and their corresponding fits, where the first row shows the magnitude Fourier transform spectra in R space, the middle row shows the real part of the Fourier transform spectra in R space, and the bottom row shows the fitted k<sup>3</sup>-weighted spectra (in the range from 2.0-9.0 Å<sup>-1</sup>).

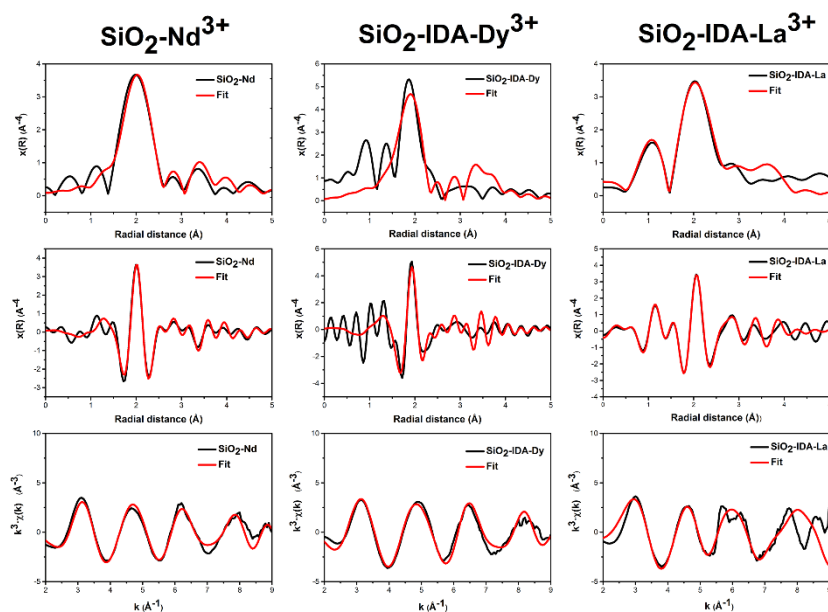


Figure 25. EXAFS spectra for SiO<sub>2</sub>-Nd<sup>3+</sup> (left), SiO<sub>2</sub>-IDA-Dy<sup>3+</sup> (middle) and SiO<sub>2</sub>-IDA-La<sup>3+</sup> (right). Experimental data in black and fitted data in red.

The spectra show good correlation between the experimental and the fitted data, both in phase and amplitude.

## 5.8 Magnetic characterization and quantification of REE by magnetometry (Paper IV)

Magnetic studies of the samples were carried out to: a) investigate how the formation of crystalline layers of REE(OH)<sub>3</sub> on the surface of the NPs can influence the magnetic properties of the system, potentially facilitating their magnetic extraction from solution and b) examine the possibilities of quantifying the amount of REE on the surface of the NPs by magnetic measurements and the correlation of these results with those from complexometry.

DC magnetization measurements were performed using a Quantum Design MPMS-XL SQUID magnetometer on the following samples: REE : IDA model compounds (where REE: Dy, Nd), SiO<sub>2</sub>-IDA-Nd<sup>3+</sup> (adsorbed at neutral pH) and SiO<sub>2</sub>-REE(OH)<sub>3</sub> (where REE: Dy, Nd, adsorbed at high pH).

Figure 26 shows magnetization vs. temperature obtained for REE : IDA model compounds. The compound with La<sup>3+</sup> was not analysed since La<sup>3+</sup> has no localized magnetic moment.

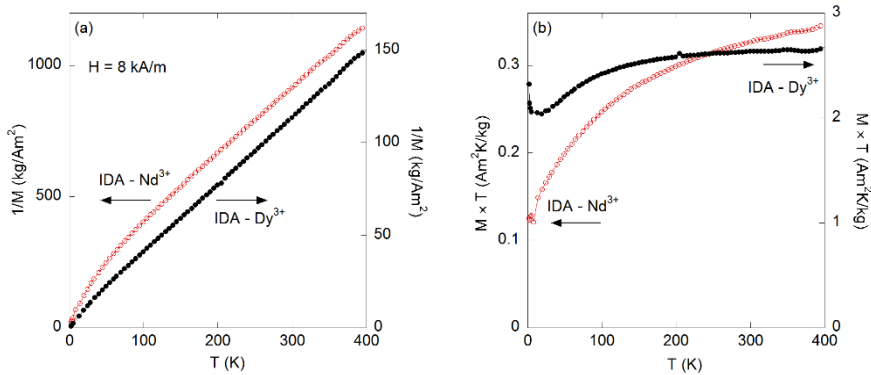


Figure 26. (a)  $1/M$  versus  $T$  and (b)  $M \times T$  versus  $T$  for the REE : IDA compounds. The magnetic moment was normalized by weight of the REE : IDA sample.

At large enough temperature, it is often found that  $M \cdot T$  approaches a constant value corresponding to the free-ion paramagnetic value (Ritchie et al., 2011), and from this, it is possible to estimate the number of RE<sup>3+</sup> ions in a sample, knowing the magnetic moment ( $m$ ) measured at a temperature where  $m \cdot T$  has approached a constant level, using the following equation:

$$m \cdot T = \frac{N \mu_0 D^2 \mu_B^2}{3k_B} H, \quad (2)$$

Where  $N$  is the number of  $\text{RE}^{3+}$  ions,  $\mathbf{p} = g\sqrt{J(J+1)}$  is the effective magnetic moment and  $\mathbf{H}$  is the applied magnetic field. Using the free-ion values for the quantum numbers,  $g = \frac{1 + J(J+1) + S(S+1) - L(L+1)}{2J(J+1)}$  and the applied magnetic field used in the magnetization versus temperature measurements, the values obtained are  $\mathbf{m} \times T = 2.72 \cdot 10^{-25} \text{N}$  and  $\mathbf{m} \times T = 2.35 \cdot 10^{-24} \text{N}$  for Nd-IDA and Dy-IDA, respectively. Using the measured magnetic moments at 400K and normalizing with the weight of sample, the obtained  $N$  are  $N \approx 1.3 \cdot 10^{21}$  ions in Nd-IDA and  $N \approx 1.1 \cdot 10^{21}$  ions Dy-IDA. Using the information obtained for this model compounds from X-ray crystallography (molar mass and molecular formula), the expected  $N$  values are slightly larger;  $N \approx 1.53 \cdot 10^{21}$  ions and  $N \approx 1.32 \cdot 10^{21}$  ions for Nd-IDA and Dy-IDA, respectively. The correlation factor is 1.18 for both  $\text{Nd}^{3+}$  and  $\text{Dy}^{3+}$  ions, and this slight difference can be explained by the fact that magnetometry results were calculated using a simplified model that uses free-ion paramagnetic moments, neglecting thus the ligand field effects.

Figure 27 shows the magnetization versus temperature for  $\text{SiO}_2\text{-Nd}(\text{OH})_3$  and  $\text{SiO}_2\text{-Dy}(\text{OH})_3$  (the notation  $\text{REE}(\text{OH})_3$  refers to adsorption at high pH, where seeding of  $\text{REE}(\text{OH})_3$  takes place).

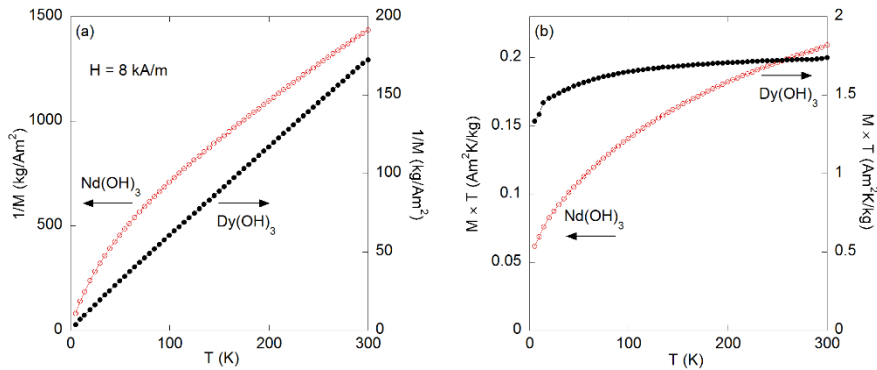


Figure 27. (a)  $1/M$  versus  $T$  and (b)  $M \times T$  versus  $T$  for the  $\text{SiO}_2$  NPs loaded with REE at high pH ( $\text{SiO}_2\text{-Dy}(\text{OH})_3$  and  $\text{SiO}_2\text{-Nd}(\text{OH})_3$ ). The magnetic moment was normalized by weight of the sample.

Using the same reasoning followed above, the amount of REE ions present in the samples were calculated and compared with the values previously obtained from complexometric titration. Table 12 shows this correlation, where a slight difference between the two methods is observed, and the reason for this might be, as explained before, the fact that ligand field effects were neglected in the analysis of magnetometry.

Table 12. Comparison of REE uptake capacity obtained from magnetometry (magn.) and from titration (titr.).

	N		mmol RE <sup>3+</sup> /g <sub>total material</sub>		Titr./Magn. correlation
	(nr. of RE <sup>3+</sup> ions/g <sub>total material</sub> )		Magnetometry	Titration	
	Magnetometry	Titration			
SiO <sub>2</sub> -Dy(OH) <sub>3</sub>	7.4 · 10 <sup>20</sup>	1.07 · 10 <sup>21</sup>	1.23	1.78	1.45
SiO <sub>2</sub> -Nd(OH) <sub>3</sub>	7.6 · 10 <sup>20</sup>	1.05 · 10 <sup>21</sup>	1.26	1.75	1.39

Finally, the increase in REE uptake that takes place when seeding of REE(OH)<sub>3</sub> occurs instead of coordination of REE was accurately quantified. Here, the magnetic measurements were compared in a sample where REE coordination takes place (SiO<sub>2</sub>-IDA-Dy<sup>3+</sup> -adsorption carried at neutral pH) and a sample where seeding of REE(OH)<sub>3</sub> takes place (SiO<sub>2</sub>-Dy(OH)<sub>3</sub> -adsorption at high pH-). Figure 28 shows the low temperature magnetization versus field curves for these two samples. The magnetization, in Am<sup>2</sup>/kg, is approximately a factor of 25 times higher for SiO<sub>2</sub>-Dy(OH)<sub>3</sub> than for SiO<sub>2</sub>-IDA-Dy<sup>3+</sup>. This is indeed in good agreement with the previously obtained results from complexometry, where we showed an increase of up to 30 times when inducing seeding of REE(OH)<sub>3</sub>.

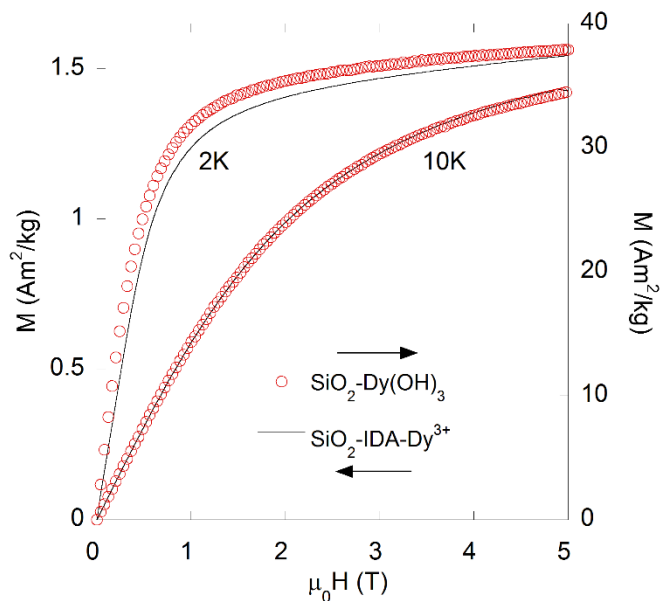


Figure 28. Magnetization versus field for SiO<sub>2</sub>-IDA-Dy<sup>3+</sup> (solid lines) and SiO<sub>2</sub>-Dy(OH)<sub>3</sub> (open circles).

## 5.9 Possible practical applications.

The notably high uptake capacity of the nanoadsorbents using the method presented in this chapter has been proven, but further testing on the actual applicability of the technology is crucial. At first glance, it can appear that this technology offers no advantage over a simple precipitation of  $\text{REE}(\text{OH})_3$  by increase of pH, but one of the greatest benefits of the process lies in its possibilities for recycling, where the material to be recycled already contains the REE mixture in the desired ratios for its end use. The magnetic nanoadsorbents can then provide an approach to efficiently extract REE after their dissolution and easily separate them thanks to the magnetic properties of the  $\gamma\text{-Fe}_2\text{O}_3\text{-SiO}_2$  NPs.

Nevertheless, the current situation is that recycling of REE is very limited: less than 1% of all REE were recycled as date of 2011, and it is mostly limited to permanent magnets and polishing compounds (Royen and Fortkamp, 2016, Tsamis and Coyne, 2015, British Geological Survey, 2011). This can be due to several reasons, such as a poor collection of the end-of-life products or the lack of competitive technologies.

Therefore, even if this method could potentially open lots of possibilities in recycling, what was mostly interesting for us was to test it in real mixtures from ores containing REE. In the frame of the EURARE project, several REE ores existing in Europe have been assessed and processed. In this case, a  $\text{REE}_2(\text{CO}_3)_3$  concentrate from the ore in Tanbreez (Greenland), that had been processed and supplied by MEAB Chemie Technik GmbH was used. The challenge with this type of material is that, besides the REE of interest, it contains many other elements that can hinder the uptake of REE by the nanoadsorbents, namely calcium, iron or chlorine. These elements could be potentially taken up by the nanoadsorbents, reducing thus their efficiency toward REE. An option is treating the concentrate in order to eliminate or reduce the amount of these elements, but adding more steps in an industrial process might translate into an increase in costs. Hence, we tried to limit the processing of the carbonate to only dissolution of the powder by acid treatment ( $\text{HNO}_3$ ) and one neutralization step with  $\text{NH}_4\text{OH}$  until  $\text{pH} \approx 6.5$ . The next step would be to put in contact the resulting neutralized solution with the nanoadsorbents and increase the pH conditions according to the procedure explained in this chapter. For this, we chose  $\text{SiO}_2$  NPs in order to be able to discern if the iron content decreased. Using magnetic  $\gamma\text{-Fe}_2\text{O}_3\text{-SiO}_2$  NPs this distinction would not have been possible, since the SEM-EDS analysis, used to characterize the samples, would not differentiate between Fe that comes from the NPs and the Fe from the leachate.

Table 13 shows the initial composition of the  $\text{REE}_2(\text{CO}_3)_3$  concentrate from the Tanbreez ore as received from MEAB and the material after  $\text{HNO}_3$  treatment and after neutralization with  $\text{NH}_4\text{OH}$ . All the analyses were made with EDS and the value shown is the average of at least 5 local measurements.

Table 13. *Chemical composition as determined by EDS analysis of the REE carbonate from Tanbreez ore and its leachate solution after treatment with  $\text{HNO}_3$ .*

Sample	%Cl	%Ca	%Fe	%La	%Ce	%Nd	%Dy	%Y	%Sc
<b>REE<sub>2</sub>(CO<sub>3</sub>)<sub>3</sub> conc.</b>	9.9	14.8	12.7	16.4	37.9	7.9	0.4	-	-
<b>REE<sub>2</sub>(CO<sub>3</sub>)<sub>3</sub> treated with HNO<sub>3</sub></b>	17.1	26.8	9.5	12.5	20.6	1.6	-	11.8	-

It is quite noticeable that both the initial carbonate and the acid treated material have a high content of chlorine, calcium and iron, which could hinder REE uptake. In the next step, we neutralized the acid-treated carbonate solution to proceed with the proposed REE uptake method with  $\text{SiO}_2$  NPs. Table 14 shows the chemical composition (from EDS) of the  $\text{SiO}_2$  NPs after adsorption and drying.

Table 14. *Chemical composition as determined by EDS of the SiO<sub>2</sub> NPs after adsorption at high pH of the leachate from Tanbreez REE carbonate..*

	%Al	%Si	%Cl	%Ca	%Ce	%Nd	%Na	%Y	%La
<b>SiO<sub>2</sub> NPs + neutralized leachate</b>	0.8	37.4	2.6	0.8	37.9	8.7	0.6	6.2	5.1

The test, although preliminary, gave some very interesting and promising results, as they suggest that the nanoadsorbents can, using the proposed method, lead to a quantitative sorption of REE together with a very significant reduction in the amount of other undesired elements present in the carbonate. More tests, ideally on an industrial or pilot plant scale, are certainly needed and could unfortunately not be carried out during this work due to lack of the required equipment and resources. Nevertheless, the process entails a potential breakthrough for industrial separation of REE, separating the REE from unwanted elements without increasing the number of steps.

## 5.10 Conclusions

In this section, a new method for uptake of REE at high pH has been presented and explained. The method, which offers a huge increase in REE uptake compared to the previously studied coordination by specific ligands (up to 30 times higher), was unknown and unforeseen for us. Therefore, we directed our focus toward finding out the mechanism behind this with different techniques, such as TEM and AFM microscopy, powder X-ray diffraction and EXAFS.

The obtained results suggest a controlled surface growth of a crystalline layer of REE(OH)<sub>3</sub> induced by the magnetic or non-magnetic SiO<sub>2</sub> NPs. The method has been tested in several consecutive adsorption-desorption cycles and showed to keep its efficiency almost intact.

Interestingly, EXAFS results imply the coexistence of both coordination and REE(OH)<sub>3</sub> seeding when the method is performed on functionalized nanoadsorbents. This could open possibilities for selective uptake/release. Also, we studied the magnetic properties of the loaded materials and the possibilities to quantify the amount of REE taken up by magnetometry. The results showed quite good correlation between the values calculated from magnetometry and those accurately obtained from complexometric titration. The small discrepancies could be explained by the fact that a slightly simplified model (where ligand field effects are neglected) was used for the magnetic calculations. In order to improve this calculations, relativistic *ab initio* calculations to determine the energy level structure of the RE<sup>3+</sup> multiplet ground state would be needed (Schilder and Lueken, 2004), but to the best of our knowledge, this was the first time magnetic measurements were used to quantify the uptake of REE and the obtained results are quite adequate.

Finally, after achieving a deeper understanding of the mechanism, the method was patented (Patent No. SE-1600165-3) and applied to a REE carbonate concentrate coming from the REE ore in Tanbreez. The tested nanoadsorbents were then able to quantitatively uptake REE from the treated REE leachate, without taking up other unwanted elements that were present in the REE carbonate. The study was preliminary and has not reached industrial scale yet, but offers an attractive potential for industrial separation of REE.



## 6 Comparative study of amino-polycarboxylic acids as complexonate ligands for molecular recognition of REEs (Paper V).

### 6.1 Background

The first two presented papers in section 4 showed the potential that specific organic ligands can have toward selective uptake of REE. In that work, the whole synthesis of the selected organosilane was carried out in lab scale in a mostly “*hand-made*” process, where the synthesis of the organosilanes required quite a number of steps. It was a very significant work to develop functional nanoadsorbents and to understand how they work, but when thinking in industrial scale, the simpler and more automated process the better. This is the reason why, in this work, we aimed at simplifying the synthetic process by choosing compounds that are readily available commercially and can be grafted on the surface of the NPs in less steps. Also, it was very interesting for us to study a series of complexonate ligands with increasing number of carboxylic functions to investigate how that influences the uptake capacity and the selectivity. The previous structural studies suggested that the coordination complexes with REE are very distinct depending on the REE, so we wanted to evaluate the influence of different ligands in this. Aminopolycarboxylic acids are great candidates for this: several are commercially available with different numbers of carboxylic groups, they are relatively cheap, and can be easily attached onto the surface of the nanoparticles. The functionalization requires a prior step of functionalization of the silica surface with an aminosilane, e.g. aminopropyltriethoxysilane (APTES), and then the aminopolycarboxylic acid

can be further attached via condensation reaction between the amino ( $-NH_2$ ) group of APTES and one carboxylic ( $-COOH$ ) group from the aminopolycarboxylic acid.

## 6.2 Synthesis of aminopolycarboxylic acid-functionalized nanoadsorbents.

Three different aminopolycarboxylic acids were studied, namely ethylenediaminetetraacetic acid (EDTA), diethylenetriaminepentaacetic acid (DTPA) and triethylenetetraaminehexaacetic acid (TTHA). Figure 29 shows schematically the synthetic routes. Although only  $SiO_2$  NPs are represented in the scheme, the procedure was analogous for magnetic  $\gamma-Fe_2O_3-SiO_2$  NPs.

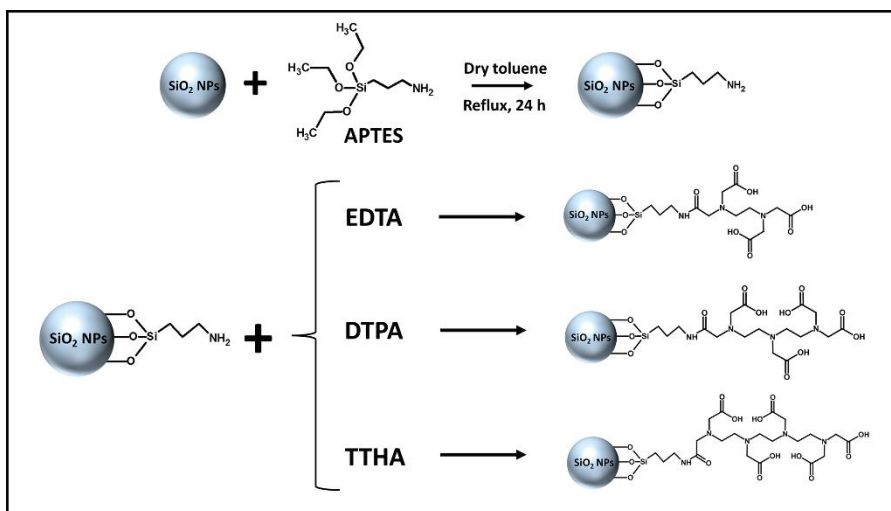


Figure 29. Synthesis scheme for the functionalization of NPs with aminopolycarboxylic acids.

## 6.3 Characterization of the functionalized nano-adsorbents.

### 6.3.1 FTIR spectroscopy.

The efficiency of the surface functionalization of NPs with EDTA, DTPA and TTHA was assessed by FTIR spectroscopy. The analysis was made on functionalized  $SiO_2$  NPs to simplify it, since the contribution from iron oxide in

the MNPs can lead to overlapping peaks. The metal oxide bands (Fe-O) usually appear in the same region as some of the characteristic bands of the silica network. Figure 30 shows the obtained FTIR spectra and Table 15 summarizes the most characteristic peaks observed and the functional groups that they are attributed to.

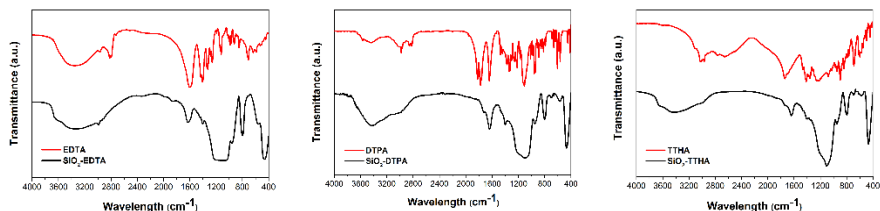


Figure 30. FTIR spectra of functionalized SiO<sub>2</sub> NPs and the corresponding aminopolycarboxylic acid.

Table 15. Summary of FTIR spectra of SiO<sub>2</sub> and functionalized SiO<sub>2</sub> NPs

Sample	Absorption peak location (cm <sup>-1</sup> )	Peak identification
SiO <sub>2</sub> NPs	1090 (saturated)	$\nu_{as}(\text{Si-O-Si})$
	950	$\nu_{as}(\text{Si-OH})$
	800	$\nu(\text{Si-O-Si})$
	460	$\delta(\text{Si-O-Si})$
SiO <sub>2</sub> -EDTA NPs	1634	$\nu(\text{C=O})$ (secondary amide)
	1404	$\delta(\text{O-H})$ (carboxylic acid)
	1250-1020	$\nu(\text{C-N})$ (overlaps with saturated $\nu_{as}(\text{Si-O-Si})$ )
SiO <sub>2</sub> -DTPA NPs	1636	$\nu(\text{C=O})$ (secondary amide)
	1728	$\nu(\text{C=O})$ (carboxylic acid)
	1397	$\delta(\text{O-H})$ (carboxylic acid)
	1250-1020	$\nu(\text{C-N})$ (overlaps with saturated $\nu_{as}(\text{Si-O-Si})$ )
SiO <sub>2</sub> -TTHA NPs	1639	$\nu(\text{C=O})$ (secondary amide)
	1734	$\nu(\text{C=O})$ (carboxylic acid)
	1250-1020	$\nu(\text{C-N})$ (overlaps with saturated $\nu_{as}(\text{Si-O-Si})$ )

All three different types of functionalized SiO<sub>2</sub> NPs show the characteristic peaks of silica. Additionally, the presence of several characteristic bands from the corresponding aminopolycarboxylic acids gives evidence of their efficient grafting. In all three cases, the  $\nu(\text{C-N})$  band, generally appearing around 1250-1020 cm<sup>-1</sup>, cannot be easily distinguished since it overlaps with the saturated  $\nu_{as}(\text{Si-O-Si})$  from the silica network.

### 6.3.2 Microscopy characterization (AFM, SEM and TEM).

The morphology of the synthesized samples was analysed by AFM using a Bruker FastScan Bio atomic force microscope operating in tapping mode, SEM using a Hitachi TM 1000-m-DEX scanning electron microscope and TEM using a JEOL JEM 2100F transmission electron microscope operating at 200 kV. Figure 31 shows the images comparing pure  $\text{SiO}_2$  NPs with those functionalized and loaded with REE and the corresponding magnetic ones. Aggregation of particles can be observed in magnetic NPs, and in both cases it can be appreciated that the functionalization of the NPs seems to not influence the morphology or size of the NPs.

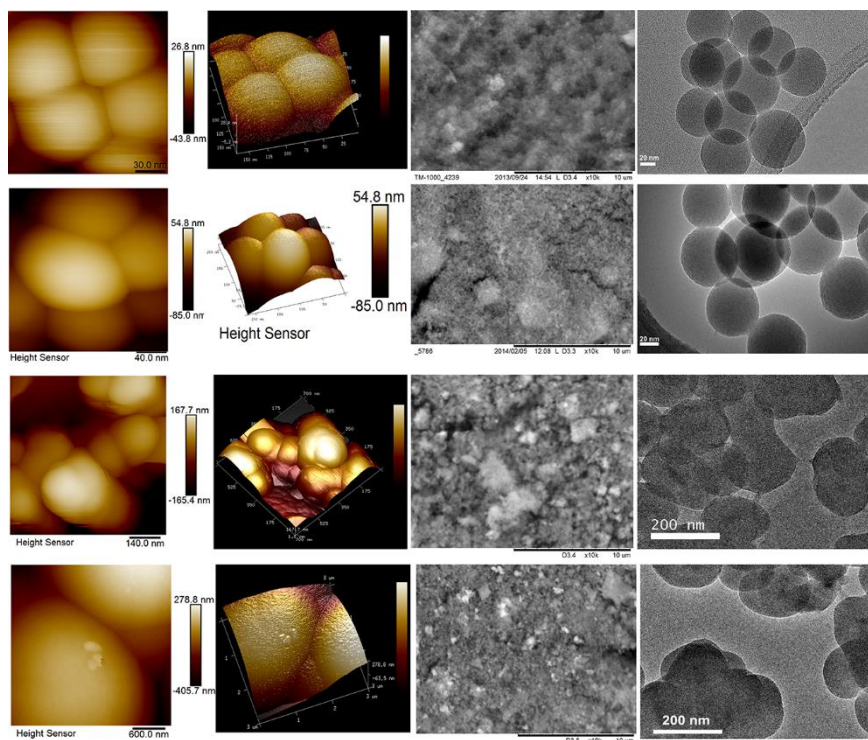


*Figure 31.* AFM, SEM and TEM images of pure  $\text{SiO}_2$  NPs (first row); EDTA-functionalized  $\text{SiO}_2$  NPs loaded with REE (second row); DTPA-functionalized  $\gamma\text{-Fe}_2\text{O}_3\text{-SiO}_2$  NPs loaded with REE (third row) and TTHA-functionalized  $\gamma\text{-Fe}_2\text{O}_3\text{-SiO}_2$  NPs loaded with REE (fourth row).

### 6.3.3 Thermogravimetric analysis (TGA).

TGA analyses were performed on functionalized SiO<sub>2</sub> NPs in order to quantify the amount of ligand grafted on the particles. The analyses were made in the temperature range from 25 to 900°C at a heating rate of 5°C/min. Table 16 shows the amount of ligand grafted in weight % and in mmol/g as obtained from the analyses.

Table 16. Amount of EDTA, DTPA and TTHA grafted onto the NPs, as obtained from TGA.

	Amount of ligand grafted (weight %)	Amount of ligand grafted (mmol/g)
SiO <sub>2</sub> -EDTA	10.6	0.33
SiO <sub>2</sub> -DTPA	16.0	0.38
SiO <sub>2</sub> -TTHA	15.2	0.29

## 6.4 REE uptake and selectivity studies.

### 6.4.1 Adsorption isotherms with La<sup>3+</sup>, Nd<sup>3+</sup> and Dy<sup>3+</sup>. Influence of different ligands.

Adsorption isotherms of the three mentioned REE were performed in the concentration range from 0 to 10 mM, on magnetic and non-magnetic SiO<sub>2</sub> NPs functionalized with EDTA, DTPA and TTHA. For this, a known amount of the corresponding functional nanoadsorbent was put in contact with the required amount of stock solutions of REE(NO<sub>3</sub>)<sub>3</sub> up to the final desired concentration (typically the points used for the isotherm were 0, 0.5, 1, 2, 3, 4 and 10 mM). After addition of NaNO<sub>3</sub> in order to keep constant ionic strength, the samples were shaken in an orbital shaker for 24 hours and after that, the amount of REE taken up by the nanoadsorbents was determined by complexometric titration, as explained in section 4.7. Figure 32 shows the obtained isotherms, which have been plotted in two types of graphs in order to facilitate the interpretation: one sorted by REE cation adsorbed and the other one sorted by type of aminopolycarboxylic acid used.

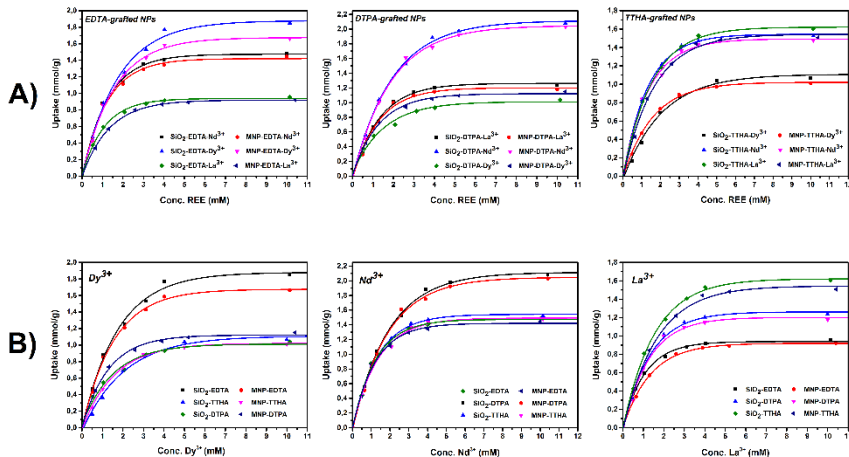


Figure 32. REE adsorption isotherms for the six different functional nanoadsorbents tested. A series shows the data sorted by type of ligand grafted (EDTA, DTPA or TTHA), and B series shows the data sorted by REE adsorbed (La<sup>3+</sup>, Nd<sup>3+</sup> or Dy<sup>3+</sup>).

The obtained isotherms show a high adsorption efficiency, with values up to 1.85 mmol REE/g. The values of average maximum adsorption capacity ( $q_e$ ) are summarized in Table 16 for the six different nanoadsorbents tested. The average is the result of three independent measurements by complexometric titration.

Table 17. Average maximum adsorption capacity ( $q_e$ ) for each nanoadsorbent, followed by the standard deviation from three measurements.

Sample	Max $q_e$ (mg REE/g adsorbent)		
	La <sup>3+</sup>	Nd <sup>3+</sup>	Dy <sup>3+</sup>
SiO <sub>2</sub> -EDTA	132.8 ± 4.9	213.9 ± 9.5	300.4 ± 10.3
MNP-EDTA	127.8 ± 5.5	208.5 ± 8.6	269.9 ± 9.5
SiO <sub>2</sub> -DTPA	171.8 ± 4.5	299.9 ± 8.2	168.6 ± 6.5
MNP-DTPA	163.4 ± 5.9	292.9 ± 7.5	186.9 ± 5.9
SiO <sub>2</sub> -TTHA	222.5 ± 5.8	219.9 ± 5.9	173.3 ± 5.7
MNP-TTHA	209.2 ± 6.7	213.1 ± 5.8	164.2 ± 5.2

It can be observed that the amount of adsorbed REE is quite high, reaching REE to EDTA ratios of about 3 : 1, REE to DTPA ratios of about 4 : 1 and REE to TTHA ratios of 5 : 1. These higher ratios of REE to L indicate a kind of monolayer formation, where the charge of the adsorbed cations is compensated apparently by anions, in this case nitrate, as can be observed in the IR spectra of

REE loaded adsorbents at neutral pH<sup>5</sup>. This means that, in principle, the selectivity in adsorption is quite low, but when performing desorption at pH  $\approx$  3-4, the REE to L ratio decreases to approximately 1 : 1 and the selectivity can strongly increase. However, considering the data sorted by type of ligand (upper row), some insights into selectivity that will be further confirmed in desorption, can be appreciated. EDTA-grafted nanoadsorbents show higher affinity for HREE, being the order of affinity  $Dy^{3+} > Nd^{3+} > La^{3+}$ . DTPA-grafted nanoadsorbents show higher affinity toward MREE, as can be observed by the fact that the  $Nd^{3+}$  uptake almost doubles the uptake for  $La^{3+}$  and  $Dy^{3+}$ . TTHA-grafted nanoadsorbents present higher affinity toward LREE ( $La^{3+}$ ).

#### 6.4.2 Selectivity studies with ternary and quinary mixtures of REE.

EDTA, DTPA and TTHA-functionalized SiO<sub>2</sub> NPs were tested in terms of selectivity with ternary ( $La^{3+}$ ,  $Nd^{3+}$ ,  $Dy^{3+}$ ) and quinary ( $La^{3+}$ ,  $Nd^{3+}$ ,  $Dy^{3+}$ ,  $Sc^{3+}/Y^{3+}$ ,  $Eu^{3+}$ ) mixtures of REE. The solutions were studied via complexometric titration for determination of total metal uptake, and the REE loaded NPs were analysed by EDS for REE qualitative analysis. Table 18 shows the obtained EDS data in average from at least five measurements in different areas of the samples. Given the fact that some peaks characteristic for REE overlap with the peak for Fe and would difficult the identification, we chose non-magnetic SiO<sub>2</sub> NPs for EDS analysis.

Table 18. EDS analysis of functionalized SiO<sub>2</sub> NPs with Ternary and Quinary Mixtures of REE

Sample	%Al	%Si	%Sc	%Y	%La	%Nd	%Eu	%Dy
SiO <sub>2</sub> -EDTA (La <sup>3+</sup> , Nd <sup>3+</sup> , Dy <sup>3+</sup> )	0.43	70.7	-	-	6.1	6.8	-	16
SiO <sub>2</sub> -EDTA (La <sup>3+</sup> , Nd <sup>3+</sup> , Dy <sup>3+</sup> , Sc <sup>3+</sup> , Eu <sup>3+</sup> )	0.24	96.4	0.74	-	0.2	0.65	0.41	1.36
SiO <sub>2</sub> -DTPA (La <sup>3+</sup> , Nd <sup>3+</sup> , Dy <sup>3+</sup> )	0.42	61.2	-	-	12.7	12.5	-	13.1
SiO <sub>2</sub> -DTPA (La <sup>3+</sup> , Nd <sup>3+</sup> , Dy <sup>3+</sup> , Sc <sup>3+</sup> , Eu <sup>3+</sup> )	0.3	91.9	2.28	-	0.75	0.57	1.35	2.88
SiO <sub>2</sub> -DTPA (La <sup>3+</sup> , Nd <sup>3+</sup> , Dy <sup>3+</sup> , Y <sup>3+</sup> , Eu <sup>3+</sup> )	0.58	69.3	-	0.92	5.72	6.1	8.38	9
SiO <sub>2</sub> -TTHA (La <sup>3+</sup> , Nd <sup>3+</sup> , Dy <sup>3+</sup> )	0.52	69.3	-	-	17.2	7.15	-	5.84
SiO <sub>2</sub> -TTHA (La <sup>3+</sup> , Nd <sup>3+</sup> , Dy <sup>3+</sup> , Y <sup>3+</sup> , Eu <sup>3+</sup> )	0.44	71.8	-	9.56	5.4	4.84	4.23	3.76

5. Provided in Supplementary Information of Paper V (FS3).

EDS analysis provides mostly surface and local information and therefore, even when taking several measurements for good statistics, the results are not as quantitative as complexometric titration. Nevertheless, they can be taken as an indication of the presence of REE, more qualitative than quantitative.

Considering this, some of the analyzed cases suggest a few of selectivity trends. For example, EDTA-functionalized nanoadsorbents present an affinity toward HREE, particularly  $\text{Dy}^{3+}$ , in ternary mixtures, and TTHA-functionalized nanoadsorbents show higher affinity toward LREE, particularly  $\text{La}^{3+}$ , in ternary mixtures. This is in agreement with the previously observed affinity trends in the adsorption isotherms, except for DTPA where no distinction among different REE could really be appreciated by EDS analysis, probably motivated by the above explained limitations of the technique and the fact that selectivity will be easier to distinguish further upon desorption, where the REE : L ratio goes down close to 1 : 1.

The nanoadsorbents saturated with ternary mixtures of REE underwent then a process of desorption at  $\text{pH} = 3$  (selective desorption conditions) and  $\text{pH} = 1$  (total desorption conditions). The results are summarized in Table 19, calculated in metal molar ratios from the obtained EDS analyses.

Table 19. *Selectivity trends in desorption for functionalized  $\text{SiO}_2$  NPs under different conditions. Expressed in molar ratios.*

	Total uptake (mmol/g)	Adsorption		Desorption $\text{pH}=3$		Desorption $\text{pH}=1$	
		Dy:Nd	Dy:La	Dy:Nd	Dy:La	Dy:Nd	Dy:La
<b><math>\text{SiO}_2</math>-EDTA</b>	1.85	2.4 : 1	2.6 : 1	3.6 : 1	76 : 1	1.6 : 1	1.9 : 1
<b><math>\text{SiO}_2</math>-DTPA</b>	1.98	1.1 : 1	1 : 1	1 : 12	1 : 1.9	1 : 1.2	1 : 1.1
<b><math>\text{SiO}_2</math>-TTHA</b>	1.54	1 : 1.2	1 : 2.9	1 : 2.5	1 : 69	1 : 1.4	1 : 1.7

Some selectivity trends can be quite apparently observed here. For EDTA-functionalized NPs, the separation factor is very pronounced for Dy:La ratio, from which can be deduced that the EDTA-functionalized nanoadsorbents have higher affinity to  $\text{Dy}^{3+}$ . DTPA-functionalized NPs show a significant separation factor for Dy:Nd although less pronounced than the previously mentioned. TTHA-functionalized NPs display the opposite trend to EDTA functionalized ones, with a separation factor of 69 for La in Dy:La ratio. It can be also observed that harsher conditions ( $\text{pH} = 1$ ) lead to total desorption.

## 6.5 Structural studies.

In the previous section, we have observed rather distinct selectivity trends for the three aminopolycarboxylic acids used. In order to get a deeper understanding of the mechanism behind this selective uptake of REE, we tried to synthesize molecular models between the corresponding aminopolycarboxylic acid and the REE at neutral pH and study them by single crystal X-ray crystallography, analogously to what we did with iminodiacetic acid in Paper II. We succeeded to synthesize one new molecular model compound, namely the complex between TTHA and  $\text{Dy}^{3+}$ , which in addition to a review of all others available in literature, allowed us to get some possible explanations to the observed selectivity.

### 6.5.1 Crystal structure of the TTHA-Dy molecular model compound.

The obtained coordination complex from  $\text{Dy}(\text{NO}_3)_3$  and TTHA at  $\text{pH} \approx 6.5$  (adjusted by dropwise addition of  $\text{NH}_4\text{OH}$  5%) featured the formula  $(\text{NH}_4)_3[\text{HDyTTHA}](\text{NO}_3) \cdot 4\text{H}_2\text{O}$  (Figure 33).

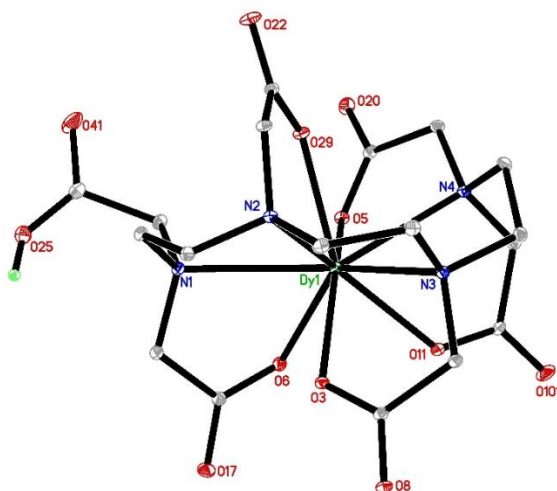


Figure 33. Molecular structure of the complex anion in  $(\text{NH}_4)_3[\text{HDyTTHA}](\text{NO}_3) \cdot 4\text{H}_2\text{O}$ .

The structure of this complex has some resemblance to those of HREE (Dy, Gd, Tb, Ho, Er) complexes with guanidinium as counterion previously reported

in the literature (Ruloff et al., 1997). Dysprosium atoms are nonacoordinated and bound to all nitrogen atoms in the ligand and to five single-bonded carboxylate oxygen atoms of the groups involved in complexation. The sixth group is unbound and protonated, which is a clear difference from the derivatives of LREE, where the coordination number is 10 and all carboxylate groups are normally involved in complexation (Mondry and Starynowicz, 1997).

### 6.5.2 Molecular insights into selective action of different complexonate functions.

The observed differences in uptake for different ligands and REE can be further understood from the X-ray single crystal structures of the complexes between REE and the different aminopolycarboxylic acids. Therefore we conducted an exhaustive study of the available literature in the matter, which together with the structure of the TTHA-Dy compound will help us understand the mechanisms. It must be kept in mind that their grafting reduces in one unit the number of carboxylic groups and that the crystal structures distinctly change with pH.

REE complexes with EDTA feature single anionic chelate structures at  $\text{pH} > 8$ , with coordination number 8 for HREE such as Er and Yb, forming  $[\text{M}(\text{EDTA})(\text{H}_2\text{O})_2]^-$  (Filippova et al., 1977). The coordination number increases to 9 already for Ho and all the lighter REE, showing  $[\text{M}(\text{EDTA})(\text{H}_2\text{O})_3]^-$  anionic units bound into dimers via coordination to two alkali-metal cations (Wang et al., 2008, Filippova et al., 1977, Liu et al., 2009).

The decrease in pH leads to a much denser packing due to the absence of negative charge (from 9-14 Å between REE atoms in anionic complexes to about 6.5 Å in “acidic” complexes) (You and Ng, 2007) (Figure 34). Part of the carboxylate groups become bridging between chelating units. For this acidic or neutral forms, there is also an apparent structural resolution with lower coordination number (8) for HREE such as Dy and Sm (Zhuang et al., 2010) and coordination number 9 for LREE such as Nd (Huang et al., 2008) and La (Xiong et al., 2007). The distance between the REE cations in these structures is about 6.3-6.6 Å, which fits very well with the distances between the grafting sites of ligands on the surface of sol-gel silica (Seisenbaeva et al., 2015). It seems then reasonable that when the acidic EDTA function is grafted onto  $\text{SiO}_2$  NPs and the adsorption occurs at neutral pH, there is an enhanced uptake capacity toward HREE. A contribution from other ligands for coordination becomes necessary and causes the “concerted action” derived selectivity previously described in Paper II (Polido Legaria et al., 2015).

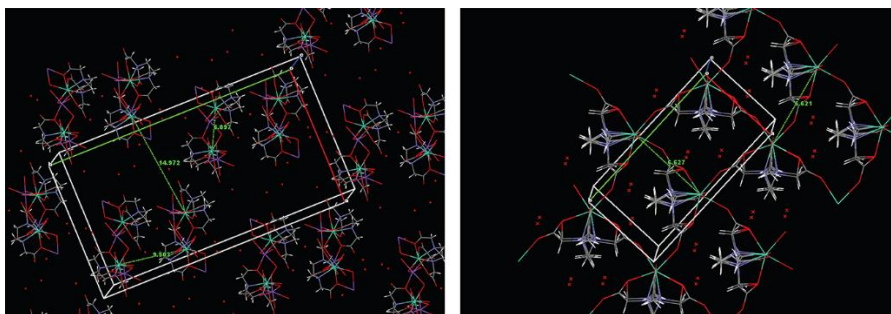


Figure 34. Crystal structures of  $\text{Na}[\text{Dy}(\text{EDTA})(\text{H}_2\text{O})_3] \cdot 5\text{H}_2\text{O}$  (left) and  $(\text{H}_3\text{O})[\text{Dy}(\text{EDTA})] \cdot \text{H}_2\text{O}$  (right). (You and Ng, 2007).

It is noteworthy to mention that the lanthanide contraction is not always manifested in the difference in coordination numbers or geometries. The discussion of REE complexes with complexonate ligands and especially EDTA in the literature, often assumes that the coordination is the same and therefore selectivity is rather low and depends only on the change in cation radii. This is true for relatively basic conditions ( $\text{pH} \geq 6.5$ ). The situation is different at  $\text{pH}$  below 6 and down to 4.5, where the difference in coordination numbers and geometries can be quite considerable and be the reason of the observed selectivity.

Complexes of REE with DTPA have never been synthesized in  $\text{pH}$  below 8. In our attempts to crystallize these compounds at  $\text{pH} \approx 6$ , we consequently obtained only the crystals of DTPA itself. In basic media, all REE reveal the same coordination number 9, in a tricapped trigonal prism coordination polyhedron. The complexes at very high  $\text{pH}$  feature the  $[\text{REE}(\text{DTPA})\text{H}_2\text{O}]_2^-$  anions, like in  $\text{K}_2[\text{Yb}(\text{DTPA})(\text{H}_2\text{O})] \cdot 7\text{H}_2\text{O}$  (Hardcastle et al., 2000), with inner sphere coordinated water molecules, while in the complexes at less basic  $\text{pH}$  the coordination sphere is completed with a carbonyl atom from a carboxylate group from another ligand, forming doubly bridged dimers like in  $(\text{NH}_4)_4[\text{Dy}_2(\text{DTPA})_2] \cdot 8\text{H}_2\text{O}$  (Figure 35) (Inomata et al., 2003). The only derivative reported at neutral  $\text{pH}$  revealed the same hydrated chelate anion construction with the difference that one carboxylic group becomes protonated and a large single charged aminoguanidinium cation was employed (Ruloff et al., 1998).

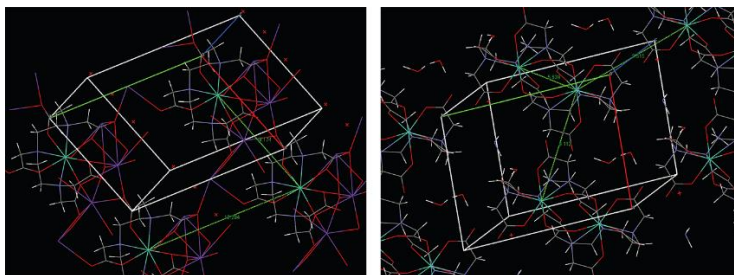


Figure 35. Crystal structures of  $K_2[Yb(DTPA)(H_2O)] \cdot 7H_2O$  (left) (Hardcastle et al., 2000) and  $(NH_4)_4[Dy_2(DTPA)_2] \cdot 8H_2O$  (right) (Inomata et al., 2003).

Grafted DTPA possesses only four carboxylate groups, which implies the need of sharing carboxylate groups to achieve sufficient filling of the coordination sphere, meaning that both chelation and concerted action will be involved.

For complexes of REE with TTHA, the whole pH range from 4.5 to 8 has been investigated. The different structures observed are related to both the size of the cations and the pH of the medium. The LREE (La, Pr, Nd) feature decacoordination with all four nitrogen and six anionic carboxylate oxygen atoms involved (Kim and Lee, 1999, Wang et al., 2006a, Mondry and Starynowicz, 1997). Heavier REE starting from Sm (Gao et al., 2011) until Yb (Wang et al., 2011) all display coordination number 9, since one carboxylate group is not attached to the central cation. The coordination polyhedron is in this case a monocapped Archimedes antiprism. In the structures obtained at basic pH, this group, deprotonated and with a negative charge, coordinates with the counterion, while at neutral pH it is protonated and uncharged (as determined in the solved structure presented in section 6.5.1). In the structures at lower pH for REEs ranging from Nd to Yb, one of the nitrogen atoms becomes protonated and the coordination is completed to 9 with two carboxylate oxygen atoms from the ligand chelated in a neighbouring complex (Figure 36) (Mondry and Starynowicz, 1998, Wang et al., 2006b). The coordination polyhedron transforms then into a tricapped trigonal prism.

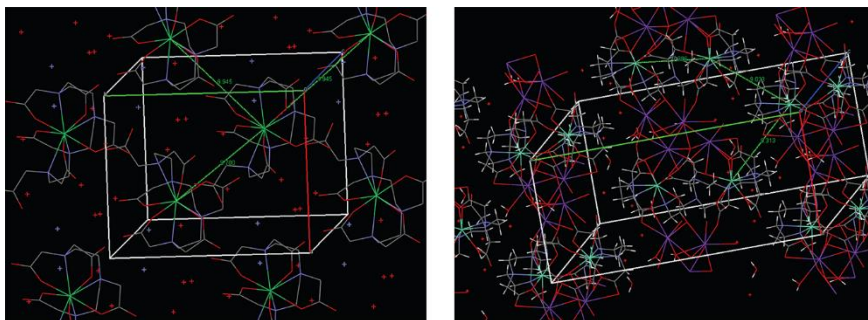


Figure 36. Crystal structures of  $K_3[\text{Dy}(\text{TTHA})] \cdot 5\text{H}_2\text{O}$  (right) and  $K_4[\text{Tb}_2(\text{HTTHA})_2] \cdot 14\text{H}_2\text{O}$  (left) (Wang et al., 2006b).

This suggests that, on the surface of nanoadsorbents with grafted TTHA, the chelating coordination is more stable for LREE, while for HREE a potential destabilization can be expected at lower pH, induced by the restructuring of the surface layer. A selectivity inverse to that observed for EDTA and IDA-grafted nanoadsorbents can be expected in this case.

Summarizing, the compiled studies imply that nanoadsorbents bearing IDA will undergo coordination of REE via concerted action of carboxylate ligands, in the EDTA-functionalized nanoadsorbents there will most likely combine concerted action and chelation, while chelation will be the predominant fashion for the DTPA- and TTHA- derived nanoadsorbents when the REE : L ratio is close to 1:1. This 1 : 1 REE : L ratio is achieved in desorption at pH = 3-4. These different coordination mechanisms give rise to the observed selectivity in adsorption and, especially in desorption, opening possibilities for selective extraction of REE.

## 6.6 Conclusions

In this part of the work, we have successfully identified three different aminopolycarboxylic acids (EDTA, DTPA and TTHA) that are commercially available and can be easily grafted on the surface of magnetic and non-magnetic SiO<sub>2</sub> NPs via a prior amination of the surface of SiO<sub>2</sub> by APTES. The resulting functional nanoadsorbents showed, not only excellent REE uptake capacities (up to 1.85 mmol REE/g), but even more interestingly, quite distinct selective REE extraction trends with separation factor of up to 70. We tried to understand this selectivity from a mechanistic point of view, like we did previously with IDA-derivative complexonates in Paper II. We succeeded to crystallize the compound from the coordination between TTHA and Dy<sup>3+</sup> and solved its structure, which together with an investigation to the existing literature gave very significant hints into the selective uptake of REE. The analyzed crystal structures suggested that, at neutral pH, EDTA-derived nanoadsorbents will feature coordination with REE via combined chelation and concerted action mechanisms, and therefore have a preference toward smaller REE (HREE), for the same reasons as described in Paper II for IDA. DTPA and TTHA-derived nanoadsorbents display chelation as the predominant mechanism for coordination with REE, resulting in a preference toward slightly lighter REE (like Nd<sup>3+</sup>), denoted as medium REE for distinction, for DTPA-derived nanoadsorbents and LREE (like La<sup>3+</sup>) for TTHA-derived ones.

This opens up great possibilities for tailoring of nanoadsorbents targeted to a specific REE or group of REE that can be potentially easily scaled up. The possibilities for upscaling are presented in the next and last work of this thesis.

## 7 Proof of concept: Evaluation of chromatographic applications for DTPA-functionalized SiO<sub>2</sub>-based adsorbents (Paper VI).

### 7.1 Background

Our previous work showed attractive opportunities for tailoring of adsorbents with ligands that are selective to a specific REE or group of REE. One of the remaining questions of the proposed technology is its applicability in industrial processes. For this, we studied the possibilities of upscaling the production of functional adsorbent materials using commercially available SiO<sub>2</sub> NPs and microparticles and exploring their potential in High-Performance Chelation Ion Chromatography (HPCIC). The use of magnetic particles in large scale would require special equipment that was not available for us. Therefore, we chose this readily available material and technique for evaluation. HPCIC is a flexible and inexpensive tool that has played an important role in individual separation of REE (Nash and Jensen, 2001, Santoyo and Verma, 2003, Roosen and Binnemans, 2014). It is a type of ion chromatography based on the formation and dissociation of complexes formed on the surface of a ligand-functionalized stationary phase (Wei et al., 2015, McGillicuddy et al., 2013a).

In this case, we chose DTPA as the first of the three aminopolycarboxylic acids studied, to be evaluated. DTPA is a chelating agent with important practical applications: it has been especially used for trivalent actinide-lanthanide separation (Braley et al., 2013, Nash, 2015, Johnson and Nash, 2015) but we have seen in our previous work that it is also applicable for REE separation. As silica-based starting material, we tested both silica NPs available

from Sigma-Aldrich (average size 20 nm) and mesoporous silica Kromasil® microparticles provided by AkzoNobel AB (average size 10 µm, average pore size 100Å). The latter ones are already functionalized with amino groups on their surface, which saves one step in the functionalization of the material.

The functionalized mesoporous Kromasil® silica particles were packed in a 4.6 mm x 250 mm column where the influence of temperature, eluent concentration, eluent flow rate and total sample load on the separation of a mixture of six REE ( $\text{La}^{3+}$ ,  $\text{Ce}^{3+}$ ,  $\text{Pr}^{3+}$ ,  $\text{Nd}^{3+}$ ,  $\text{Dy}^{3+}$  and  $\text{Y}^{3+}$ ) has been evaluated, as well as the long-term stability of the column.

## 7.2 Upscaling of the production of functional adsorbents.

### 7.2.1 DTPA-functionalization of $\text{SiO}_2$ NPs from Sigma-Aldrich.

Silica NPs with a specific surface area in the range from 175-225  $\text{m}^2\text{g}^{-1}$  and average diameter about 20 nm were acquired from Sigma-Aldrich. Their functionalization with DTPA requires prior amination of the surface of silica, which was done with APTES as explained in section 6.2. About 5 g of the  $\text{SiO}_2$  nanopowder were reacted with the corresponding amount of APTES (twice the stoichiometrically required amount for the creation of a monolayer) and after washing and drying of the particles, the amount of APTES attached was determined by TGA, to use this as a reference for the further reaction with DTPA. The reaction of  $\text{SiO}_2$ -APTES with DTPA was carried out in dry toluene as solvent and at 80°C. It is very important to control the temperature, since too high temperature can lead to destruction of the ligand DTPA by condensation. The procedure was repeated until a total production of 25 g of  $\text{SiO}_2$ -DTPA nanoparticles.

### 7.2.2 DTPA-functionalized Kromasil® silica particles.

Kromasil® silica particles are, as mentioned before, already amino-functionalized, therefore the functionalization can be made in just one-step reaction with DTPA. The reaction was carried out in dry toluene as solvent and at a controlled temperature of 80°C under  $\text{N}_2$  (g.) atmosphere. After washing and drying of the particles, the final amount of material obtained was around 20g.

## 7.3 Characterization of the adsorbents.

### 7.3.1 Thermogravimetric analysis.

TGA was used to quantify the degree of functionalization of the materials. The analyses were carried out in the range from 25 to 900°C at a heating rate of 5°C/min. For both silica nanoparticles and Kromasil® microparticles, the decomposition of the grafted DTPA ligand was associated with two thermal effects- a smaller weight loss at about 220°C, supposedly resulting from the partial decarboxylation of grafted DTPA, and a bigger loss at 340°C, corresponding to the degradation of the ligand and formation of residual carbon, which later burns out after 600°C. The organic material content was about 23% for SiO<sub>2</sub> NPs and 26% for Kromasil® microparticles<sup>6</sup>.

### 7.3.2 SEM, TEM and AFM imaging.

The morphology of the produced adsorbents was characterized by SEM, TEM and AFM microscopy. Figure 37 shows SEM and AFM analyses of Kromasil® microparticles. SEM images show uniform and smooth spheres, where it can be observed that the grafting of the ligands does not change the appearance of the particles. AFM images show a hierarchical structure built up of blocks with a diameter of about 20-30nm. The blocks are quite densely packed, revealing almost a dense packing in the cross-cut. No morphology change caused by the functionalization of the particles can be observed in either SEM or AFM.

The same preservation of the morphology and particle size was observed for the SiO<sub>2</sub> NPs by TEM (Figure 38). The nanoparticles, with an average size of 20 nm are aggregated in the form of randomly cross-linked chains. Their appearance remains unchanged after amination and grafting of DTPA. No visible transformation was visible either after sorption and release of REE.

---

6. TGA graphs are provided in Supplementary of Paper VI.

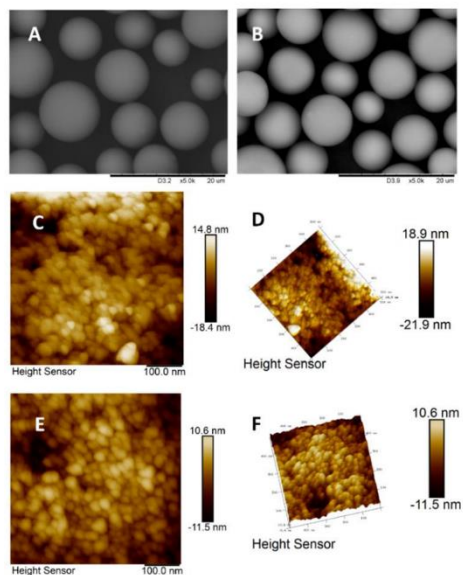


Figure 37. SEM (A-B) and AFM (C-F) images of Kromasil® microparticles (A, C and D correspond to pure Kromasil® and B,E, F to DTPA-functionalized Kromasil®)

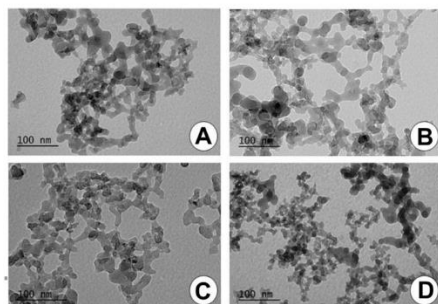


Figure 38. TEM images of A) DTPA-functionalized SiO<sub>2</sub> NPs; B) DTPA functionalized SiO<sub>2</sub> NPs bearing La<sup>3+</sup>, Nd<sup>3+</sup> and Dy<sup>3+</sup>; C) Acid treated DTPA-functionalized SiO<sub>2</sub> NPs (pH= 1.9) and D) Acid treated DTPA-functionalized SiO<sub>2</sub> NPs (pH=1.3).

The commercially available SiO<sub>2</sub> NPs were mostly used as models to test the production of bigger quantities of functional adsorbent and evaluate their efficiency in selective uptake of REE (see Paper VI), whereas the functionalized Kromasil® microparticles were used to fill chromatography columns and tested for chromatographic separation of REE, which will be discussed in the next section.

## 7.4 HPCIC evaluation of DTPA-functionalized Kromasil® column.

### 7.4.1 Isocratic and gradient elution.

In chromatography, isocratic elution means that the composition of the mobile phase remains constant, and it can have some advantages over gradient elution, such as the robustness, easy and straightforward application. Several isocratic experiments were carried out, but the obtained chromatograms (Figure 39) showed that it did not lead to separation of the six REE studied. Therefore, linear gradient elution was investigated, using  $\text{HNO}_3$  as the eluent with a concentration increasing linearly from zero to a final value in the range 0.1-0.24M. The column temperature was kept at  $55^\circ\text{C}$  and the mobile phase flow rate at  $1 \text{ mL min}^{-1}$ . The chromatogram (Figure 39 right) shows that a good overall separation can be achieved using relatively low  $\text{HNO}_3$  concentrations with a linear gradient elution process.

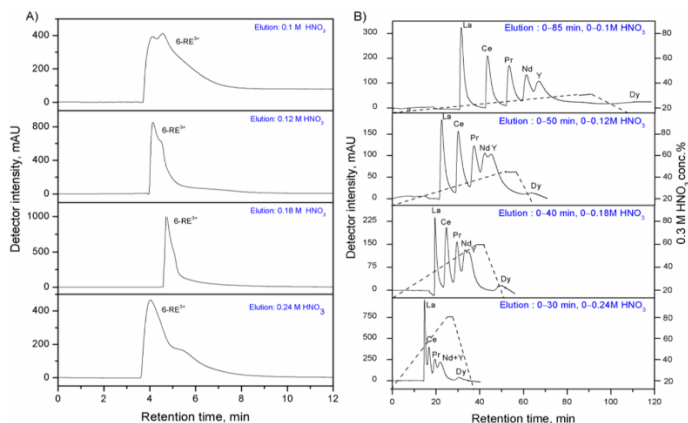
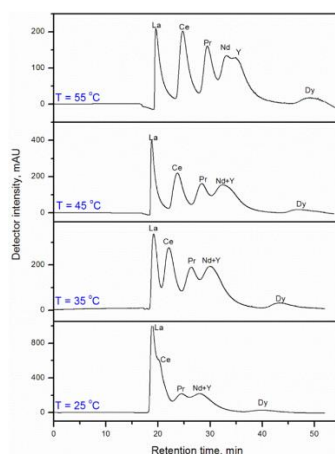


Figure 39. Chromatograms from A) isocratic and B) linear gradient elution studies at different concentrations of  $\text{HNO}_3$  in the eluent. Eluent flow rate =  $1 \text{ mL min}^{-1}$ , column temperature =  $55^\circ\text{C}$ , injected volume =  $50 \mu\text{L}$  and total REE concentration =  $1000 \text{ mg L}^{-1}$ .

In all runs,  $\text{Y}^{3+}$  co-eluted with  $\text{Nd}^{3+}$  before  $\text{Dy}^{3+}$  and the separation between them was difficult.

## 7.4.2 Influence of column temperature.

Previous studies have documented that the column temperature can influence on the retention and the separation of metal ions in HPCIC (Dybczyński et al., 2015). Additionally, a higher temperature can also reduce the pressure drop over the column (Dybczyński and Kulisa, 2005). Therefore, the effect of temperature on the retention and separation of REE was evaluated in the range 25-55°C, keeping the eluent linear gradient profile and flow rate unchanged (Figure 40). The chromatograms show that the overall peak resolution improves with temperature. At 25°C only a rudimentary separation could be achieved, while at 55°C there was a good separation between La<sup>3+</sup>, Ce<sup>3+</sup>, Pr<sup>3+</sup> and Dy<sup>3+</sup>, whereas Y<sup>3+</sup> and Nd<sup>3+</sup> partially co-eluted.



*Figure 40.* Chromatograms obtained at different column temperatures for linear gradient elution experiments (from 0M - 0.15M HNO<sub>3</sub> over 55 min). Eluent flow rate= 1 mL min<sup>-1</sup>, injected volume = 50μL, total REE concentration= 1000mg L<sup>-1</sup>.

## 7.4.3 Column efficiency and long-term stability.

The efficiency of a chromatography column is measured by the height of a theoretical plate (HETP), which for a column of a given length (L) results in a number of plates (N) equal to L/HETP. For an efficient separation between adjacent peaks, the band broadening, and hence the HETP, should be as low as possible. The efficiency depends on the flow rate, with a minimum in HETP at some optimum value. The effect of the eluent flow rate (in the range from 0.5-1.5 mL min<sup>-1</sup>) on the HETP was evaluated (calculated from the van Deemter equation –equation 2), as well as the retention factor.

$$HETP = \frac{L}{16} \left( \frac{W}{t_R} \right)^2 \quad (2)$$

L is the column length and W is the peak width. Figure 41 shows the obtained HETP, where it can be noticed that the HETP has an overall minimum at a flow rate of 0.8 mL min<sup>-1</sup>, and the column efficiency for all the evaluated REE decreases with increasing flow rate above this value.

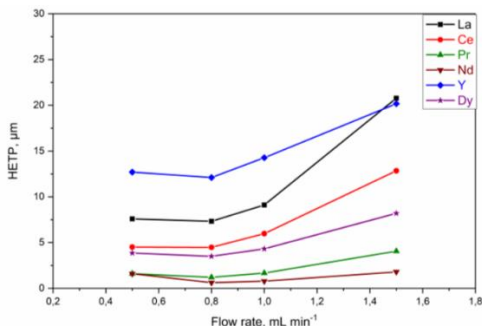


Figure 41. Effect of the eluent flow rate on the column efficiency (HETP) for La<sup>3+</sup>, Ce<sup>3+</sup>, Pr<sup>3+</sup>, Nd<sup>3+</sup>, Y<sup>3+</sup> and Dy<sup>3+</sup>, for linear gradient elution experiments (from 0M-0.15M HNO<sub>3</sub> over 55 min). Column temperature = 55°C, injected volume = 50μL, and total REE concentration = 1000 mg L<sup>-1</sup>.

In theory, the column efficiency can be increased by reducing the particle size, due to reduced diffusion and faster mass transfer. However, the pressure drop over a packed column is inversely proportional to the square of the particle diameter, hence a reduction in particle size can rapidly lead to requirements on the pump pressure that can be prohibitive for a scaled up process. Table 3 shows the optimum experimental conditions and the highest obtained efficiency compared against previously reported studies of REE separation by HPCIC. The results show that the proposed column is very competitive, with a relatively high efficiency considering the moderate temperature and pressure drop.

Table 20. Experimental parameters and column efficiency for some reported HPCIC REE separation studies and the present work.

Column specifications	Material and particle size	Temp. (°C)	Flow rate (mL/min)	Efficiency, N (m <sup>-1</sup> )
NTA gel functionalized macroporous hydrophilic resin column (Inoue et al., 1996)	(150 x 4.6 mm) GMA gel polymer resin (10 µm)	40	1.0	Not reported
IDA modified silica column (Nesterenko and Jones, 1998)	(250 x 4 mm) Silica particles (6µm)	65	0.8	12000
HEIDA modified core-shell silica column (McGillicuddy et al., 2013b)	(50 x 2.1 mm) Core-shell silica particles (1.7 µm)	70	0.8	200000
DTPA functionalized Kromasil silica column	(250 x 4.6 mm) Kromasil silica particles (10 µm)	55	1.0	400000

The long-term stability of the column was evaluated by comparing the change in retention times ( $t_R$ ) of REE after 54 experimental runs. Only a minor deterioration in the column performance was observed after 54 runs, with a 2% peak shift toward lower retention times, as shown in Figure 42.

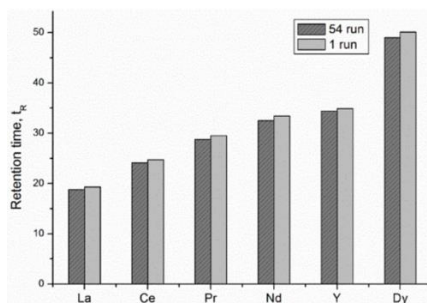
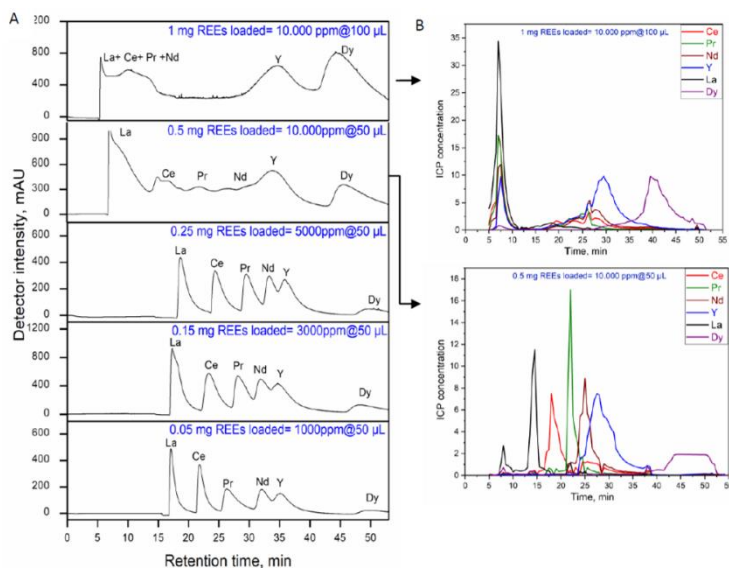


Figure 42. Comparison of retention times obtained for the six REE with a freshly packed column after 54 experimental runs.

#### 7.4.4 Column overloading.

For an economically viable process, it is necessary to be able to obtain a high productivity for a given degree of separation. Considering this, the response of the chromatographic process to an increasing sample load was investigated in a series of experiments. The total REE concentration was in the range of 1000 ppm to 10000 ppm, and the injected REE volume was 50  $\mu\text{L}$  or 100  $\mu\text{L}$ . All other experimental conditions were kept constant. The resulting chromatograms are shown in Figure 43 together with the ICP analyses of two fractions collected.



*Figure 43.* A) Chromatograms of experiments with increasing sample load, with linear gradient elution (0M-0.15M  $\text{HNO}_3$  over 55 min), eluent flow rate = 1  $\text{mL min}^{-1}$ , column temperature = 55  $^\circ\text{C}$ . B) ICP element-resolved fraction analysis of experiments with the highest total sample loads.

The chromatograms with total REE sample amounts between 0.05 and 0.25 mg are quite similar: the peaks appear at similar retention times and display similar shapes, with an overall good separation of REE. The chromatograms obtained at 0.5 mg and 1 mg total REE load are distinctly different, with peak displacements and triangular peak shapes characteristic of column overloading. The ICP graph shows, however, that the separation between most of the REE is still satisfactory at a total load of 0.5 mg, not being that the case for 1 mg total load, where ICP reveals that the separation is severely compromised.

Using this column under the evaluated conditions, the analyses suggest that the optimum productivity is located close to a total REE load of 0.25 mg per

cycle. For a 50 mm diameter pilot-scale column and a 1.2m diameter industrial scale column, this translates into 59 mg/cycle and 34g/cycle, respectively.

## 7.5 Conclusions

Functionalization of SiO<sub>2</sub>-based adsorbents has been successfully scaled up with commercially available SiO<sub>2</sub> nano- and microparticles. SiO<sub>2</sub> NPs of 20 nm in average size were acquired from Sigma-Aldrich and successfully functionalized with DTPA on their surface. These particles were fully characterized and used as models to ensure their efficiency for REE uptake. The SiO<sub>2</sub> microparticles (Kromasil®) were produced and provided by AkzoNobel AB, and after their DTPA-functionalization, they were further evaluated as new packing material for separation of REE by HPCIC technique. Several chromatographic parameters were evaluated and optimized, such as gradient elution, flow rate, temperature and column loading. Using a 4.6x250 mm lab-scale column, an optimal separation of La<sup>3+</sup>, Ce<sup>3+</sup>, Pr<sup>3+</sup>, Nd<sup>3+</sup> and Dy<sup>3+</sup> was achieved with a linear gradient elution from 0M to 0.15M HNO<sub>3</sub> over 55 min with an eluent flow rate of 1 mL min<sup>-1</sup> and a column temperature of 55°C up to a total load of 0.5 mg REE. The stability of the column was also evaluated and proved to perform reproducible separations for at least 54 runs. The material showed to be very promising for chromatographic separation of REE, and since their functionalization process is rather simple thanks to the fact that Kromasil® are already functionalized with amino groups on their surface, the particles can be functionalized with different ligands that have specific selectivities (as it has been studied in Paper V) and potentially build chromatographic columns with different selectivity.

## 8 Conclusions and future prospects.

This thesis work has focused on exploring the possibilities of SiO<sub>2</sub>-based nanoadsorbents for extraction and separation of REE, aiming to develop a technology that can meet the requirements from industry yet being efficient and environmentally friendlier than some of the currently used techniques.

The work started with the synthesis of optimal magnetic and non-magnetic SiO<sub>2</sub> nanoadsorbents and the search and synthesis of suitable organic ligands efficient for REE uptake that could be attached on their surface. Three organosilanes were successfully synthesized, characterized and grafted on the surface of the nanoadsorbents. These contained carboxylic (-COOH) and amine (-NH<sub>2</sub>) groups, in the view that these functional groups would participate in the chelation with REE. One of the three organosilanes, an IDA derivative, proved to be quite efficient for the uptake of REE, and what was even more interesting, it showed a clear preference toward HREE (Dy<sup>3+</sup>) upon desorption. This selectivity mechanism was further understood thanks to the structural studies of molecular model compounds with IDA and REE, which showed that, despite our initial hypothesis, the coordination of REE happens not via chelation, but via concerted action of the carboxylic groups of the ligands. The coordination complexes are then very distinct for each REE, with different coordination numbers and structures, and the observed selectivity could be explained based on that.

The next work arose from the attempt to involve the N atoms of the ligand in the coordination with REE. In the previous work we had seen that, with the adsorption conditions used (neutral pH), the N atoms are protonated and cannot play a role in chelation. Therefore, we modified the adsorption conditions (basic pH), expecting to double the previously achieved REE uptake. However, what we observed was a REE uptake up to 30 times higher than previously achieved. This huge increase in uptake was unforeseen and could not be explained by chelation, therefore we focused on unravelling this new mechanism by different

techniques and found out that the enhanced adsorption of REE was governed by an induced seeding of a crystalline phase of  $\text{REE}(\text{OH})_3$  on the surface of the nanoadsorbents. In this process, organic ligands are not crucial, simplifying thus its potential application to industry. The process proved to be, at least preliminarily, very efficient with leachate solutions from actual REE ores, showing that the nanoadsorbents can be selective to the sum of REE, without taking up other unwanted elements that commonly appear in REE ores, like iron or calcium.

The final stage of the thesis was devoted to increasing selectivity toward REE and upscaling. For the first point, we studied a series of three aminopolycarboxylic acids (EDTA, DTPA and TTHA) that could be easily attached onto the surface of the nanoadsorbents and evaluated their efficiency. Our previous structural study on REE : IDA model compounds had revealed that the coordination was specific for each REE cation and this led to different selectivities, which made us think that the ligand has most likely an influence in this as well. We identified indeed rather specific preferences for different groups of REE: EDTA-functionalized nanoadsorbents showed preference toward HREE, DTPA-functionalized nanoadsorbent toward MREE and TTHA-functionalized nanoadsorbent toward LREE. The reasons for this observed selectivity were found one more time thanks to model compounds structural studies.

As for upscaling, commercially available  $\text{SiO}_2$  NPs (Sigma-Aldrich) and microparticles (Kromasil®, Akzo Nobel AB) were successfully functionalized with DTPA up to several dozens of grams. The latter were evaluated as packing material for chromatographic separation of REE by HPCIC technique. DTPA-functionalized Kromasil®  $\text{SiO}_2$  microparticles proved to be very efficient for the separation of a mixture of six REE and competed quite favorably against other packing materials used for HPCIC.

In the future, more chromatographic tests could be performed with the other type of ligands that have been studied at lab scale, since it can potentially offer to build specific chromatographic columns for a certain group of REE.

The process of  $\text{REE}(\text{OH})_3$  induced seeding by nanoadsorbents should also be tested on real leachates on a bigger scale, to confirm all the possibilities that it can bring for the industrial extraction and separation of REE.

## References

- A.KAVOSI; F. FARIDBOD; GANJALI, M. R. 2015. Solid Phase Extraction of Some Lanthanide Ions by Functionalized SBA-15 from Environmental Samples. *International Journal of Environmental Research*, 9, 8.
- ABBAS, M., RAO, B. P., ISLAM, M. N., NAGA, S. M., TAKAHASHI, M. & KIM, C. 2014. Highly stable- silica encapsulating magnetite nanoparticles (Fe<sub>3</sub>O<sub>4</sub>/SiO<sub>2</sub>) synthesized using single surfactantless- polyol process. *Ceramics International*, 40, 1379-1385.
- ABSALAN, G., ASADI, M., KAMRAN, S., SHEIKHIAN, L. & GOLTZ, D. M. 2011. Removal of reactive red-120 and 4-(2-pyridylazo) resorcinol from aqueous samples by Fe<sub>3</sub>O<sub>4</sub> magnetic nanoparticles using ionic liquid as modifier. *J Hazard Mater*, 192, 476-84.
- AI, H., FLASK, C., WEINBERG, B., SHUAI, X., PAGEL, M. D., FARRELL, D., DUERK, J. & GAO, J. 2005. Magnetite-loaded polymeric micelles as ultrasensitive magnetic-resonance probes. *Advanced Materials*, 17, 1949-1952.
- AL-SAYARI, S., CARLEY, A. F., TAYLOR, S. H. & HUTCHINGS, G. J. 2007. Au/ZnO and Au/Fe<sub>2</sub>O<sub>3</sub> catalysts for CO oxidation at ambient temperature: Comments on the effect of synthesis conditions on the preparation of high activity catalysts prepared by coprecipitation. *Topics in Catalysis*, 44, 123-128.
- ALAMMAR, T., CYBINSKA, J., CAMPBELL, P. S. & MUDRING, A.-V. 2016. Sonochemical synthesis of highly luminescent Ln<sub>2</sub>O<sub>3</sub>:Eu<sup>3+</sup> (Y, La, Gd) nanocrystals. *Journal of Luminescence*, 169, 587-593.
- ALMEIDA, S. D. N. & TOMA, H. E. 2016. Neodymium(III) and lanthanum(III) separation by magnetic nanohydrometallurgy using DTPA functionalized magnetite nanoparticles. *Hydrometallurgy*, 161, 22-28.
- ALONSO, E., SHERMAN, A. M., WALLINGTON, T. J., EVERSON, M. P., FIELD, F. R., ROTH, R. & KIRCHAIN, R. E. 2012. Evaluating Rare Earth Element Availability: A Case with Revolutionary Demand from Clean Technologies. *Environmental Science & Technology*, 46, 3406-3414.
- ANDRES, J. & CHAUVIN, A.-S. 2011. Lanthanides: Luminescence Applications. *Encyclopedia of Inorganic and Bioinorganic Chemistry*. John Wiley & Sons, Ltd.
- ANIKINA, L. I. & KARYAKIN, A. V. 1964. LUMINESCENCE OF THE RARE-EARTH ELEMENTS AND ITS APPLICATIONS IN ANALYTICAL CHEMISTRY. *Russian Chemical Reviews*, 33, 571.
- ARCE, V. B., GARGARELLO, R. M., ORTEGA, F., ROMANANO, V., MIZRAHI, M., RAMALLO-LOPEZ, J. M., COBOS, C. J., AIROLDI, C., BERNARDELLI, C., DONATI, E. R. & MARTIRE, D. O. 2015. EXAFS and DFT study of the cadmium and lead adsorption on modified silica nanoparticles. *Spectrochimica Acta Part a-Molecular and Biomolecular Spectroscopy*, 151, 156-163.
- ARIGA, K., ITO, H., HILL, J. P. & TSUKUBE, H. 2012. Molecular recognition: from solution science to nano/materials technology. *Chemical Society Reviews*, 41, 5800-5835.
- AZHAR UDDIN, M., TSUDA, H., WU, S. & SASAOKA, E. 2008. Catalytic decomposition of biomass tars with iron oxide catalysts. *Fuel*, 87, 451-459.
- BABAI, A., KOPIEC, G., LACKMANN, A., MALLICK, B., PITULA, S., TANG, S. & MUDRING, A.-V. 2014. Eu<sup>3+</sup> as a dual probe for the determination of IL anion donor power: A

- combined luminescence spectroscopic and electrochemical approach. *Journal of Molecular Liquids*, 192, 191-198.
- BADRUDDOZA, A. Z. M., SHAWON, Z. B. Z., TAY, W. J. D., HIDAJAT, K. & UDDIN, M. S. 2013. Fe<sub>3</sub>O<sub>4</sub>/cyclodextrin polymer nanocomposites for selective heavy metals removal from industrial wastewater. *Carbohydrate Polymers*, 91, 322-332.
- BALCI, M. 2005. *Basic 1H- and 13C-NMR Spectroscopy*, Elsevier.
- BAUTISTA, F. M., CAMPELO, J. M., LUNA, D., MARINAS, J. M., QUIRÓS, R. A. & ROMERO, A. A. 2007. Screening of amorphous metal-phosphate catalysts for the oxidative dehydrogenation of ethylbenzene to styrene. *Applied Catalysis B: Environmental*, 70, 611-620.
- BINNEMANS, K. 2015. Rare Earths: essential elements for the transition to a low-carbon economy. *Bauxite Residue Valorisation and Best Practices Conference*. Leuven.
- BITAR, A., AHMAD, N. M., FESSI, H. & ELAISSARI, A. 2012. Silica-based nanoparticles for biomedical applications. *Drug Discovery Today*, 17, 1147-1154.
- BRALEY, J. C., MCALISTER, D. R., HORWITZ, E. P. & NASH, K. L. 2013. Explorations Of Talspeak Chemistry In Extraction Chromatography: Comparisons of TTHA with DTPA and HDEHP with HEH EHP. *Solvent Extraction and Ion Exchange*, 31, 107-121.
- BRITISH GEOLOGICAL SURVEY 2011. Rare Earth Elements.
- BUNZLI, J. C. G., COMBY, S., CHAUVIN, A. S. & VANDEVYVER, C. D. B. 2007. New opportunities for lanthanide luminescence. *Journal of Rare Earths*, 25, 257-274.
- BÜNZLI, J.-C. G. & PIGUET, C. 2002. Lanthanide-Containing Molecular and Supramolecular Polymetallic Functional Assemblies. *Chemical Reviews*, 102, 1897-1928.
- CALVIN, S. 2013. XAFS for Everyone. In: PRESS, C. (ed.) *XAFS for Everyone*.
- CAPELLO, C., FISCHER, U. & HUNGERBUHLER, K. 2007. What is a green solvent? A comprehensive framework for the environmental assessment of solvents. *Green Chemistry*, 9, 927-934.
- CAREY, F. A. & SUNDBERG, R. J. 2007. *Advanced Organic Chemistry: Part B: Reaction and Synthesis*
- CARRON, S., BLOEMEN, M., VANDER ELST, L., LAURENT, S., VERBIEST, T. & PARAC-VOGT, T. N. 2016. Ultrasmall Superparamagnetic Iron Oxide Nanoparticles with Europium(III) DO3A as a Bimodal Imaging Probe. *Chemistry-a European Journal*, 22, 4521-4527.
- CHEN, Y., QIAN, H., WU, F. & ZHOU, J. 2011. Clearance and recovery of Cd(II) from aqueous solution by magnetic separation technology. *Chemosphere*, 83, 1214-9.
- CLARAMUNT, R. M., ELGUERO, J., HERRANZ, F., PINILLA, E., SANTA MARIA, M. D. & TORRES, M. R. 2005. Molecular recognition of biotin, barbital and tolbutamide with new synthetic receptors.
- CONDOMITTI, U., ZUIN, A., SILVEIRA, A. T., ARAKI, K. & TOMA, H. E. 2012. Magnetic nanohydrometallurgy: A promising nanotechnological approach for metal production and recovery using functionalized superparamagnetic nanoparticles. *Hydrometallurgy*, 125, 148-151.
- CORNELL, R. M. & SCHWERTMANN, U. 2003. *The iron oxides: structure, properties, reactions, occurrences and uses*, Weinheim, Germany, WILEY-VCH Verlag GMBH & Co. KGaA.
- DASARI, S., SINGH, S., SIVAKUMAR, S. & PATRA, A. K. 2016. Dual-Sensitized Luminescent Europium(III) and Terbium(III) Complexes as Bioimaging and Light-Responsive Therapeutic Agents. *Chemistry-a European Journal*, 22, 17387-17396.
- DAVIS, M. E. 2002. Ordered porous materials for emerging applications. *Nature*, 417, 813.
- DIETZ, M. L. 2006. Ionic Liquids as Extraction Solvents: Where do We Stand? *Separation Science and Technology*, 41, 2047-2063.
- DUDARKO, O. A., GONCHARIK, V. P., SEMENII, V. Y. & ZUB, Y. L. 2008. Sorption of Hg<sup>2+</sup>, Nd<sup>3+</sup>, Dy<sup>3+</sup>, and UO<sub>2</sub><sup>2+</sup> ions at polysiloxane xerogels functionalized with phosphonic acid derivatives. *Protection of Metals*, 44, 193-197.
- DUNN, P. J. 2012. The importance of Green Chemistry in Process Research and Development. *Chemical Society Reviews*, 41, 1452-1461.
- DUPONT, D., BRULLOT, W., BLOEMEN, M., VERBIEST, T. & BINNEMANS, K. 2014. Selective Uptake of Rare Earths from Aqueous Solutions by EDTA-Functionalized Magnetic and Nonmagnetic Nanoparticles. *ACS Applied Materials & Interfaces*, 6, 4980-4988.

- DUTTA, D., THAKUR, D. & BAHADUR, D. 2015. SnO<sub>2</sub> quantum dots decorated silica nanoparticles for fast removal of cationic dye (methylene blue) from wastewater. *Chemical Engineering Journal*, 281, 482-490.
- DYBCZYŃSKI, R. & KULISA, K. 2005. Effect of Temperature and the Mechanism of Zone Spreading During Cation-Exchange Separation of Rare Earth Elements by Ion Chromatography. *Chromatographia*, 61, 573-580.
- DYBCZYŃSKI, R. S., KULISA, K., PYSZYŃSKA, M. & BOJANOWSKA-CZAJKA, A. 2015. New reversed phase-high performance liquid chromatographic method for selective separation of yttrium from all rare earth elements employing nitrilotriacetate complexes in anion exchange mode. *Journal of Chromatography A*, 1386, 74-80.
- EARLE, M. J. & SEDDON, K. R. 2002. Ionic Liquids: Green Solvents for the Future. *Clean Solvents*. American Chemical Society.
- EFYTHYMOS BALOMENOS, E. D., JASON YANG, DIMITRIS PANIAS, BERND FRIEDRICH, KOEN BINNEMANS, GULAIM SEISENBAEVA, CARSTEN DITTRICH, PER KALVIG, IOANNIS PASPALIARIS 2017. The EURARE Project: Development of a Sustainable Exploitation Scheme for Europe's Rare Earth ore Deposits. *Johnson Matthey Technol. Rev.*, 61.
- EL-SOFANY, E. A. 2008. Removal of lanthanum and gadolinium from nitrate medium using Aliquat-336 impregnated onto Amberlite XAD-4. *J Hazard Mater*, 153, 948-54.
- EURARE. 2013. *Development of a sustainable exploitation scheme for Europe's Rare Earth ore deposits* [Online]. Available: <http://www.eurare.eu/> [Accessed].
- EUROPEAN COMMISSION 2010. Critical Raw Materials for the EU. Report of the Ad-hoc Working group on Defining Critical Raw Materials. . *European Commission, Enterprise and Industry*
- EUROPEAN COMMISSION, E. 2014. Report on Critical Raw Materials for the EU. *DG Enterprise & Industry*.
- FANG, Z., QIU, X., CHEN, J. & QIU, X. 2011a. Degradation of the polybrominated diphenyl ethers by nanoscale zero-valent metallic particles prepared from steel pickling waste liquor. *Desalination*, 267, 34-41.
- FANG, Z., QIU, X., HUANG, R., QIU, X. & LI, M. 2011b. Removal of chromium in electroplating wastewater by nanoscale zero-valent metal with synergistic effect of reduction and immobilization. *Desalination*, 280, 224-231.
- FILIPPOVA, T. V., POLYNOVA, T. N., ILINSKII, A. L., PORAIKOSHITS, M. A. & MARTYNYENKO, L. I. 1977. CRYSTAL-STRUCTURE OF PENTAHYDRATE AMMONIUM SALT OF ERBIUM(III) ETHYLENEDIAMINETETRAACETATE. *Journal of Structural Chemistry*, 18, 895-896.
- FLOREK, J., MUSHTAQ, A., LARIVIERE, D., CANTIN, G., FONTAINE, F.-G. & KLEITZ, F. 2015. Selective recovery of rare earth elements using chelating ligands grafted on mesoporous surfaces. *RSC Advances*, 5, 103782-103789.
- FRANVILLE, A. C., ZAMBON, D., MAHIOU, R., CHOU, S., TROIN, Y. & COUSSEINS, J. C. 1998. Synthesis and optical features of an europium organic-inorganic silicate hybrid. *Journal of Alloys and Compounds*, 275-277, 831-834.
- GAO, J. Q., LI, D., WANG, J., JIN, X. D., WU, T., LI, K., KANG, P. L. & ZHANG, X. D. 2011. Syntheses, structural determination, and binding studies of mononuclear nine-coordinate (enH<sub>2</sub>)[SmIII(egta)(H<sub>2</sub>O)]<sub>2</sub> · 6H<sub>2</sub>O and 2-D ladder-like nine-coordinate (enH<sub>2</sub>)<sub>1.5</sub>[SmIII(ttha)] · 4.5H<sub>2</sub>O. *J. Coord. Chem.*, 64, 2234.
- GEUS 2017. Road map for free material supply autonomy in europe.
- GHANDI, K. 2014. A Review of Ionic Liquids, Their Limits and Applications. *Green and Sustainable Chemistry*, Vol.04No.01, 10.
- GHERNAOUT, D., GHERNAOUT, B. & NACEUR, M. W. 2011. Embodying the chemical water treatment in the green chemistry—A review. *Desalination*, 271, 1-10.
- GONZALES, M. & KRISHNAN, K. M. 2005. Synthesis of magnetoliposomes with monodisperse iron oxide nanocrystal cores for hyperthermia. *Journal of Magnetism and Magnetic Materials*, 293, 265-270.
- GUPTA, A. K. & GUPTA, M. 2005. Synthesis and surface engineering of iron oxide nanoparticles for biomedical applications. *Biomaterials*, 26, 3995-4021.
- GUPTA, C. K. & KRISHNAMURTHY, N. 2004. *Extractive Metallurgy of Rare Earths*, CRC Press.
- HARDCASTLE, K. I., BOTTA, M., FASANO, M. & DIGILIO, G. 2000. Experimental Evidence for a Second Coordination Sphere Water Molecule in the Hydration Structure of YbDTPA –

- Insights for a Re-Assessment of the Relaxivity Data of GdDTPA. *Eur. J. Inorg. Chem.*, 2000, 971.
- HAXEL, G. B., HEDRICK, J. B. & ORIS, G. J. 2002. US. Geological survey.
- HE, C. S., REN, L., ZHU, W. P., XU, Y. F. & QIAN, X. H. 2015. Removal of mercury from aqueous solution using mesoporous silica nanoparticles modified with polyamide receptor. *Journal of Colloid and Interface Science*, 458, 229-234.
- HENRIQUES, C. 2012. Catalysis by Zeolites. EUCHEME.
- HUANG, X. H., XU, X. H., PAN, W. B. & ZENG, R. H. 2008. Poly[aqua- $[\mu\text{-N}^{\prime}$ - (carboxymethyl)ethylene-diamine--N,N,N'-triacetato]neodymium(III)]. *Acta Crystallogr Sect E Struct Rep Online*, 64, m1194.
- IM, S. H., HERRICKS, T., LEE, Y. T. & XIA, Y. 2005. Synthesis and characterization of monodisperse silica colloids loaded with superparamagnetic iron oxide nanoparticles. *Chemical Physics Letters*, 401, 19-23.
- INOMATA, Y., SUNAKAWA, T. & HOWELL, F. S. 2003. The syntheses of lanthanide metal complexes with diethylenetriamine-N,N,N',N''-pentaacetic acid and the comparison of their crystal structures. *Journal of Molecular Structure*, 648, 81-88.
- INOUE, Y., KUMAGAI, H., SHIMOMURA, Y., YOKOYAMA, T. & SUZUKI, T. M. 1996. Ion Chromatographic Separation of Rare-Earth Elements Using a Nitrotriacetate-Type Chelating Resin as the Stationary Phase. *Analytical Chemistry*, 68, 1517-1520.
- IRAM, M., GUO, C., GUAN, Y., ISHFAQ, A. & LIU, H. 2010. Adsorption and magnetic removal of neutral red dye from aqueous solution using Fe<sub>3</sub>O<sub>4</sub> hollow nanospheres. *Journal of Hazardous Materials*, 181, 1039-1050.
- IUPAC 2005. *Nomenclature of Inorganic Chemistry. IUPAC Recommendations 2005.*, Cambridge, UK.
- IZATT, N. E., BRUENING, R. L., KRAKOWIAK, K. E. & IZATT, S. R. 2000. Contributions of Professor Reed M. Izatt to Molecular Recognition Technology: From Laboratory to Commercial Application. *Industrial & Engineering Chemistry Research*, 39, 3405-3411.
- IZATT, S. R., MCKENZIE, J. S., BRUENING, R. L., IZATT, R. M., IZATT, N. E. & KRAKOWIAK, K. E. 2016. Selective Recovery of Platinum Group Metals and Rare Earth Metals from Complex Matrices Using a Green Chemistry/Molecular Recognition Technology Approach. *Metal Sustainability*. John Wiley & Sons, Ltd.
- JIANG, J. Z., ZOU, J., ZHU, L. H., HUANG, L., JIANG, H. P. & ZHANG, Y. X. 2011. Degradation of Methylene Blue with H<sub>2</sub>O<sub>2</sub> Activated by Peroxidase-Like Fe(3)O(4) Magnetic Nanoparticles. *Journal of Nanoscience and Nanotechnology*, 11, 4793-4799.
- JIN, T., INOUE, S., MACHIDA, K. & ADACHI, G. 1997. Photovoltaic cell characteristics of hybrid silicon devices with lanthanide complex phosphor-coating film. *Journal of the Electrochemical Society*, 144, 4054-4058.
- JOHNSON, A. T. & NASH, K. L. 2015. MIXED MONOFUNCTIONAL EXTRACTANTS FOR TRIVALENT ACTINIDE/LANTHANIDE SEPARATIONS: TALSPK-MME. *Solvent Extraction and Ion Exchange*, 33, 642-655.
- JULIE KLINGER 2016. Rare Earth Elements. In: KLINGER, J. (ed.) *Generation Anthropocene*.
- JURGONS, R., SELIGER, C., HILPERT, A., TRAHMS, L., ODENBACH, S. & ALEXIOU, C. 2006. Drug loaded magnetic nanoparticles for cancer therapy. *Journal of Physics Condensed Matter*, 18, S2893-S2902.
- KANAZAWA, Y. & KAMITANI, M. 2006. Rare earth minerals and resources in the world. *Journal of Alloys and Compounds*, 408-412, 1339-1343.
- KIM, C.-H. & LEE, S.-G. 1999. Crystal Structure and Thermal Properties of the Lanthanum(III) Complex with Triethylenetetraaminehexaacetic Acid: K<sub>3</sub>La(TTHA)]·5H<sub>2</sub>O. *Bulletin of the Korean Chemical Society*, 20, 417-421.
- KUMAR, M. 1994. Recent trends in chromatographic procedures for separation and determination of rare earth elements. A review. *Analyst*, 119, 2013-2024.
- LARSSON, K. & BINNEMANS, K. 2015. Separation of rare earths by split-anion extraction. *Hydrometallurgy*, 156, 206-214.
- LARSSON, K. & BINNEMANS, K. 2017. Separation of Rare Earths by Solvent Extraction with an Undiluted Nitrate Ionic Liquid. *Journal of Sustainable Metallurgy*, 3, 73-78.
- LEE, H., SHAO, H., HUANG, Y. & KWAK, B. 2005. Synthesis of MRI contrast agent by coating superparamagnetic iron oxide with chitosan. *IEEE Transactions on Magnetics*, 41, 4102-4104.

- LI, C., SHEN, Y., JIA, M., SHENG, S., ADEBAJO, M. O. & ZHU, H. 2008. Catalytic combustion of formaldehyde on gold/iron-oxide catalysts. *Catalysis Communications*, 9, 355-361.
- LIYOU, T.-H. 2004. Preparation and characterization of nano-structured silica from rice husk. *Materials Science and Engineering: A*, 364, 313-323.
- LIU, B., HU, P., WANG, J., XU, R., ZHANG, L. Q., GAO, J., WANG, Y. F. & ZHANG, X. D. 2009. Synthesis and Structures of Nine-Coordinate K[SmIII(Edta)(H<sub>2</sub>O)<sub>3</sub>] · 2H<sub>2</sub>O and Ten-Coordinate K<sub>2</sub>[SmIII(Pdta)(H<sub>2</sub>O)<sub>2</sub>]<sub>2</sub> · 4.5H<sub>2</sub>O Complexes. *Russ. J. Coord. Chem.*, 35, 758.
- LU, A.-H., SALABAS, E. L. & SCHÜTH, F. 2007a. Magnetic Nanoparticles: Synthesis, Protection, Functionalization, and Application. *Angewandte Chemie International Edition*, 46, 1222-1244.
- LU, C.-W., HUNG, Y., HSIAO, J.-K., YAO, M., CHUNG, T.-H., LIN, Y.-S., WU, S.-H., HSU, S.-C., LIU, H.-M., MOU, C.-Y., YANG, C.-S., HUANG, D.-M. & CHEN, Y.-C. 2007b. Bifunctional Magnetic Silica Nanoparticles for Highly Efficient Human Stem Cell Labeling. *Nano Letters*, 7, 149-154.
- LÜBBE, A. S., BERGEMANN, C., BROCK, J. & MCCLURE, D. G. 1999. Physiological aspects in magnetic drug-targeting. *Journal of Magnetism and Magnetic Materials*, 194, 149-155.
- MAJEWSKI, P. 2008. *Maghemite* [Online]. Encyclopaedia Britannica Online: Encyclopaedia Britannica Online. Available: <http://search.eb.com/eb/article-9049986> [Accessed].
- MAJEWSKI, P. & THIERRY, B. 2007. Functionalized Magnetite Nanoparticles—Synthesis, Properties, and Bio-Applications. *Critical Reviews in Solid State and Materials Sciences*, 32, 203-215.
- MARTIN, K. R. 2007. The chemistry of silica and its potential health benefits. *J Nutr Health Aging*, 11, 94-7.
- MARTÍNEZ-MERA, I., ESPINOSA-PESQUEIRA, M. E., PÉREZ-HERNÁNDEZ, R. & ARENAS-ALATORRE, J. 2007. Synthesis of magnetite (Fe<sub>3</sub>O<sub>4</sub>) nanoparticles without surfactants at room temperature. *Materials Letters*, 61, 4447-4451.
- MASSARI, S. & RUBERTI, M. 2013. Rare earth elements as critical raw materials: Focus on international markets and future strategies. *Resources Policy*, 38, 36-43.
- MATERNE, T., DE BUYL, F., WITUCKI, G. L. 2004. Organosilane Technology in Coating Applications: Review and Perspectives. Dow Corning S.A. .
- MCGILLICUDDY, N., NESTERENKO, E. P., NESTERENKO, P. N., JONES, P. & PAULL, B. 2013a. Chelation ion chromatography of alkaline earth and transition metals a using monolithic silica column with bonded N-hydroxyethyliminodiacetic acid functional groups. *Journal of Chromatography A*, 1276, 102-111.
- MCGILLICUDDY, N., NESTERENKO, E. P., NESTERENKO, P. N., STACK, E. M., OMAMOGHO, J. O., GLENNON, J. D. & PAULL, B. 2013b. A new N-hydroxyethyliminodiacetic acid modified core-shell silica phase for chelation ion chromatography of alkaline earth, transition and rare earth elements. *Journal of Chromatography A*, 1321, 56-64.
- MELNYK, I., GONCHARYK, V., STOLYARCHUK, N., KOZHARA, L., LUNOCHKINA, A., ALONSO, B. & ZUB, Y. 2012. Dy(III) sorption from water solutions by mesoporous silicas functionalized with phosphonic acid groups. *Journal of Porous Materials*, 19, 579-585.
- MELNYK, I. V. & ZUB, Y. L. 2012. Preparation and characterization of magnetic nanoparticles with bifunctional surface layer ≡Si(CH<sub>2</sub>)<sub>3</sub>NH<sub>2</sub>/≡SiCH<sub>3</sub> (or ≡SiC<sub>3</sub>H<sub>7</sub>-n). *Microporous and Mesoporous Materials*, 154, 196-199.
- MOHAPATRA, P. K., LAKSHMI, D. S., BHATTACHARYYA, A. & MANCHANDA, V. K. 2009. Evaluation of polymer inclusion membranes containing crown ethers for selective cesium separation from nuclear waste solution. *Journal of Hazardous Materials*, 169, 472-479.
- MONDRY, A. & STARYNOWICZ, P. 1997. Crystal Structure and Absorption Spectroscopy of a Neodymium(III) Complex with Triethylenetetraaminehexaacetic Acid, Na<sub>3</sub>[Nd(TTHA)] · 2.5NaClO<sub>4</sub> · 7.617H<sub>2</sub>O. *Inorganic Chemistry*, 36, 1176-1180.
- MONDRY, A. & STARYNOWICZ, P. 1998. Crystal structure and absorption spectroscopy of a dimeric neodymium(III) complex with triethylenetetraaminehexaacetic acid (H<sub>6</sub>ttha), Na<sub>0.5</sub>H<sub>5.5</sub>[Nd<sub>2</sub>(ttha)<sub>2</sub>] · 7.5NaClO<sub>4</sub> · 16.83H<sub>2</sub>O. *J. Chem. Soc., Dalton Trans.*, 859.
- NAGAO, D., OSUZU, H., YAMADA, A., MINE, E., KOBAYASHI, Y. & KONNO, M. 2004. Particle formation in the hydrolysis of tetraethyl orthosilicate in pH buffer solution. *Journal of Colloid and Interface Science*, 279, 143-149.
- NASH, K. L. 2015. The Chemistry of TALSPEAK: A Review of the Science. *Solvent Extraction and Ion Exchange*, 33, 1-55.

- NASH, K. L. & JENSEN, M. P. 2001. ANALYTICAL-SCALE SEPARATIONS OF THE LANTHANIDES: A REVIEW OF TECHNIQUES AND FUNDAMENTALS. *Separation Science and Technology*, 36, 1257-1282.
- NASSAR, N. N. 2010. Rapid removal and recovery of Pb(II) from wastewater by magnetic nanoadsorbents. *Journal of Hazardous Materials*, 184, 538-546.
- NAZAROV, M. & NOH, D. Y. 2010. Rare earth double activated phosphors for different applications. *Journal of Rare Earths*, 28, 1-11.
- NESTERENKO, P. N. & JONES, P. 1998. Isocratic separation of lanthanides and yttrium by high-performance chelation ion chromatography on iminodiacetic acid bonded to silica. *Journal of Chromatography A*, 804, 223-231.
- PENG, C., ZHANG, H., YU, J., MENG, Q., FU, L., LI, H., SUN, L. & GUO, X. 2005. Synthesis, Characterization, and Luminescence Properties of the Ternary Europium Complex Covalently Bonded to Mesoporous SBA-15. *The Journal of Physical Chemistry B*, 109, 15278-15287.
- POGORILYI, R. P., MELNYK, I. V., ZUB, Y. L., CARLSON, S., DANIEL, G., SVEDLINDH, P., SEISENBAEVA, G. A. & KESSLER, V. G. 2014. New product from old reaction: uniform magnetite nanoparticles from iron-mediated synthesis of alkali iodides and their protection from leaching in acidic media. *Rsc Advances*, 4, 22606-22612.
- POLIDO, E. 2016. *Hybrid Nanoadsorbents for Extraction and Separation of Rare Earth Elements in Solution*. Licentiate Thesis, Swedish University of Agricultural Sciences.
- POLIDO LEGARIA, E., TOPEL, S. D., KESSLER, V. G. & SEISENBAEVA, G. A. 2015. Molecular insights into the selective action of a magnetically removable complexone-grafted adsorbent. *Dalton Transactions*, 44, 1273-1282.
- POPAT, A., HARTONO, S. B., STAHR, F., LIU, J., QIAO, S. Z. & QING LU, G. 2011. Mesoporous silica nanoparticles for bioadsorption, enzyme immobilisation, and delivery carriers. *Nanoscale*, 3, 2801-2818.
- QIANG, Y., ANTONY, J., SHARMA, A., NUTTING, J., SIKES, D. & MEYER, D. 2006. Iron/iron oxide core-shell nanoclusters for biomedical applications. *Journal of Nanoparticle Research*, 8, 489-496.
- QIU, J., YANG, R., LI, M. & JIANG, N. 2005. Preparation and characterization of porous ultrafine Fe<sub>2</sub>O<sub>3</sub> particles. *Materials Research Bulletin*, 40, 1968-1975.
- RAKSHAE, R. & PANAHANDEH, M. 2011. Stabilization of a magnetic nano-adsorbent by extracted pectin to remove methylene blue from aqueous solution: A comparative studying between two kinds of cross-liked pectin. *Journal of Hazardous Materials*, 189, 158-166.
- RAPAPORT, A., MILLIEZ, J., BASS, M., CASSANHO, A. & JENSSSEN, H. 2006. Review of the properties of up-conversion phosphors for new emissive displays. *Journal of Display Technology*, 2, 68-78.
- RASHEED, Q. J., PANDIAN, K. & MUTHUKUMAR, K. 2011. Treatment of petroleum refinery wastewater by ultrasound-dispersed nanoscale zero-valent iron particles. *Ultrason Sonochem*, 18, 1138-42.
- REDDY, M. L. P., RAMAMOCHAN, T. R., BHAT, C. C. S., SHANTHI, P. B. & DAMODARAN, A. D. 1992. Mathematical Modelling of the Liquid-Liquid Extraction Separation of Rare Earths. *Mineral Processing and Extractive Metallurgy Review*, 9, 273-282.
- REISS, G. & HUTTEN, A. 2005. Magnetic nanoparticles - Applications beyond data storage. *Nature Materials*, 4, 725-726.
- RENU, AGARWAL, M. & SINGH, K. 2017. Heavy metal removal from wastewater using various adsorbents: a review. *Journal of Water Reuse and Desalination*, 7, 387-419.
- RITCHIE, C., SPELDRIK, M., GABLE, R. W., SORACE, L., KÖGERLER, P. & BOSKOVIC, C. 2011. Utilizing the Adaptive Polyoxometalate [As<sub>2</sub>W<sub>19</sub>O<sub>67</sub>(H<sub>2</sub>O)]<sub>14</sub>- To Support a Polynuclear Lanthanoid-Based Single-Molecule Magnet. *Inorganic Chemistry*, 50, 7004-7014.
- RONDA, C. R., JÜSTEL, T. & NIKOL, H. 1998. Rare earth phosphors: fundamentals and applications. *Journal of Alloys and Compounds*, 275-277, 669-676.
- ROOSEN, J. & BINNEMANS, K. 2014. Adsorption and chromatographic separation of rare earths with EDTA- and DTPA-functionalized chitosan biopolymers. *Journal of Materials Chemistry A*, 2, 1530-1540.
- ROSKILL LTD 2016. Rare Earths: Global industry, markets and outlook to 2026.
- ROYEN, H. & FORTKAMP, U. 2016. Rare Earth Elements- Purification, Separation and Recycling. IVL Swedish Environmental Research Institute.

- RULOFF, R., GELBRICH, T., HOYER, E., SIELER, J. & BEYER, L. 1998. Gesteuerte Kristallisation des Gadolinium(III)-Komplexes von Diethylenetriaminpentaacetat: Monomere und dimere Struktur / Controlled Crystallization of the Gadolinium(III) Complex of Diethylenetriamine-Pentaacetate: Monomeric and Dimeric Structure. *Zeitschrift für Naturforschung B*.
- RULOFF, R., GELBRICH, T., SIELER, J., HOYER, E. & BEYER, L. 1997. Strukturen zweier isomerer Gadolinium(III)-Polyaminopolycarboxylate -Argumente für signifikante Unterschiede ihrer 1H-NMR-Relaxation/Structures of Two Isomeric Gadolinium(III) Polyamino Polycarboxylates -Relation to their Significant Differences in 1H NMR Relaxation. *Zeitschrift für Naturforschung B*.
- SADEGHIANI, N., BARBOSA, L. S., GLIEDES, M. H. A., CHAVES, S. B., SANTOS, J. G., SILVA, O., PELEGRINI, F., AZEVEDO, R. B., MORALS, P. C. & LACAVALA, Z. G. M. 2005. Magnetic resonance of polyaspartic acid-coated magnetite nanoparticles administered in mice. *IEEE Transactions on Magnetics*, 41, 4108-4110.
- SANTOYO, E. & VERMA, S. P. 2003. Determination of lanthanides in synthetic standards by reversed-phase high-performance liquid chromatography with the aid of a weighted least-squares regression model estimation of method sensitivities and detection limits. *Journal of chromatography. A*, 997, 171-182.
- SANTRA, S., TAPEC, R., THEODOROPOULOU, N., DOBSON, J., HEBARD, A. & TAN, W. 2001. Synthesis and Characterization of Silica-Coated Iron Oxide Nanoparticles in Microemulsion: The Effect of Nonionic Surfactants. *Langmuir*, 17, 2900-2906.
- SCHILDER, H. & LUEKEN, H. 2004. Computerized magnetic studies on d, f, d-d, f-f, and d-S, f-S systems under varying ligand and magnetic fields. *Journal of Magnetism and Magnetic Materials*, 281, 17-26.
- SEISENBAEVA, G. A., MELNYK, I. V., HEDIN, N., CHEN, Y., ERIKSSON, P., TRZOP, E., ZUB, Y. L. & KESSLER, V. G. 2015. Molecular insight into the mode-of-action of phosphonate monolayers as active functions of hybrid metal oxide adsorbents. Case study in sequestration of rare earth elements. *RSC Advances*, 5, 24575-24585.
- SHAHRIARI, T., BIDHENDI, G. N., MEHRDADI, N. & TORABIAN, A. 2014. Effective parameters for the adsorption of chromium(III) onto iron oxide magnetic nanoparticle. *International Journal of Environmental Science and Technology*, 11, 349-356.
- SHARMA, R. K. & SHARMA, S. 2014. Silica nanosphere-supported palladium(II) furfural complex as a highly efficient and recyclable catalyst for oxidative amination of aldehydes. *Dalton Trans*, 43, 1292-304.
- SHELDON, R. A. 2012. Fundamentals of green chemistry: efficiency in reaction design. *Chemical Society Reviews*, 41, 1437-1451.
- SHEN, Y. F., TANG, J., NIE, Z. H., WANG, Y. D., REN, Y. & ZUO, L. 2009. Preparation and application of magnetic Fe<sub>3</sub>O<sub>4</sub> nanoparticles for wastewater purification. *Separation and Purification Technology*, 68, 312-319.
- SHI, F., TSE, M. K., POHL, M. M., BRÜCKNER, A., ZHANG, S. & BELLER, M. 2007. Tuning catalytic activity between homogeneous and heterogeneous catalysis: Improved activity and selectivity of free nano-Fe<sub>2</sub>O<sub>3</sub> in selective oxidations. *Angewandte Chemie - International Edition*, 46, 8866-8868.
- SHIBASAKI, M. & YOSHIKAWA, N. 2002. Lanthanide complexes in multifunctional asymmetric catalysis. *Chemical Reviews*, 102, 2187-2209.
- SHIRI-YEKTA, Z., YAFTIAN, M. R. & NILCHI, A. 2013. Silica nanoparticles modified with a Schiff base ligand: An efficient adsorbent for Th(IV), U(VI) and Eu(III) ions. *Korean Journal of Chemical Engineering*, 30, 1644-1651.
- SILVERSTEIN, R. M., WEBSTER, F. X., KIEMLE, D. J. & BRYCE, D. L. 2014. *Spectrometric Identification of Organic Compounds*, Wiley.
- SINGH, L. P., BHATTACHARYYA, S. K., KUMAR, R., MISHRA, G., SHARMA, U., SINGH, G. & AHALAWAT, S. 2014. Sol-Gel processing of silica nanoparticles and their applications. *Adv Colloid Interface Sci*, 214c, 17-37.
- SLATER, C. S. & SAVELSKI, M. 2007. A method to characterize the greenness of solvents used in pharmaceutical manufacture. *Journal of Environmental Science and Health, Part A*, 42, 1595-1605.
- SOENEN, S. J., DE CUYPER, M., DE SMEDT, S. C. & BRAECKMANS, K. 2012. Chapter ten - Investigating the Toxic Effects of Iron Oxide Nanoparticles. In: NEJAT, D. (ed.) *Methods in Enzymology*. Academic Press.

- SOUSA-AGUIAR, E. F., TRIGUEIRO, F. E. & ZOTIN, F. M. Z. 2013. The role of rare earth elements in zeolites and cracking catalysts. *Catalysis Today*, 218-219, 115-122.
- SPRECHER, B., XIAO, Y. P., WALTON, A., SPEIGHT, J., HARRIS, R., KLEIN, R., VISSER, G. & KRAMER, G. J. 2014. Life Cycle Inventory of the Production of Rare Earths and the Subsequent Production of NdFeB Rare Earth Permanent Magnets. *Environmental Science & Technology*, 48, 3951-3958.
- STJERNDAHL, M., ANDERSSON, M., HALL, H. E., PAJEROWSKI, D. M., MEISEL, M. W. & DURAN, R. S. 2008. Superparamagnetic Fe<sub>3</sub>O<sub>4</sub>/SiO<sub>2</sub> Nanocomposites: Enabling the Tuning of Both the Iron Oxide Load and the Size of the Nanoparticles. *Langmuir*, 24, 3532-3536.
- STÖBER, W., FINK, A. & BOHN, E. 1968. Controlled growth of monodisperse silica spheres in the micron size range. *Journal of Colloid and Interface Science*, 26, 62-69.
- TANI, T., WATANABE, N. & TAKATORI, K. 2003. Emulsion Combustion and Flame Spray Synthesis of Zinc Oxide/Silica Particles. *Journal of Nanoparticle Research*, 5, 39-46.
- TANIGUCHI, V. T. & DOTY, A. W. 1989. Large scale chromatographic separation using 'continuous displacement chromatography' (CDC). *Proceedings of Rare Earths: Extraction, Preparation and Application*, 147-161.
- TARTAJ, P., DEL PUERTO MORALES, M., VEINTEMILLAS-VERDAGUER, S., GONZÁLEZ-CARREÑO, T. & SERNA, C. J. 2003. The preparation of magnetic nanoparticles for applications in biomedicine. *Journal of Physics D: Applied Physics*, 36, R182-R197.
- TECHNOLOGY METALS RESEARCH 2015. Advanced Rare Earth projects index.
- TEJA, A. S. & KOH, P.-Y. 2009. Synthesis, properties, and applications of magnetic iron oxide nanoparticles. *Progress in Crystal Growth and Characterization of Materials*, 55, 22-45.
- TEXIER, A.-C., ANDRÈS, Y. & LE CLOIREC, P. 1999. Selective Biosorption of Lanthanide (La, Eu, Yb) Ions by *Pseudomonas aeruginosa*. *Environmental Science & Technology*, 33, 489-495.
- THAKUR, N. V. 2000. Separation of Rare Earths by Solvent Extraction. *Mineral Processing and Extractive Metallurgy Review*, 21, 277-306.
- TSAMIS, A. & COYNE, M. 2015. Recovery of Rare Earths from Electronic wastes: An opportunity for high-tech SMEs. . European Parliament.
- TU, Y. J., YOU, C. F. & CHANG, C. K. 2012. Kinetics and thermodynamics of adsorption for Cd on green manufactured nano-particles. *J Hazard Mater*, 235-236, 116-22.
- U.S. DEPARTMENT OF ENERGY 2010. Critical Materials Strategy.
- U.S. GEOLOGICAL SURVEY 2017. Mineral Commodity Summary 2017.
- U.S GEOLOGICAL SURVEY 2013. Going Critical: Being Strategic with Our Mineral Resources.
- WANG, C. T. & WILLEY, R. J. 1998. Oxidation of methanol over iron oxide based aerogels in supercritical CO<sub>2</sub>. *Journal of Non-Crystalline Solids*, 225, 173-177.
- WANG, J., HU, P., HAN, G., ZHANG, L., LI, D., XU, R., CHEN, X. & ZHANG, X. D. 2011. New nine-coordinate (NH<sub>4</sub>)<sub>3</sub>[YbIII(ttha)]·5H<sub>2</sub>O and eight-coordinate (NH<sub>4</sub>)[YbIII(pdta)(H<sub>2</sub>O)<sub>2</sub>]·5H<sub>2</sub>O complexes: Structural determination. *Russ. J. Struct. Chem.*, 52, 592.
- WANG, J., LIU, X. H., ZHANG, Z. H., ZHANG, X. D., GAO, G. R., KONG, Y. M. & LI, Y. 2006a. The syntheses and structures of ten-coordinate K<sub>6</sub>[PrIII(ttha)]<sub>2</sub> · 10H<sub>2</sub>O and nine-coordinate K<sub>4</sub>[SmIII<sub>2</sub>(Htha)<sub>2</sub>] · 14H<sub>2</sub>O complexes. *J. Coord. Chem.*, 59, 2103.
- WANG, J., LIU, X. Z., WANG, X. F., GAO, G. R., XING, Z. Q., ZHANG, X. D. & XU, R. 2008. Nine-coordinate rare earth metal complexes with aminopolycarboxylic acids: Mononuclear (NH<sub>4</sub>)<sub>3</sub>[TbIII(ttha)]·5H<sub>2</sub>O and binuclear (NH<sub>4</sub>)<sub>4</sub>[Tb 2 III (dtpa)<sub>2</sub>]·9H<sub>2</sub>O. *Journal of Structural Chemistry*, 49, 75-83.
- WANG, J., WANG, Y., ZHANG, Z., ZHANG, X., LIU, X., LIU, X., LIU, Z., ZHANG, Y., TONG, J. & ZHANG, P. 2006b. Rare earth metal complexes with triethylenetetraminehexaacetic acid. *Journal of Coordination Chemistry*, 59, 295-315.
- WANG, Y. & DAVIS, B. H. 1999. Fischer-Tropsch synthesis. Conversion of alcohols over iron oxide and iron carbide catalysts. *Applied Catalysis A: General*, 180, 277-285.
- WEI, Z., SANDRON, S., TOWNSEND, A. T., NESTERENKO, P. N. & PAULL, B. 2015. Determination of trace labile copper in environmental waters by magnetic nanoparticle solid phase extraction and high-performance chelation ion chromatography. *Talanta*, 135, 155-162.
- VEMURY, S., PRATSINIS, S. E. & KIBBEY, L. 2011. Electrically Controlled Flame Synthesis of Nanophase TiO<sub>2</sub>, SiO<sub>2</sub>, and SnO<sub>2</sub> Powders. *Journal of Materials Research*, 12, 1031-1042.

- WENG, Z., JOWITT, S. M., MUDD, G. M. & HAQUE, N. 2015. A Detailed Assessment of Global Rare Earth Element Resources: Opportunities and Challenges\*. *Economic Geology*, 110, 1925-1952.
- WILDEN, A., MODOLO, G., KAUFHOLZ, P., SADOWSKI, F., LANGE, S., MUNZEL, D. & GEIST, A. 2015. Process Development and Laboratory-Scale Demonstration of a Regular-SANEX Process Using C5-BPP (2,6-Bis (5-(2,2-dimethylpropyl)-1H-pyrazol-3-yl)pyridine). *Separation Science and Technology*, 50, 2467-2475.
- WILKINSON, K., EKSTRAND-HAMMARSTROM, B., AHLINDER, L., GULDEVALL, K., PAZIK, R., KEPINSKI, L., KVASHNINA, K. O., BUTORIN, S. M., BRISMAR, H., ONFELT, B., OSTERLUND, L., SEISENBAEVA, G. A. & KESSLER, V. G. 2012. Visualization of custom-tailored iron oxide nanoparticles chemistry, uptake, and toxicity. *Nanoscale*, 4, 7383-7393.
- XIE, F., ZHANG, T. A., DREISINGER, D. & DOYLE, F. 2014. A critical review on solvent extraction of rare earths from aqueous solutions. *Minerals Engineering*, 56, 10-28.
- XIONG, D.-B., CHEN, H.-H., YANG, X.-X. & ZHAO, J.-T. 2007. Hydrothermal synthesis and characterization of a new 1-D polymeric lanthanum ethylenediaminetetraacetate with less metal-aqua coordination: {[La(EDTA)(H<sub>2</sub>O)]<sub>2</sub>}<sub>n</sub>. *Inorganica Chimica Acta*, 360, 1616-1620.
- XU, Z. P., ZENG, Q. H., LU, G. Q. & YU, A. B. 2006. Inorganic nanoparticles as carriers for efficient cellular delivery. *Chemical Engineering Science*, 61, 1027-1040.
- YE, S., XIAO, F., PAN, Y. X., MA, Y. Y. & ZHANG, Q. Y. 2010. Phosphors in phosphor-converted white light-emitting diodes: Recent advances in materials, techniques and properties. *Materials Science and Engineering: R: Reports*, 71, 1-34.
- YOU, X.-L. & NG, S. W. 2007. Poly[hydronium [dysprosium(III)-μ<sub>3</sub>-(ethylenediaminetetraacetato-κ<sup>8</sup>N,N',O,O',O'',O''':O''''':O''''')]] monohydrate]. *Acta Crystallographica Section E*, 63, m1819-m1819.
- YURCHENKO, G. R., MATKOVSKII, A. K., MEL'NIK, I. V., DUDARKO, O. A., STOLYARCHUK, N. V., ZUB, Y. L. & ALONSO, B. 2012. Adsorption properties of silica-based sorbents containing phosphonic acid residues. *Colloid Journal*, 74, 386-390.
- ZHANG, H., ZHAO, Z., XU, X. & LI, L. 2011. Study on industrial wastewater treatment using superconducting magnetic separation. *Cryogenics*, 51, 225-228.
- ZHANG, H. J., MCDOWELL, R. G., MARTIN, L. R. & QIANG, Y. 2016. Selective Extraction of Heavy and Light Lanthanides from Aqueous Solution by Advanced Magnetic Nanosorbents. *Acs Applied Materials & Interfaces*, 8, 9523-9531.
- ZHANG, P., ZHANG, L., WANG, C., XUE, S. F., LIN, S. Y. & TANG, J. K. 2014. Equatorially Coordinated Lanthanide Single Ion Magnets. *Journal of the American Chemical Society*, 136, 4484-4487.
- ZHANG, R., HUANG, J., ZHAO, J., SUN, Z. & WANG, Y. 2007. Sol-gel auto-combustion synthesis of zinc ferrite for moderate temperature desulfurization. *Energy and Fuels*, 21, 2682-2687.
- ZHENG, Y. H., CHENG, Y., BAO, F. & WANG, Y. S. 2006. Synthesis and magnetic properties of Fe<sub>3</sub>O<sub>4</sub> nanoparticles. *Materials Research Bulletin*, 41, 525-529.
- ZHUANG, X., LONG, Q. & WANG, J. 2010. Poly[[[μ(3)-N'-(carboxymethyl)ethylene-di-amine-N,N,N'-triacetato]dysprosium(III)] trihydrate]. *Acta Crystallographica Section E: Structure Reports Online*, 66, m1436-m1436.



## Popular science summary

Rare Earth Elements (REE) are a group of 17 chemically similar elements from the periodic table that are crucial for many applications, mostly technological, which to a greater or lesser extent define the basis of our modern life. They are colloquially known as “the vitamins of modern industry”, since they are essential but needed in quite small amounts. Despite their name, they are not “rare” in the Earth’s crust, but their beneficiation and separation is a challenging process from many points of view. Historically, we have been reliant on China for their supply, but in the last years there has been an effort from other political unions, such as the European Union, to develop their own REE supply industry. This thesis work is part of a multi-disciplinary European project and aims to tackle some of the challenges of the REE supply chain, specifically dealing with the extraction and separation of REE.

The hereby proposed approach is focused on the study of magnetic silica-based nanoadsorbents and their potential for REE extraction and separation. The nanoadsorbents are surface decorated with organic molecules (ligands) that have affinity toward REE and can take them up. Doing a comprehensive study of different ligands and how they interact with different REE, tailoring of nanoadsorbents for a specific REE or group of REE can be achieved. The possibilities of these type of nanoadsorbents for increasing the total REE uptake, as well as upscaling of the process, were also studied in this thesis. This technology provided very competitive results and advantages over the currently most used industrial processes, mostly from an environmental point of view, but also in terms of simplicity and reusability of the materials.

## Populärvetenskaplig sammanfattning

Sällsynta jordartsmetaller (REE) är en grupp bestående av 17 kemiskt snarlika grundämnen i Periodiska systemet som är avgörande för många tillämpningar. Dessa är kända för att i större eller mindre utsträckning utgör grunden för vårt moderna liv. REE är allmänt kända som ”Den moderna industrins vitaminer”, detta då de är livsnödvändiga men i ganska små mängder. Deras namn till trots, så är de inte ”sällsynta” i jordskorpan, men dess anrikning och separation är på många sätt utmanande. Historiskt sett har vi varit beroende av deras produktion i Kina. På senare år har det dock gjorts insatser på andra håll i världen, t.ex. i EU för att utveckla en egen REE-framställande industri. Den här avhandlingen är en del i ett multidisciplinärt europeiskt projekt som syftar till att tackla några av de utmaningar som den REE-framställande industrin står inför, mer specifikt extraktion och separation av REE.

Det härmed föreslagna tillvägagångssättet fokuserar på studier av magnetiska kiseloxidbaserade nanoadsorbenter och deras potential för extrahering och separering av REE. Nanoadsorbenterna är ytbesmyckade med organiska molekyler (ligander) som har affinitet mot REE och kan binda dem till sig. Genom omfattande studier av olika ligander och deras interaktioner med olika REE, så kan skräddarsydda nanoadsorbenter för specifika REE eller REE-grupper åstadkommas. Avhandlingen redovisar även möjligheterna att använda den här typen av nanoadsorbenter för att öka det totala REE-upptaget samt ger exempel på processuppskalning.

## Acknowledgements

So, this is it. Here comes the section that will probably be the most read of the entire thesis. If you have reached here after actually reading all the previous pages, you can already feel deeply thanked for. If, like many times I've done myself, you have skipped pages up to here, well...you will have to go through these pages to see if, hopefully, I haven't forgotten many people and you can find your name in the following lines☺.

First of all, I would like to thank my main supervisor, **Gulaim A. Seisenbaeva**, from whom I have learnt a lot along these four years, both professionally and personally. You have always helped me whenever I needed it, even if you had plenty of other things to do, there was always a space for everyone and that is something I truly appreciate. Thank you for guiding me through these years.

Thank you **Vadim G. Kessler**, my co-supervisor, for always showing an optimistic attitude, for sharing your knowledge, your passion for research and your always appreciated stories. Thanks to both of you, **Gulaim** and **Vadim** for choosing me for this position and giving me the opportunity to live one of my most life-changing experiences.

Thanks to my second co-supervisor, **Peter Svedlindh**, with whom I have perhaps not spent as much time as I would have liked to, but every time I did he has shown his willingness to help and to contribute to my thesis with his great knowledge.

Thanks to all the wonderful people in the EURARE project. You are all amazing professionals and even better humans. We have done a great job and had some unforgettable moments in beautiful cities all over Europe within our Work Package 0 :P. Special mention to **Miranda**, who has done a huge work proof-reading my thesis and correcting the language. But even more importantly, thank you for encouraging me to apply for that position in Kemakta, I am really looking forward to start working with you and all the great people there.

All my colleagues at the department of, first Chemistry, then Chemistry and Biotechnology, and finally Molecular Sciences, have made my time at work a joy. The department is now quite big so I am most likely going to miss many names here, but every and each of you has my gratitude. One of the first persons to make me feel welcome and helped me was our recently retired administrator **Sonja Jansson**, thank you so much for all your patience and help with all my questions. Thanks to all the current administrative team as well, for they have made everything work very smooth. **Daniel Lundberg**, your constant enthusiasm is something I admire and I thank you for, as well as your interest in my research. Thank you **Gunnar** for your kindness from the very first minute. **Eva**, thank you for delighting us with tasty cakes in the fika room ☺. Thank you **Ievgen** for entertaining my boring writing days by tracking the number of lunches and fikas that one person can have in a day. Despite starting a very creative war with us (well I don't remember who started it anymore), the *organic people* has also a place in my heart. Thank you **Christina, Lena, Frida** for your sense of humour, creativity, and generally just being people that you know you can always have a fun conversation with. **Johnny**, gracias por tu amabilidad y por tener siempre una sonrisa en la cara ☺. **Hanna**, we have had some very nice chats and at times of weakness I think we have been of great support for each other, for which I am very thankful. You are a hard-working and very organized person and I admire you for that. I wish you the best for the rest of your PhD. Thank you **Gustav** for always being a nice and calm person. Thank you **Ali** and **Elisabeth** for always being kind and interested in how I was doing, I wish you the best in life and with the nice family that you have created ☺. Thanks to my office mates for some very remarkable memories. **Fredric**, thanks for never giving up trying to drag me to the gym :P. Thank you **Tobias** for very nice times during the time that we shared office. **Kayly**, thank you for your kindness and always being willing to help. **Martin**, gracias por una gran amistad desde el minuto cero, que seguro durará más que este PhD :P. **Anja**, one of the most recent PhD students, although we haven't had much time together I thank you for showing your friendliness from the very beginning and I wish you the best for the coming 4 years, they'll go faster than you think! Thanks to the lunch-bunch, **Kerstin, Pernilla** and **Alyona** for some very memorable lunches and times inside and outside the department. Alyona, I will give you your drill back don't you worry :P.

Special thanks also to some people that is no longer in the department, **Anke, Yina** and **Seda**. Thanks for making my beginning here much easier and for great memories both at work and outside.

To one of the best friends I got in my life thanks to SLU, **Olga**, I don't think I have enough lines to thank you for everything I should. You are one of the

most kind-hearted people I know, you have always been good and kind to me no matter what your personal situation was. Having you in my life is a gift and you know you will always find a friend in me no matter where life takes us.

To all my friends in Uppsala, **Joanna, Joy, Pia, Berta...**for making my start in a new country much easier and being great friends even if we don't always see each other as often as we would like to.

A mis amigas **Bea, Maite, María y Virginia**, por ser las mejores amigas que alguien podría tener y por hacer que la lista de anécdotas que contar a nuestros futuros nietos sea interminable. A **Saioa**, además de por ser una buena amiga, por querer verme cada vez que voy a Pamplona y hacerme sentir importante :P. A **Miguel**, una de las personas más inteligentes que conozco, por estar siempre orgulloso de mí y ser un buen amigo. A mis químicas guapas **María y Blanca**, tenemos que repetir nuestra aventura campestre pronto ☺. **Gupo!** Gracias por amenizar mis horas de trabajo y de no trabajo con interminables conversaciones que en más de una ocasión han causado una carcajada en medio de la oficina.

A mi familia, porque aunque a veces no entiendan muy bien qué narices estoy haciendo exactamente en Suecia, siempre me han apoyado y han creído en mí. Gracias **Papá y mamá** por todo, está claro que sin vosotros no habría llegado hasta aquí. Gracias por educarme para ser una persona trabajadora e independiente. **Hermana**, gracias loqui!! Por estar siempre feliz por mí y creer en mí a veces incluso demasiado :P. Aunque seamos personas bastante distintas, creo que no me equivoco si digo que ninguna de las dos podría vivir sin la otra. Cuqui and loqui forever! No tengo espacio para toda mi familia (mi tesis ya es suficientemente tostón, se me acaban las páginas), pero gracias a todos, a mi tía **Sol** y mi prima **Isa** por nuestras comidas con temas de conversación siempre muy agradables. A mis primas **Ana y Nanin**, a mi tía **Mary** y a los tres soles **Xabier, Fermín y Leyre**, que algún día leerán esto ☺ .

Tack **Marie** för att du är bara den bästa svärmor man kan ha och det är alltid en sann glädje att besöka dig eller ha dig på besök. Tack också för att du skapade Jon, den bästa mannen i världen!

The last paragraph is always left for the most important, right? To my beloved **Jon**, who would deserve a whole chapter for himself for everything he does and every way in which he makes me happy. You are the best I have in life, thank you for bearing with me lately when I haven't exactly been an easy person to be around. For always loving me till the sun (like Maite would say :P) and always try to put a smile on my face. Being able to share my life with you is the best gift, I don't have enough words to express how lucky I feel and I hope there are many more coming stories and experiences to live with you. Jag älskar dig, mi guapo.